Université de Montréal

Study of NAD(P)H fluorescence in living cardiomyocytes by spectrally resolved time-correlated single photon counting

par

Cheng Ying

Programme de Sciences Biomédicales

Faculté de Médecine

Thèse présentée à la Faculté des études supérieures

en vue de l'obtention du grade de Maître ès Sciences (M.Sc.)

en Sciences Biomédicales

Décembre 2007

Université de Montréal
Faculté des études supérieures

Cette thèse intitulée :

Study of NAD(P)H fluorescence in living cardiomyocytes by spectrally resolved time-correlated single photon counting

présentée par :
Cheng Ying

a été évaluée par un jury composé des personnes suivantes :

Jean-Yves Lapointe, président-rapporteur
Alzbeta Chorvatova, directeur de recherche
Grant Mitchell, membre du jury

RÉSUMÉ

Dans les cellules cardiaques, la fonction première des mitochondries est la production d'énergie, processus crucial pour la contraction et le bon fonctionnement du cœur. Dans des conditions physiopathologiques telles que l'ischémie et/ou le rejet des cœurs transplantés, l'analyse de l'état métabolique mitochondrial chez les patients ainsi que dans les modèles animaux permettrait donc de déceler les signes précoces de dysfonctions mitochondriales par conséquent de dysfonction cardiaque. Dans cette étude, nous examinons dans les myocytes cardiaques, la fluorescence endogène ou autofluorescence (AF) du nicotinamide adénine dinucléotide (phosphate), ou NAD(P)H, le principal donneur d'électrons dans la respiration mitochondriale, responsable de la production d'ATP. Le NAD(P)H est étudié comme un marqueur non invasif pour sonder la fonction mitochondriale et ainsi leur état métabolique. Notre objectif est d'étudier l'état du métabolisme oxydatif des mitochondries dans les myocytes cardiaques isolés de rats adultes ou de patients pédiatriques ayant subi une transplantation cardiaque. Pour réaliser cette étude, nous utiliserons une nouvelle méthode de spectroscopie avec résolution temporelle, afin d'établir les spectres d'émission et les caractéristiques dynamiques du temps de vie des molécules NAD(P)H. La fluorescence de NAD(P)H a été enregistrée dans les myocytes suite à l'excitation par un laser UV pulsatile et les spectres ainsi que les durées de vie de fluorescence ont été enregistrés de manière simultanée. Nous avons évalué l'AF en fonction de la modulation de la production de NADH et/ou de la respiration mitochondriale. Nous avons comparé les conditions physiopathologiques, telles que l'ischémie et/ou les stades différents de rejet des cœurs transplantés dans le but de trouver de nouveaux outils permettant d'établir le diagnostic précoce de ces conditions et ainsi d'améliorer le pronostic de ces patients.

Nos résultats montrent qu'un modèle de décomposition triexponentielle de durée de vie de fluorescence, notamment 0.4-0.7ns, 1.2-1.9ns et 8.0-13.0ns, a été nécessaire pour décrire la fluorescence de NAD(P)H dans les myocytes cardiaques dans la gamme spectrale

de 420-560nm. L'augmentation de la production mitochondriale de NADH par des corps cétoniques a renforcée l'intensité de l'AF, sans pour autant induire un changement significatif de sa durée de vie. La roténone, l'inhibiteur du Complexe I de la chaîne respiratoire mitochondriale, a augmenté l'intensité de l'AF, tout en raccourcissant sa durée de vie moyenne. Le dinitrophénol (DNP), un agent découplant la phosphorylation oxydative des mitochondries a provoqué une diminution de l'intensité de l'AF et une augmentation de sa durée de vie moyenne. Ces effets, comparables à ceux induits par l'augmentation de la concentration de NADH et/ou de ses taux de déshydrogénation *in vitro*, ont été également examinés dans des conditions qui imitent l'ischémie.

Cette étude est aussi la première à montrer les caractéristiques dynamiques de la fluorescence de NAD(P)H dans les cellules cardiaques humaines isolées d'une biopsie endomyocardique des patients pédiatriques qui ont subi une transplantation cardiaque. La fluorescence endogène de NAD(P)H a été retrouvée significativement plus faible dans les cœurs humains par rapport à ceux des rats isolés dans les mêmes conditions. La roténone a augmenté l'intensité de fluorescence dans les cellules cardiaques humaines, les rendant ainsi comparables aux modèles expérimentaux chez le rat. Nous avons aussi observé une corrélation entre les changements de l'intensité de la fluorescence avec le stade de rejet des cœurs transplantés. En effet, l'intensité de fluorescence a augmentée de manière significative en cas de rejet léger (R1), par comparaison au stade sans rejet (R0). Ces résultats suggèrent que les cellules cardiaques humaines sont métaboliquement plus actives que celles des rats dans les mêmes conditions, alors que cette activité (par conséquent la production de l'ATP) semble baisser au cours de processus de rejet.

La méthode spectrométrique avec la résolution temporelle représente un outil prometteur pour analyser le NAD(P)H mitochondrial des cardiomyocytes. Cette approche permettra d'améliorer les connaissances sur le métabolisme oxydatif et/ou son dysfonctionnement au niveau cellulaire. Il pourrait éventuellement constituer un nouvel outil diagnostique pour évaluer les changements métaboliques associés au rejet des cœurs transplantés. Dans le futur, cette approche pourrait se révéler utile pour la détection précoce

des cas bénins ou de rejet, notamment dans le cadre de résultats histologiques douteux, et donc dans la prise de décision pour débuter le traitement adéquat. Ainsi, ce travail pourrait donc avoir un impact direct sur la prise en charge des enfants avec des cœurs transplantés et qui risquent le rejet.

Mots-clés : NAD(P)H, autofluorescence (AF), spectroscopie avec résolution temporelle, mitochondrie, myocytes cardiaques, rejet des cœurs transplantés

ABSTRACT

The primary function of cardiac mitochondria is the production of ATP to support rhythmic contraction of the heart. Examination of the mitochondrial redox state in patients and experimental animals is therefore crucially important to sensitively detect early signs of mitochondrial function in pathophysiological conditions, such as ischemia and/or the allograft rejection of heart transplantations, a major cause of death of transplanted patients. In this study, we monitor cellular fluorescence of nicotinamide adenine dinucleotide (phosphate), or NAD(P)H, the principal electron donor in mitochondrial respiration responsible for vital ATP supply of cardiomyocytes. Here, NAD(P)H is studied as a marker for non-invasive fluorescent probing of the mitochondrial function. Our objects are to study fingerprinting of mitochondrial metabolic oxidative state in living cardiomyocytes by spectrally-resolved time-correlated single photon counting (TCSPC) to report dynamic characteristics of NAD(P)H fluorescence decay in living rat cardiomyocytes, as well as in human cardiac cells from pediatric patients with transplanted hearts. NAD(P)H fluorescence is recorded in living cardiomyocytes following excitation by UV-pulsed laser diode and detection by spectrally-resolved TCSPC, based on the simultaneous measurement of the fluorescence spectra and fluorescence lifetimes. Modulation of NADH production and/or mitochondrial respiration is tested and pathophysiological conditions are compared to search for new diagnostic tools for early detection of rejection of transplanted hearts and therefore to improve the prognosis in this population of patients.

Our results show that at least a 3-exponential decay model, with 0.4-0.7ns, 1.2-1.9ns and 8.0-13.0ns lifetime pools is necessary to describe cardiomyocyte autofluorescence (AF) within 420-560nm spectral range. Increased mitochondrial NADH production by ketone bodies enhanced the fluorescence intensity, without significant change in fluorescent lifetimes. Rotenone, the inhibitor of Complex I of the mitochondrial respiratory chain, increased AF intensity and shortened the average fluorescence lifetime. Dinitrophenol (DNP), an uncoupling agent of the mitochondrial oxidative phosphorylation, lowered AF

intensity, broadened the spectral shoulder at 520 nm and increased the average fluorescence lifetime. These effects, comparable to the changes in the concentration and in the rate of dehydrogenation of NADH *in vitro*, were also examined under ischemia-mimetic conditions.

Furthermore, we report for the first time dynamic characteristics of NAD(P)H fluorescence decays in living human cardiac cells, isolated from one endomyocardial biopsies (EMB) of pediatric heart transplanted patients with different rejection grades. NAD(P)H fluorescence in human hearts was found significantly lower in comparison to rat ones in same conditions. Rotenone increased the fluorescence intensity in human cardiac cells, making them more comparable to experimental rat model. We observed a correlation between changes in steady-state NAD(P)H fluorescence spectra and rejection grades, namely significantly increased fluorescence intensity in mild rejection (R1) vs. no rejection (R0). These results suggest that human cardiac cells are more metabolically active than the rat ones in the same conditions, while this activity (and thus ATP production) seems lowered during rejection process.

Spectrally-resolved fluorescence lifetime technique provides promising new tool for analysis of mitochondrial NAD(P)H fluorescence in living cardiomyocytes. This approach will enhance our knowledge about cardiomyocyte oxidative metabolism and /or its dysfunction at a cellular level. It can eventually become a new diagnostic tool for evaluation of oxidative metabolism changes in transplanted hearts. In the future, this approach can prove helpful in the detection of early or mild cases of rejection, particularly in the case of doubtful histological results and hence in the decision-making for rapid initiation of the necessary treatment. It may therefore have a direct impact on the care of children with transplanted hearts that are at risk of rejection.

Keywords: NAD(P)H, autofluorescence (AF), spectrally-resolved fluorescence lifetimes, mitochondria, living cardiomyocyte, rejection of heart transplantation.

TABLE OF CONTENTS

RÉSUMÉ ..... **iii**

ABSTRACT ..... **vi**

LIST OF TABLES ..... **xi**

LIST OF FIGURES ..... **xii**

LIST OF ABBREVIATIONS AND SYMBOLS ..... **xv**

ACKNOWLEDGEMENTS ..... **xix**

1. INTRODUCTION **1**

1.1. Oxidative metabolism in cardiomyocyte mitochondria **1**

1.1.1. ATP generation for heart functional activities 1

1.1.2. Substrates for cardiomyocyte metabolism 3

1.1.3. Structure and function of NAD(P)H molecule 7

1.1.4. Mitochondrial respiratory chain 9

1.1.5. Oxidative phosphorylation and ATP synthesis 14

1.1.6. Control of mitochondrial respiration and ATP synthesis 16

1.1.7. Change in respiration and oxidative metabolism in pathophysiological conditions 18

1.2. NAD(P)H fluorescence in cardiomyocytes **21**

1.2.1. Physics of fluorescence 21

1.2.2. Endogenous fluorescence of living cells 23

1.2.3. Spectral characteristics of NAD(P)H fluorescence 25

1.2.4. NAD(P)H fluorescence lifetime pools in mitochondria 27

1.2.5. Latest experimental approaches for monitoring cellular autofluorescence 29

1.3. Aim of present study **30**

2. MATERIAL AND METHODS 32

2.1. Material 32

2.1.1. Isolation of left ventricular myocytes from rat hearts 32

2.1.2. Isolation of cardiomyocytes from endomyocardial biopsies of pediatric heart transplanted patients 34

2.1.3. Solutions 35

2.1.4. Reagents 36

2.2. Methods 37

2.2.1. Confocal microscopy 37

2.2.2. Spectrally-resolved time-correlated single photon counting 37

2.2.3. Recording of spectrally-resolved autofluorescence data in living cardiac cells 40

2.2.4. Definitions of terms and derived quantities 46

2.2.5. Data analysis 48

3. RESULTS 49

3.1. Recording of NADH flurescence *in vitro* 49

3.1.1. Kinetics of free NADH fluorescence decay 49

3.1.2. Concentration-dependence of NADH fluorescence decay kinetics 49

3.1.3. pH-dependence of NADH fluorescence decay kinetics 50

3.1.4. Binding of NADH to lipoamide dehydrogenase 50

3.2. Study of NAD(P)H fluorescence in living cardiomyocytes 60

3.2.1. Distribution of NAD(P)H fluorescence 60

3.2.2. Spectral and lifetime characteristics of NAD(P)H fluorescence 60

3.2.3. Inhibition of the mitochondrial respiratory chain 61

3.2.4. Stimulation of NADH dehydrogenation by uncoupling of ATP synthesis 63

3.2.5. Modulation of NADH production in living cardiomyocytes 64

3.2.6. NAD(P)H fluorescence in cardiomyocytes under ischemia-mimicking conditions 74

3.3. Investigation of NAD(P)H fluorescence in living cells from human endomyocardial biopsies 79

3.3.1. Isolation of living cardiac cells from endomyocardial biopsies 79

3.3.2. NAD(P)H fluorescence in human cells: comparison to rat 80

3.3.3. Study of NAD(P)H fluorescence in heart transplanted patients with different rejection grades 81

3.4. Perspectives 87

3.4.1. Decay associated spectra of NAD(P)H fluorescence 87

3.4.2. Analysis of time-resolved emission spectra of NAD(P)H fluorescence 88

4. DISCUSSION 91

4.1. Fingerprinting of metabolic oxidative state in living cardiomyocytes 92

4.2. Changes of metabolic oxidative state in living cardiomyocytes under pathophysiological conditions 100

5. CONCLUSIONS AND PERSPECTIVES 104

6. BIBLIOGRAPHY 105

APPENDIX I: I

APPENDIX II: II

LIST OF TABLES

Table 1: Inhibitors of oxidative phosphorylation 13

Table 2: Theoretical yields of ATP from fully oxidized glucose molecule 15

Table 3: Fluorescence parameters of NADH in the absence and in the presence of LipDH in intracellular solutions (λex/λem = 375 nm/450 nm) 58

Table 4: Fluorescence parameters of rat cardiomyocytes AF (λex/λem = 375 nm/450 nm) 72

Table 5: Fluorescence parameters of cardiomyocytes AF in ischemia-mimetic solutions (λex/λem = 375 nm/450 nm) 78

Table 6: Fluorescence parameters of human cardiomyocytes AF (λex/λem = 375 nm/450 nm) 86

LIST OF FIGURES

Figure 1: Processes of excitation-contraction coupling and mitochondrial energetics ·····2

Figure 2: Pathways and regulatory points of myocardial substrate metabolism·····5

Figure 3: Structure of $NAD(P)^+$ and NAD(P)H molecules ·····8

Figure 4: Complex I of the mitochondrial respiratory chain ·····10

Figure 5: Mitochondrial respiratory chain and its inhibition points·····12

Figure 6: General scheme of the fluorescence process·····22

Figure 7: Transmission images of living cardiomyocytes·····33

Figure 8: Principle of classic TCSPC measurement·····38

Figure 9: The spectrally-resolved TCSPC instrumentation·····39

Figure 10: Original recording of spectrally and time-resolved fluorescence decay·····42

Figure 11: Original recording of AF decay·····44

Figure 12: Analysis of fluorescence decay·····45

Figure 13: NADH fluorescence spectra and lifetimes *in vitro*·····52

Figure 14: Concentration-dependence of NADH fluorescence lifetimes and their relative amplitudes *in vitro*·····53

Figure 15: pH-dependence of NADH fluorescence decay kinetics *in vitro* ·····54

Figure 16: Spectral and fluorescence lifetime characteristics of NADH after binding to LipDH *in vitro*·····55

Figure 17: Fluorescence lifetimes and their relative amplitudes after binding of NADH to LipDH *in vitro* ····· 56

Figure 18: pH-dependence of NADH fluorescence decay kinetics after binding to LipDH *in vitro* ····· 57

Figure 19: Confocal image of NAD(P)H fluorescence in one cardiac cell ····· 66

Figure 20: NAD(P)H fluorescence spectral characteristics in living cardiomyocytes ····· 67

Figure 21: Steady-state NAD(P)H fluorescence in living cardiomyocytes following application of the modulators of respiratory chain ····· 68

Figure 22: NAD(P)H fluorescence lifetimes and their relative amplitudes following application of Rotenone and DNP ····· 69

Figure 23: Steady-state NADH fluorescence spectra in living cardiomyocytes following application of metabolic substrates ····· 70

Figure 24: NAD(P)H fluorescence lifetimes and their relative amplitudes following application of BHB/AcAc (2:1) and BHB/AcAc (20:1) ····· 71

Figure 25: Steady-state NAD(P)H fluorescence spectra of cardiomyocytes under ischemia-mimicking condition ····· 76

Figure 26: NAD(P)H fluorescence lifetimes and their relative amplitudes in ischemia-mimicking conditions ····· 77

Figure 27: Steady-state NAD(P)H fluorescence of human cardiomyocytes isolated from EMB of pediatric heart transplanted patients ····· 83

Figure 28: NAD(P)H fluorescnece lifetimes and relative amplitudes in human cells ····· 84

Figure 29: Steady-state NAD(P)H fluorescence of human cardiomyocytes with different grade of rejection (ISHLT) 85

Figure 30: Decay-associated spectra (DAS) of NAD(P)H fluorescence in cardiomyocytes 89

Figure 31: Time-resolved emission spectroscopy (TRES) of NAD(P)H fluorescence in cardiomyocytes 90

LIST OF ABBREVIATIONS AND SYMBOLS

AcAc:	Acetoacetate
Acetyl-CoA:	Acetyl-coenzyme A
a_i:	Relative amplitude
ATP (ADP):	Adenosine triphosphate (diphosphate)
AF:	Autofluorescence
AP:	Action potential
BDM	2,3-butanedione monoxime
BHB:	β-hydroxybutyrate
BSA:	Bovine serum albumin
χ^2:	Chi-square values
CCCP:	Carbonyl cyanide *m*-chlorophenyl hydrazone
CICR:	Ca^{2+}-induced Ca^{2+}-release
DCI:	1,1'-diethyl-2,2'-carbocyanine iodide
DNP:	Dinitrophenol
DPA:	9,10-diphenylanthracene
DAS:	Decay-associated spectra
E:	Energy
ECC:	Excitation-contraction coupling
ETC:	Electron transport chain
ETF:	Electron transport flavoprotein
EMB:	Endomyocardial biopsy
FAD:	Flavin adenine dinucleotides
FCCP:	Carbonylcyanide-*p*-trifluoromethoxy phenylhydrazone
FMN:	Flavin mononucleotide
FRET:	Förster resonant energy transfer
FWHM:	Full width in half-maximum

GCAD:	Graft coronary artery disease
GTP:	Guanosine trisphosphate
h:	Planck's constant
I_{Na}	Na^+-current
$I_{Ca,L}$:	L-type Ca^{2+}-current
IRF:	Instrument response function
ISHLT:	International Society for Heart and Lung Transplantation
λem:	Emission wavelength
λex	Excitation wavelength
LipDH:	Lipoamide dehydrogenase
ΔμH:	Proton motive force
Δψ:	Mitochondrial membrane potential
NAD(P)H:	Nicotinamide adenine dinucleotide (phosphate)
[NADH]	NADH concentration
ns:	Nano-second
***v*:**	Frequency of light
PCA:	Principal component analysis
PDH:	Pyruvate dehydrogenase
Pcr:	Phosphocreatine
P_i:	Inorganic phosphate
PML:	Photomultiplier
ps:	Pico-second
R0:	Rejection grade 0: no rejection
R1:	Rejection grade 1: mild rejection
ROS:	Reactive oxygen species
ΔpH:	Proton gradient
RyR2:	Ryanodine receptor type 2
S_0:	Ground state of a fluorophore

S_1:	Excited state of a fluorophore
SD:	Standard deviation
SEM:	Standard error
SERCA:	SR Ca^{2+} ATPase
SR:	Sarcoplasmic reticulum
τ:	Fluorescence lifetime
TAC:	Time-to-amplitude converter
TCA:	Tricarboxylic acid cycle
TCSPC:	Time-correlated single photon counting
TRES:	Time-resolved emission spectra
2D/3D:	Two/three dimension
UV:	Ultraviolet

子曰：「學而時習之，不亦悅乎？」

論語, 學而第一

Confucius said: "Isn't it a pleasure to study and practice what you have learned?"

From THE ANALECTS (Sayings)

ACKNOWLEDGEMENTS

First I would like to thank my supervisor, Dr. Alzbeta Chorvatova, for taking me into her research team and opened new horizons to me, while giving me an opportunity to study in a new field of scientific research. These 2 years of my M.Sc program have been a steep learning curve for me. I am grateful for the exceptional guidance and unconditional devotion that she has given me.

Special thanks in particular to Dr. D. Chorvat Jr. and his colleagues, from International Laser Centre, Bratislava, Slovak Republic, for helping compute our experimental data for DAS and TRES. Thanks Dr. N. Dahdah, Dr. N. Poirier and Dr. J. Miro, for their kindly providing endomyocardial biopsies, and S. Michaud for kindly providing information about histological grade of cardiac allograft rejection, thank Dr. B. Comte for fruitful discussion. Thanks also to A. Mateasik for custom-written procedures for data correction and Q. Wu for creation of database for data management. Acknowledgement extends to V. Bassien Capsa, F. Elzwiei, S. Aneba and all other colleagues in Dr. Chorvatova's laboratory for their friendship, assistance, and for making work in the laboratory so enjoyable.

In my courses of M.Sc program, I also received friendly help from my teachers, Dr. J. Noel, Dr. L. Parent, Dr. A. Calderone, Dr. J.M. Therrien, and Dr. J. Lambert. I have learned a lot of knowledge from them. Finally, the love, support, and patience of my wife, my daughter and the family are appreciated more than words can say.

Based on all the help I have received, not only academically but also for my time here in Montreal. Therefore, I apologize if I have missed anyone out, it was done without intentions.

1. INTRODUCTION

1.2. Oxidative metabolism in cardiomyocyte mitochondria

1.2.1. ATP generation for heart functional activities

Life critically depends on the heart functional activities. The most important function of the heart is to pump blood to supply the body with oxygen and substrates. The heart increases its output to adapt to constantly changing demand of blood and energy through three major mechanisms: (1) the force-frequency relationship [1], (2) the Frank-Starling mechanism [2], (3) and the sympathetic activation [3]. In order to support myocardial contractile activity to adapt the varying workload, the heart requires a continuous supply of energy, which tight coupling mechanisms are essential to maintain cellular pools of adenosine triphosphate (ATP), phosphocreatine (PCr) and nicotinamide adenine dinucleotide (NADH). An energy-releasing process is the hydrolysis of ATP to adenosine diphosphate (ADP), when the ATP converts to ADP, it is usually immediately recycled in the mitochondria where it is recharged and comes out again as ATP. Almost all (>95%) of ATP is produced in mitochondria, which take up ~30% of cellular volume and are located in close vicinity to the main sites of energy consumption, i.e., the myofilaments, the sarcoplasmic reticulum (SR) and t-tubules [4-7]. Approximately 60-70% of ATP generation contribute to myocardial contractile, and remaining 30-40% is primarily used for the SR Ca^{2+}-ATPase (SERCA) and other ion pumps [8, 9].

Cardiac contraction and relaxation are based on the process of excitation-contraction (EC) coupling [6, 10] which consumes vast amounts of energy (Fig. 1). Briefly, when a cardiomyocyte is depolarized during an action potential (AP), voltage-gated Na^+-channels are activated and the inward Na^+-current (I_{Na}) induces a rapid depolarization of the cell membrane, facilitating voltage-dependent opening of L-type Ca^{2+}-channels ($I_{Ca,L}$). The Ca^{2+} influx triggers the opening of the ryanodine receptor (RyR2 subtype), inducing the release

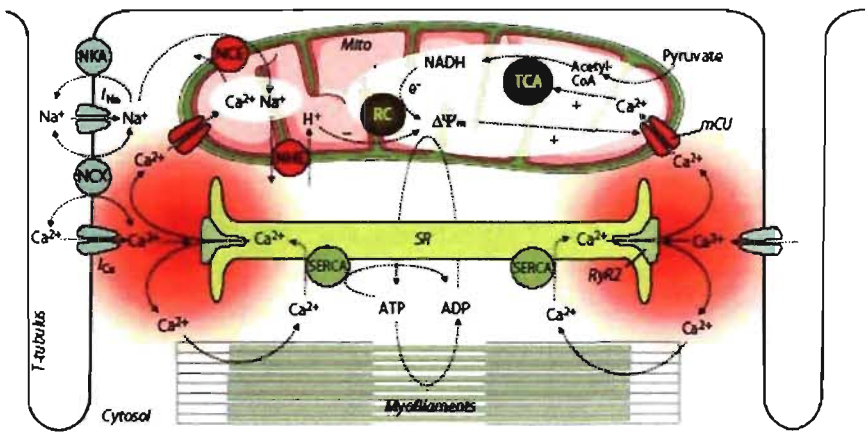

Figure 1: Processes of excitation-contraction coupling and mitochondrial energetics. SR, sarcoplasmic reticulum; SERCA, SR Ca^{2+} ATPase; Mito, mitochondria; TCA, tricarboxylic acid cycle; RC, respiratory chain; $\Delta\psi m$, mitochondrial membrane potential; NCE, mitochondrial Na^+/Ca^{2+}-exchanger; NHE, mitochondrial Na^+/H^+-exchanger; NKA, sarcolemmal Na^+/K^+-ATPase; NCX, sarcolemmal Na^+/Ca^{2+}-exchanger; RyR2, ryanodine receptor type 2; mCU, mitochondrial Ca^{2+}-uniporter; I_{Na} and I_{Ca}, currents of voltage-gated Na^+- or Ca^{2+}-channels, respectively. (Adapted from Maack, C. *et al.*)[5]

of even greater amounts of Ca^{2+} from the SR, a process termed Ca^{2+}-induced Ca^{2+}-release (CICR). The increasing cytosolic Ca^{2+} binds to the myofilaments such as troponin C, and induces the contraction of the cardiomyocyte. Binding of Ca^{2+} to the troponin C induces a conformational change of troponin C with exposes the binding site of the actin filaments for myosin head, that are able to bind to the myosin ATPase located on the myosin head. This binding results in ATP hydrolysis that supplies energy for a conformational change to occur in the actin-myosin cross bridge formation. The result of these changes is a movement ("ratcheting") between the myosin heads and the actin filaments, such that the actin and myosin filaments slide past each other thereby shortening the sarcomere length. Relaxation is initiated by the diffusion of Ca^{2+} from the myofilaments back to the cytosol, then Ca^{2+} actively being removed from cytosol. The main mechanisms removing Ca^{2+} from the cytosol are the SR Ca^{2+}-ATPase, the sarcolemmal Na^{+}/Ca^{2+}-exchanger and the plasmalemmal Ca^{2+}-ATPase (Fig. 1). The myosin ATPase of the contractile filaments, the SR Ca^{2+}-ATPase, and the plasmalemmal Na^{+}/K^{+}-ATPase are the main cellular energy consumers in the process of EC coupling [5]. The processes of excitation-contraction coupling and mitochondrial bioenergetics are highly interrelated, defects in EC coupling may directly translate into defects in mitochondrial bioenergetics in pathological situations, and may trigger altered supply of the respiratory chain with NADH.

1.1.2. Substrates for cardiomyocyte metabolism

In cardiomyocytes, to convert the potential energy in various metabolic substrates into ATP is the main function of mitochondria. These organelles are able to use a wide variety of circulating substrates, including fatty acids, glucose, lactate and ketone bodies. Under normal physiological conditions, fatty acids and glucose are main sources for intracellular ATP production, lactate and ketone bodies are used to a lesser extent [11, 12]. The heart utilizes these highly reduced metabolic substrates to produce energy from electrons by dehydrogenation reactions. However, electrons from the fuel molecules are not directly transported to the final electron acceptor oxygen; instead substrates are oxidized into reduced forms of NADH and flavin adenine dinucleotides ($FADH_2$) as electron carriers.

Each of these molecules contains two electrons, and will release energy upon oxidation. Metabolic substrates convey reducing equivalents (NADH and $FADH_2$) to the mitochondrial respiratory chain via three interconnected pathways, (1) the fatty acid β-oxidation pathway, (2) the citric acid cycle (Krebs' cycle), which is also known as tricarboxylic acid cycle (TCA cycle), (3) and to a lesser extent from the pyruvate dehydrogenase reaction and glycolysis (Fig. 2) [11]. Under physiological conditions, glucose is transformed to pyruvate, which enters mitochondria and is converted to acetyl-coenzyme A (CoA) by pyruvate dehydrogenase (PDH). Fatty acids are activated to fatty acyl-CoA in the cytosol and transported into mitochondria via the carnitine-acyltranslocase. Acetyl-CoA from both decarboxylation of pyruvate and fatty acid β-oxidation enters the citric acid cycle, resulting in the formation of NADH and $FADH_2$. In the well-perfused heart, □60-90% of the acetyl-CoA comes from β-oxidation of fatty acids, while 10-40% comes from the oxidation of pyruvate that is derived in approximately equal amounts glycolysis and lactate oxidation [11, 13, 14]. Acetyl-CoA metabolized through the citric acid cycle yields 3 NADH, 1 $FADH_2$, and 1 guanosine triphosphate (GTP) [15]. The reducing equivalents (NADH and $FADH_2$) that are either generated by the dehydrogenases of glycolysis, the oxidation of lactate, pyruvate and fatty acid β-oxidation, or the citric acid cycle, deliver electrons to the mitochondrial respiratory chain, resulting in ATP formation by oxidative phosphorylation.

The regulation of the Krebs' cycle is largely determined by substrate availability, product inhibition and competitive feedback inhibition mechanisms. Fuel enters the Krebs' cycle primarily as acetyl-CoA. The generation of acetyl-CoA from fatty acid β-oxidation and from pyruvate oxidation is, therefore, a major control-point of the Krebs' cycle. The rate of acetyl-CoA production in the heart is strictly coordinated with the rate of acetyl-CoA utilization by Krebs' cycle. The reaction of the PDH complex serves to interconnect the metabolic pathways of glycolysis, gluconeogenesis and fatty acid synthesis to the Krebs' cycle. The PDH activity is inhibited by NADH, acetyl-CoA and ATP, and activated by pyruvate, NAD^+, non-acetylated CoA (CoASH), ADP, Ca^{2+} and Mg^{2+} [16-20]. Regulation

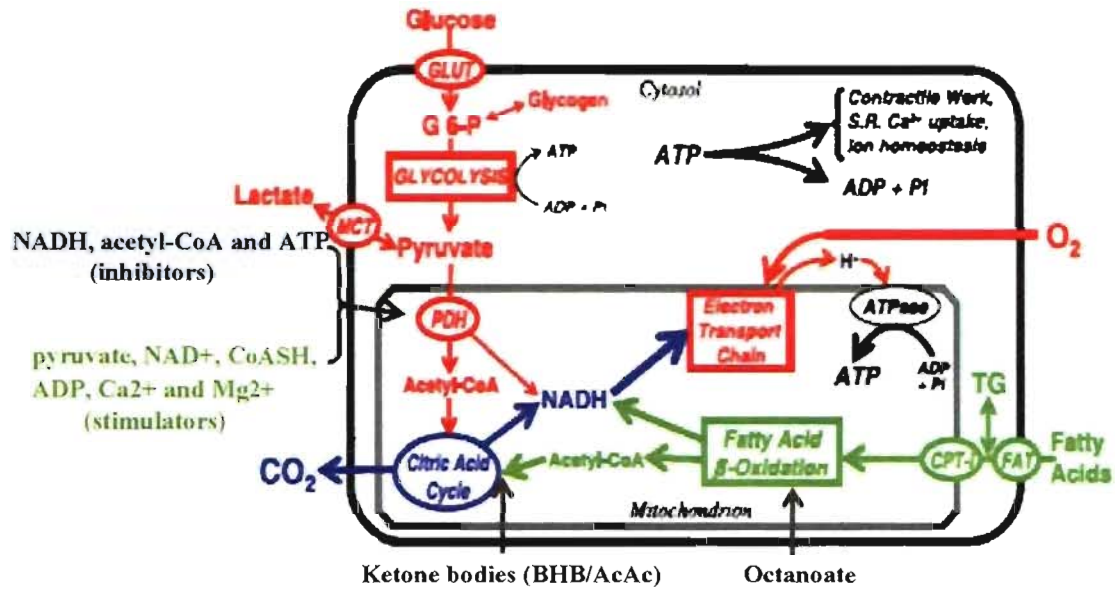

Figure 2: Pathways and regulatory points of myocardial substrate metabolism. The reducing equivalents are produced primarily in the fatty acid β-oxidation pathway, the citric acid cycle, and to a lesser extent from the pyruvate dehydrogenase reaction and glycolysis. CPT-I, carnitine palmitoyltransferase-I; FAT, fatty acid transporter/CD36; G 6-P, glucose 6-phosphate; GLUT, glucose transporters; MCT, monocarboxylic acid transporters; PDH, pyruvate dehydrogenase; SR, sarcoplasmic reticulum; CoASH, non-acetylated CoA; BHB, β-hydroxybutyric; AcAc, acetoacetic. (Adapted from Stanley, W. C. *et al.*)[11]

of the flux and activity of PDH are therefore determined by alteration of the $NADH/NAD^+$, acetyl-CoA/CoASH and ATP/ADP ratio. NADH and $FADH_2$ produced from the acetyl-CoA are strongly dependent on appropriate balance of fatty acids, carbohydrates and ketone bodies utilization. Pyruvate is one important metabolite. Under anaerobic conditions, pyruvate is fermented into lactate or alcohol to regenerate NAD^+. Under aerobic conditions pyruvate is converted into acetyl-CoA by pyruvate dehydrogenase. Zhou *et al.* [21] studied myocardial substrate metabolism and showed that an elevation in arterial lactate concentration greatly increased the cytosolic $NADH/NAD^+$ ratio but had a lesser effect on the mitochondrial $NADH/NAD^+$ ratio. On the other hand, stimulation of diabetic conditions reduced pyruvate oxidation and the cytosolic $NADH/NAD^+$ ratio but did not effect mitochondrial $NADH/NAD^+$ ratio. The ratio of $NADH/NAD^+$ in the mitochondria is comparatively stable. Octanoate is another crucial substrate. This medium chain fatty acid is not regulated by the carnitylpalmitoyl transport system in cardiomyocytes [22-24], but is completely oxidized through the mitochondrial β-oxidation and respiration pathways [25, 26]. It induces both, the NADH generation by the Krebs' cycle following dehydrogenation of octanoyl-CoA [27] and an uncoupling effect [28]. Ketone bodies consist of the molecules β-hydroxybutyrate (BHB), acetoacetate (AcAc) and acetone, which are produced from fatty acids, the heart extracts and oxidizes ketone bodies in a concentration-dependent manner. The concentration of ketone bodies in the arterial plasma is normally very low, and a minor contribution of substrates for the myocardial metabolism. However, during starvation or poorly controlled diabetes, plasma ketone body concentrations are elevated, and become a major substrate for the myocardial metabolism[11, 17]. BHB is oxidized into AcAc and NADH is produced dependently on the BHB/AcAc ratio [29]. Oxidation of glucose and lactate are inhibited by elevated plasma ketone bodies [17, 30], elevated rates of BHB and AcAC oxidation could inhibit fatty acids β-oxidation by increasing the intramitochondrial $NADH/NAD^+$ ratio [26, 31].

1.1.3. Structure and function of NAD(P)H molecule

Nicotinamide adenine dinucleotide phosphate (NADPH) and NADH (Fig. 3) are two of the most important coenzymes in the cardiac cell. Both molecules are synthesized from nicotinamide. NADH consists of two nucleotides joined by a pair of bridging phosphate groups, while NADPH is NADH with a third phosphate group attached to the hydroxyl group(-OH) on the position of 2' carbon in the ribose sugars. Because of the positive charge on the nitrogen atom in the nicotinamide ring (upper right), the oxidized forms of these redox reagents are often depicted as NAD^+ and $NADP^+$ respectively. The contribution of NADH and NADPH intrinsic fluorescence signal response to UV excitation are much less clearly identified in living cell [32] (see also Appendix I)[33] when both coenzymes are discussed, they are therefore referred to collectively as NAD(P)H. Each molecule of NAD^+ (or $NADP^+$) can acquire two electrons to be reduced (equation 1), however, only one proton accompanies the reduction. The other proton produced as two hydrogen atoms are removed from the molecule which being oxidized and is liberated into the surrounding medium. The reaction is thus:

$$NAD^+ + 2H + 2e^- \leftrightarrow NADH + H^+ \qquad (1)$$

Both coenzymes play crucial roles in most bioenergetic and biosynthetic processes as intracellular carriers of reducing equivalents and participants in both metabolic redox reaction, as well as in cell signaling [34-36]. NADH and NADPH are distinct in their biochemical roles: NADH is employed to generate proton motive force that can drive the synthesis of ATP. NADPH is not used for ATP synthesis but its electrons provide the energy for certain biosynthesis reactions. Furthermore, NADPH is an important co-factor for several enzymes, some involved in antioxidant processes put in place to counteract the generation of reactive oxygen species (ROS) by oxidative respiration and/or oxidative stress [37]. NADH is the predominant reduced pyridine nucleotide, and it has been found that, in isolated heart mitochondria, the concentration of NADH is greater than that of NADPH by a factor of ~ 10 [38-41]. The balance between the reduced and oxidized forms of NAD(P)H

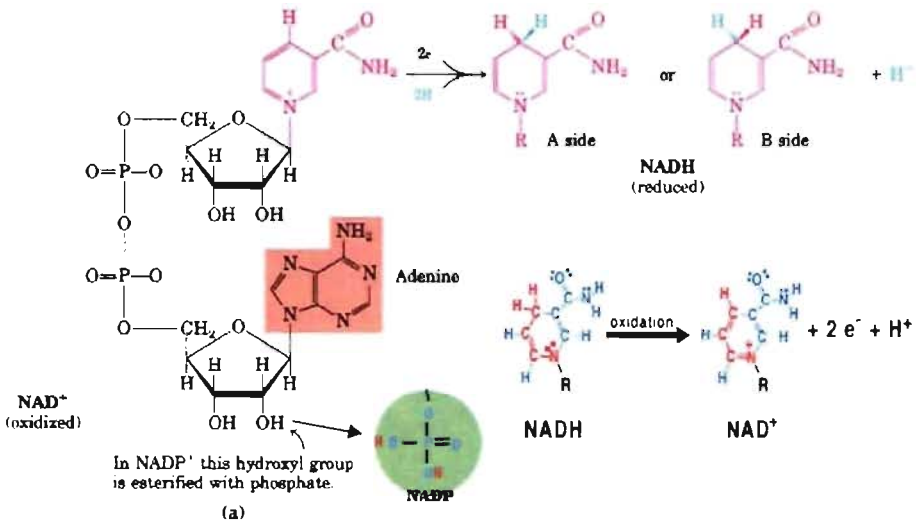

Figure 3: Structure of NAD(P)$^+$ and NAD(P)H molecules. Left, Oxidized form of NAD$^+$ (left), reduced form of NADH (upper right), NADPH is NADH with a third phosphate group attached at the bottom (lower left). Oxidation of NADH to NAD$^+$ removes two electrons and hydrogen atoms from NADH (right lower). (Adapted from Biochemistry) [15]

is called NAD(P)H/NAD(P)$^+$ ratio, which can be regarded as an indicator of cellular redox status. The NADP$^+$/NADPH ratio is ~ 200 times lower than the NAD$^+$/NADH ratio [42, 43], these different ratios reflect the different metabolic roles of NADH and NADPH.

1.1.4. Mitochondrial respiratory chain

As mentioned in previous section (1.1.2), energy sources such as glucose and fatty acids are initially metabolized in the cytoplasm, converted to acetyl-CoA in TCA cycle and the products of NADH and $FADH_2$ are then imported into mitochondria. Electrons from these donors are passed through a series of redox reactions protein complexes called the electron transport chain (ETC) [4, 7], located in the mitochondrial inner membrane, and are delivered to oxygen, forming water. By definition, O_2 consumption at the electron transport system is known as respiration; the protein complex that carry it out are known as the respiratory chain. Electrons from NADH and $FADH_2$ are transported via the respiratory chain as follows:

NADH → Complex I → Q → Complex III → cytochrome C → Complex IV → O_2

↑

Complex II

Complexes I, III and IV are proton pumps, while Q and cytochrome C are mobile electron carriers. Complex II is not a proton pump, it serves to funnel additional electrons into the quinone pool (Q) by removing electrons from succinate and transferring them (via $FADH_2$) to Q. The electron acceptor is molecular oxygen. The redox reactions catalyzed by Complex I and Complex III exist roughly at equilibrium. This means that these reactions are readily reversible, simply by increasing the concentration of the products relative to the concentration of the reactants (for example, by increasing the proton gradient). ATP synthase is also readily reversible. Thus ATP can be used to make a proton gradient, which in turn can be used to make NADH.

In cardiomyocytes, the primary electron source for the mitochondrial respiratory

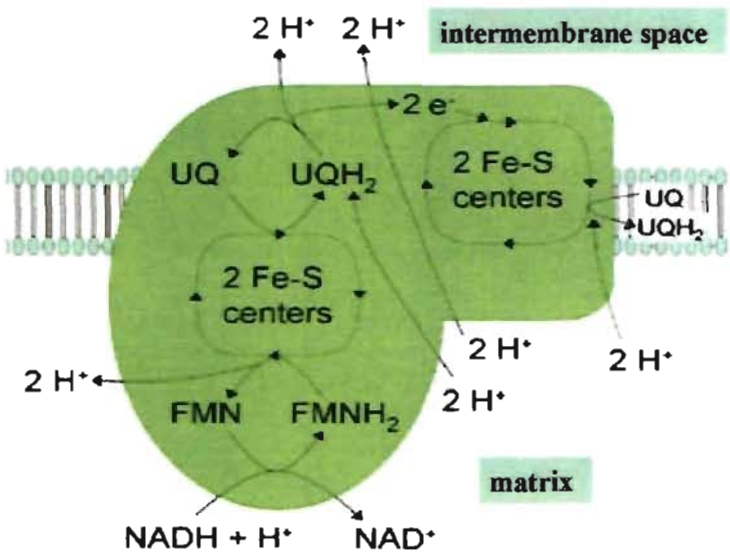

Figure 4: Complex I of the mitochondrial respiratory chain. Electrons and protons from NADH oxidation on their way from $FMNH_2$ to UQH_2 are translocated across the inner mitochondrial membrane, from the matrix to the intermembrane space in the Complex I of the mitochondrial respiratory chain. (Adapted from Biochemistry) [44]

chain is the NADH, which accounts for 95% of ATP generation via dehydrogenation of NADH to NAD^+ by Complex I of the mitochondrial respiratory chain [45, 46]. Binding of NADH to Complex I results in oxidation of NADH to NAD^+, electrons and hydrogen atoms are removed from NADH, reducing flavin mononucleotide (FMN) to $FMNH_2$ in one two-electron step (equations 2). The next electron carrier is a Fe-S cluster which can only accept one electron at a time to reduce the ferric ion into a ferrous ion. The electron then travels from the Fe-S cluster to the oxidized a coenzyme Q (UQ) to give the free-radical (semiquinone) form of UQH_2 (equation 4), eventually the electrons flow through all three on their way from $FMNH_2$ to UQH_2, involving the uptake of two protons as UQ is reduced to UQH_2 due to the transferring of 2 electrons from the aforementioned iron-sulphur cluster (Fig. 4). The equations of the reaction at Complex I as follows:

$$NADH + H^+ + FMN \Rightarrow NAD^+ + FMNH_2 \qquad (2)$$

$$FMNH_2 \Rightarrow FMN + 2e^- + 2H^+ \qquad (3)$$

$$UQ + 2e^- + 2H^+ \Rightarrow UQH_2 \qquad (4)$$

NADH feeds electrons into the respiratory chain at Complex I, and succinate enters via $FADH_2$ at Complex II (Figure 5). As the electrons are shuttled through the inner membrane to generate the flow of electrons (Δp) consisting of membrane potential ($\Delta\psi$) (negative inside), four protons (H^+) are concomitantly translocated from the matrix to the intermembrane space located between the inner and outer mitochondrial membranes, establishing a proton gradient (ΔpH) (alkaline inside), eventually constituting the proton motive force ($\Delta\mu H$). The electrons that travel down the respiratory chain by sequential redox reactions at complexes I–IV are eventually transferred to O_2 (Fig. 5), molecular oxygen is thereby reduced to water, and a large amount of stored energy is liberated for ATP synthesis when H^+ gradient reduced across the mitochondrial inner membrane[17]. Protons return down their gradient either via a proton leak (as is the case during uncoupling effect) or via the ATP synthase. At complex V(the F_1F_0-ATPase) of the respiratory chain, proton motive force provides the free energy for the generation of ATP from ADP via oxidative phosphorylation [11, 47].

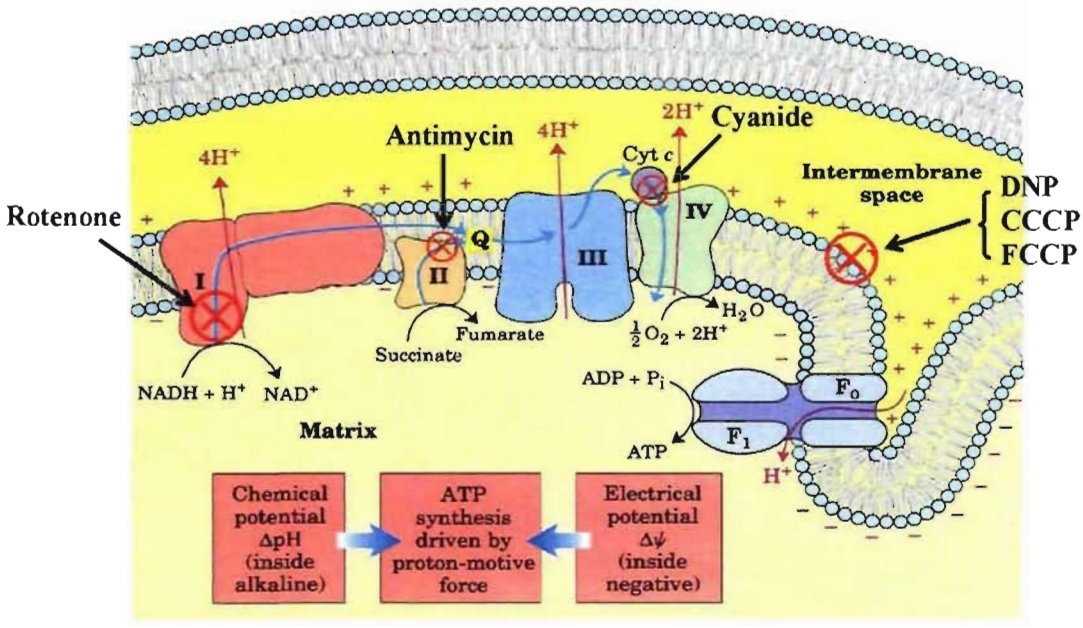

Figure 5: Mitochondrial respiratory chain and its inhibition points. Rotenone, inhibition of NADH-CoQ reductase at Complex I; Antimycin, inhibition of electron transfer from cytochrome b to cytochrome c1 at Complex III; Cyanide, inhibition of cytochrome oxidase at Complex IV; Dinitrophenol (DNP), Carbonyl cyanide *m*-chlorophenyl hydrazone (CCCP) and Carbonylcyanide-*p*-trifluoromethoxy phenyl hydrazone (FCCP), both are uncoupling agents, uncoupling oxidative phosphorylation by carrying protons across the mitochondrial membrane, leading to a rapid consumption of energy without generation of ATP, hence stimulating NADH dehydrogenation. (Adapted from Biochemistry) [15].

	Function	Site of action	Effects on oxidative phosphorylation
Rotenone	**Respiration inhibitor**	**NADH-CoQ reductase at Complex I**	**Inhibition of NADH oxidation. NADH becomes reduced; substrates such as succinate that enter via $FADH_2$ is still oxidized and make 2 ATPs/mol.**
Antimycin A	**Respiration inhibitor**	**electron transfer from cytochrome b to cytochrome c1 at Complex III**	**All intermediates before and in cluding cytochrome a will be in the reduced state; all intermediates after and including cytochrome c1 will be in the oxidized state. It therefore prevents the oxidation of both NADH and succinate.**
Cyanide	**Respiration inhibitor**	**Cytochrome oxidase at Complex IV.**	**Blocks transfer of electrons to O_2, prevents both coupled and uncoupled respiration with all substrates, including NADH and succinate.**
FCCP (CCCP)	**Uncoupling agent**	**transmembrane H^+ carrier at complex IV**	**Disrupt the proton gradient by carrying protons across the membrane. This uncouples proton pumping from ATP synthesis.**
Dinitrophenol (DNP)	**Uncoupling agent**	**transmembrane H^+ carrier at complex IV**	**It uncouples oxidative phosphorylation by carrying protons across the mitochondrial membrane, leading to a rapid consumption of energy without generation of ATP.**
Oligomycin	**Phosphorylation inhibitor**	**ADP phosphorylation at complex V**	**Inhibition of ADP phosphorylation. Does not inhibit uncoupled oxidations.**

Table 1: Inhibitors of oxidative phosphorylation

The described pathway of electron flow through the ETC, together with the unique properties of the proton motive force, have been determined using a number of drugs and toxins, which inhibit oxidative phosphorylation (Fig. 5 and Table 1) [48-51]. Some of these agents are inhibitors of electron transport at specific sites in the ETC, while others stimulate electron transport by discharging the proton gradient. For example, Rotenone inhibits the transfer of electrons from Fe-S cluster to UQ at the Complex I. The oxidation of substrates that generate NADH pathway is, therefore, blocked. However, substrates that are oxidized to generate $FADH_2$ (such as succinate or α-glycerol phosphate) can still be oxidized and generate ATP. Furthermore, cyanide inhibit cytochrome oxidase at Complx IV, blocks both site of NADH and $FADH_2$ oxidation [49]. On the other hand, 2,4-Dinitrophenol (DNP), an uncoupling agent, which can deplete the proton gradient and collapse the proton motive force leading to less efficient ATP synthesis, thus stimulating NADH dehydrogenation by drive oxidative phosphorylation [50].

1.1.5. Oxidative phosphorylation and ATP synthesis

Oxidative phosphorylation is defined as complex and multi-step processes in which ATP is produced by an electron transport chain, using oxygen as the final electron acceptor (Fig. 5). As mentioned in section 1.1.4., cardiomyocyte mitochondria produce an electrical chemical gradient by accumulating hydrogen ions in the intermembrane space. This generates an electrochemical gradient, composed of membrane electrical potential and pH difference across the mitochondrial inner membrane, while creating a proton motive force, which will be used by the F_1F_0-ATPase complex to make ATP via oxidative phosphorylation. The ETC and oxidative phosphorylation are coupled by a proton gradient across the inner mitochondrial membrane, as Dr. Peter D. Mitchell (Nobel Prize in Chemistry winner, 1978) described in his chemiosmotic coupling hypothesis [52-54].

The F_1F_0-ATPase located in the inner mitochondrial membrane uses the free energy charge provided by proton motive force to synthesize ATP from ADP and inorganic phosphate (P_i) in the matrix space. The F_0 component of ATP synthase acts as an ion

Step	coenzyme yield	ATP yield	Source of ATP
Glycolysis preparatory phase		-2	Phosphorylation of glucose and fructose 6-phosphate uses two ATP from the cytoplasm.
Glycolysis pay-off phase		4	Substrate-level phosphorylation
	2 NADH	4 (6)	Oxidative phosphorylation. Only 2 ATP per NADH since the coenzyme must feed into the electron transport chain from the cytoplasm rather than the mitochondrial matrix. If the malate shuttle is used to move NADH into the mitochondria this might count as 3 ATP per NADH.
Oxidative decarboxylation	2 NADH	6	Oxidative phosphorylation
Krebs cycle		2	Substrate-level phosphorylation
	6 NADH	18	Oxidative phosphorylation
	2 $FADH_2$	4	Oxidative phosphorylation
Total yield		36 (38) ATP	From the complete oxidation of one glucose molecule to carbon dioxide and oxidation of all the reduced coenzymes.

Table 2: Theoretical yields of ATP from fully oxidized glucose molecule

channel for return of protons back to mitochondrial matrix. As their return, the free energy produced during the generation of the oxidized forms of NAD^+ and FAD is released. This energy is used to drive ATP synthesis, catalyzed by the F_1 component of the complex [55]. The P_i for phosphorylation is imported into the mitochondria by the phosphate translocator, and ATP is subsequently exported to the cytosol in exchange for ADP by the adenine nucleotide translocator. ATP synthase catalyses the following reaction:

$$ADP^{3-} + H^+ + P_i \leftrightarrow ATP^{4-} + H_2O \qquad (5)$$

Components of this remarkable enzyme rotate as a part of its catalytic mechanism. It acts as revolving doors, resembling a molecular water wheel that harnesses the flow of hydrogen ions in order to build ATP molecules [56]. Each NADH molecule contributes to proton motive force to generate 2.5-3.0 ATP, while each $FADH_2$ molecule is worth 1.5-2.0 ATP. Alltogether, when glucose is completely oxidized to CO_2 and H_2O during cellular respiration, produced 10 NADH and 2 $FADH_2$ molecules theoretical yield of 36-38 ATP molecules (Table 2). However, such conditions are generally not achieved due to losses such as proton leakage across the membrane, cost of ATP for moving pyruvate, phosphate, and/or ADP into the mitochondria, resulting in reduced efficiency of the whole process with the maximum yields closer to 28-30 ATP molecules [15, 57].

1.1.6. Control of mitochondrial respiration and ATP synthesis

Control of mitochondrial respiration and ATP synthesis allows the cell to adjust its energy metabolism to demands of cellular ATP-utilizing reactions that can fluctuate rapidly. Such demands include not only ATP production, but also various biosynthetic activities of mitochondria, regulation of cellular calcium levels, etc. The demand for ATP by various tissues is dependent on the specific task of each organ. Nevertheless, the stimulation of mitochondrial function is common in all tissues in the body. The heart can almost instantaneously modulate its rate of ATP production and oxygen consumption over at least a 5-fold range in response to different workloads with only relatively minor changes in the concentration of the various intermediates involved in the oxidative pathway [17, 58]. Control mechanisms responsible for matching energy supply with high energetic demands

remain controversial. There are no simple answers to question: "what controls the process of oxidative phosphorylation?" For decades biochemists have investigated enzymes with the view to determine binding constants for substrates, products and inhibitors, turnover rates, feed-back control, allosteric mechanisms and the relevant ligands, regulation of activity by protein modifications, etc. Ideas such as rate-limiting enzymes[4] evolved, for example, from assumption that NADH and O_2 are present in abundance, through high levels of NADH in mitochondria are present in limiting amounts, to its activity being subject to feed-back mechanisms. Feedback inhibition of PDH and α-ketoglutarate dehydrogenase activity can shut down the Krebs' cycle, thus reducing NADH production.

The cellular regulation of oxidative phosphorylation is a very complex process control network, with numerous potential rate-limiting steps affected by a variety of signaling molecules, including ADP, P_i, PCr, Ca^{2+} and Mg^{2+} [59-63]. Many studies observed that the level of energy-rich adenine intermediates can be remarkably constant as the metabolic rate changes [58, 59, 64]. Several hypotheses have been put forward to explain the control of oxidative phosphorylation. The classical respiratory control hypothesis of Chance and Williams [65] implies that the rate of respiration is regulated by the availability of ADP to the F_1F_0-ATPase. The study has shown that the activation of mitochondria by increased ADP is coupled with oxidation of NADH, resulting in decreased NADH levels in isolated mitochondria. Bose *et al.*[63] have shown that oxidative phosphorylation is activated by P_i at three levels: (1) the generation of NADH, (2) the distribution of free energy throughout the cytochrome chain, (3) and as a substrate for ADP phosphorylation at the F_1F_0-ATPase. As a result, P_i is capable of increasing the ATP generation. However, a series of experiments in isolated rat hearts or instrumented dogs by Katz *et al.* [66 67] have shown enhanced cardiac workload that increased oxygen consumption, but without change in ADP, ATP, P_i or PCr. They concluded that respiration is regulated up-stream by the availability of electrons to the respiratory chain, i.e., the redox state of $NADH/NAD^+$, rather than ADP.

Consequently, mitochondrial respiration and ATP synthesis are controlled by the mitochondrial $NADH/NAD^+$ ratio, the phosphorylation potential, and the effectors of

cytochrome oxidase, such as pH or oxygen. ADP or P_i –dependent, as well as Ca^{2+}-dependent regulatory mechanisms are activation in parallel, adjusting ATP production from resting conditions to increased cardiac workload [5, 21, 58, 60, 63, 64, 68, 69]. Such parallel activation of the respiratory chain and mitochondrial dehydrogenases by either Ca^{2+} or P_i, together with very rapid response in the NADH production and oxidation process virtually eliminate transients in metabolite levels during changes in work [63, 69]. ADP and Ca^{2+} are two principal regulatory factors. Since NADH production is activated by Ca^{2+} stimulation of the Krebs' cycle dehydrogenases (PDH, isocitrate- and α-ketoglutarate dehydrogenase), Ca^{2+} also activates the F1Fo-ATPase [70, 71]. Changes in ATP/ADP in the cytoplasmic and mitochondrial compartments mediate rapid changes in the mitochondrial NADH/NAD^+ ratio to regulate oxidative phosphorylation, primarily reflecting the effects of Ca^{2+} on the rate of NADH production by Krebs' cycle. As a result Ca^{2+} rather than ADP regulate cellular respiration and ATP production. But any mechanism that increases the rate of NADH oxidation concomitantly activation of NADH production.

1.1.7. Change in respiration and oxidative metabolism in pathophysiological conditions

It is well known that cardiac mitochondrial dysfunction following mitochondrial respiration and/or oxidative metabolism disorder is involved in many pathophysiological conditions, such as ischemia, hypoxia, stroke, hypertension, diabetes, cardiomyopathy, heart failure, and in the myocardial apoptotic process [4, 7, 11, 13, 31, 34, 36, 37, 72]. Ischemia is described as an inadequate flow of blood and oxygen delivery to an organ, caused by constriction or blockage of the blood vessels supplying it. Insufficient blood supply causes tissue to become hypoxic, or anoxic (if no oxygen is supplied at all). This can cause tissue necrosis (i.e. cell death). In very aerobic tissues such as heart, over 90% of ATP formation comes from oxidative phosphorylation, with remaining 10% being derived from glycolysis and GTP formation in normoxic conditions [11]. Hypoxia or ischemia are induced following reduction in coronary blood flow, and result in a series of detrimental biochemical reactions

in cardiac cells. After seconds to minutes of ischemia, lack of oxygen delivery to the respiratory chain blocks the Krebs' cycle. As aerobic ATP formation from oxidative phosphorylation are insufficient to support the energy demand for heart functional activities, the cell immediately switches to anaerobic metabolism, with the production of anaerobic ATP and lactic acid by glycolysis, to maintain ATP levels. This leads to a lesser use of NADH by oxidative phosphorylation, hence accumulation of cytoplasmic NADH, and is accompanied by accumulation of lactate and H^+ in the cell [72-74].

Cell functions are greatly disrupted by the decrease in pH and ATP. ATP-linked ion transport pumps fail, causing the cell depolarization, poor ion homeostasis, and Ca^{2+} accumulation in the cell. Resulting excess of calcium entry overexcites cells and leads to generation of harmful chemicals, such as free radicals, reactive oxygen species (ROS) and stimulation of calcium-dependent enzyme, resulting in mitochondrial damage, myocardial apoptosis and necrosis [13, 72]. Many researchers have identified Complex I as a major site of damage to the respiratory chain in ischemia [75, 76]. They observed a reduction in oxidation rate for NADH-linked substrates by up to 60%, however, oxidation rates with succinate were unchanged, suggesting that damage was restricted to Complex I. Simultaneously, NADPH is involved in antioxidant process put in place to counteract the generation of ROS by oxidative respiration and/or oxidative stress [37].

Paradoxically, however, the major damage to ischemic cells comes from the re-introduction of oxygen (reperfusion). During reperfusion, the cells typically undergo further contraction (hypercontracture) and membrane damage, followed by cell death [77, 78]. It is widely acknowledged that ischemia and reperfusion lead to mitochondrial, as well as cellular damage in cardiac cells [79-81]. Because of the high oxidative metabolism, cardiac cells have a high oxidative capacity, demonstrated by their ultrastructure: 25–35% of total cardiomyocyte volume is occupied by mitochondria [82]. Cardiomyocyte apoptosis has been identified as an early event during ischemia-reperfusion injury [83 84]. NADH fluorescence has long been considered as a tool to study cardiac ischemia [46, 85] and NADH changes were proposed to play a crucial role in ischemia/reperfusion injury [86]. The production of ROS,

such as superoxide, by Complex I of mitochondrial respiratory chain is a major cause of cellular oxidative stress and contribute to ischemia reperfusion injury [87-92]. The $NADH/NAD^+$ ratio determine the rate of superoxide formation [87, 90, 91].

Based on what we know, the changes in mitochondrial respiration and oxidative metabolic state can also contribute to deterioration of the heart in specific cardiac pathologies, including the process of rejection of transplanted hearts. The allograft rejection is the most important cause of death of heart transplanted patients. Search for new diagnostic tools is therefore crucial to insure its early detection and hence efficient prevention. Rejection of heart transplantation includes hyperacute rejection, acute rejection and chronic rejection. The risk of rejection, highest in the first three post-operative months, decreases six month following transplantation mainly thanks to routine rejection surveillance and adequacy of immunosuppressive therapy. Acute rejection is defined as lymphatic inflammatory infiltration with associated damage and/or necrosis of cardiac cells [93]. Alteration of coronary vascular regulation during acute rejection may induce graft dysfunction and promote the occurrence of coronary atherosclerosis in transplant recipients [94]. Moreover, ischemia-reperfusion injury was also proposed to be an important alloantigen-independent factor [95] observed during cardiac rejection and leading to hypoxia of cardiomyocytes. After six months of transplantation, the main problems of the heart transplant recipients includes acute allograft rejection, cardiac allograft vasculopathy and infections, which can occur at anytime in several years after the operation [93, 96]. In these conditions, the coronary arteries develop progressive and diffuse focal (scattered and spread out) narrowing throughout their entire length. Such type of narrowing is different from the fatty or calcified plaque that typically causes atherosclerotic coronary artery disease, but can, as well, result in nutrient and oxygen deprivation of the heart and lead to the failure of normal function of cardiac cells. For these reasons, in the presence of rejection, cardiac cells can be in a state of hypoxia or ischemia, and cell death with impaired mitochondrial respiration and oxidative metabolic state.

1.2. NAD(P)H fluorescence in cardiomyocyte

1.2.1. Physics of fluorescence

In physics, fluorescence is an optical phenomenon describing the fact that absorption of a photon by certain molecules triggers the emission of another photon with a longer wavelength (λ). Such molecule is called fluorophore. The energy difference between the absorbed and emitted photons ends up as molecular vibrations or heat. As the emitted photon has always less energy than the excited one ($E_{em} < E_{ex}$), in regard to the equation 6, the emitted wavelength is always longer than the excited wavelength ($\lambda_{em} > \lambda_{ex}$). Usually, when the absorbed photon is in the ultraviolet (UV) range, the emitted light is in the visible range. Fluorescence occurs when a fluorophore molecule relaxes to its ground state (S_0) after being electronically excited (equation 7). When a fluorophore molecule absorbs a photon, it goes into its first excited state (S_1') from electronic ground state (S_0) (process 1 at Fig. 6), vibrational energy is lost thermally after excitation within picoseconds and the molecule drop to the ground vibrational state (S_1) of the excited electronic state, the molecule then returns back to the level of S_0 (equation 8) accompanied by the emission of the photon (process 3 at Fig. 6) and by converting the absorbed energy internally (process 2 at Fig. 6), or by transferring the energy to the environment after a short period of the order of nanoseconds (ns) (Fig. 6) [97]. The process of fluorescence can be described following equations:

Photon energy: $E = h\nu = h\frac{c}{\lambda}$ (6)

Excitation: $S_0 + h\nu \rightarrow S_1'$ (7)

Emission: $S_1 \rightarrow S_0 + h\nu$ (8)

where $h\nu$ is a generic term for photon energy where: h = Planck's constant and $\nu = \frac{c}{\lambda}$, is frequency of light, **c** is speed of light. State S_0 is called the ground state of the fluorophore and S_1' is an excited vitrarational state of the first (electronically) excited state (Fig. 6).

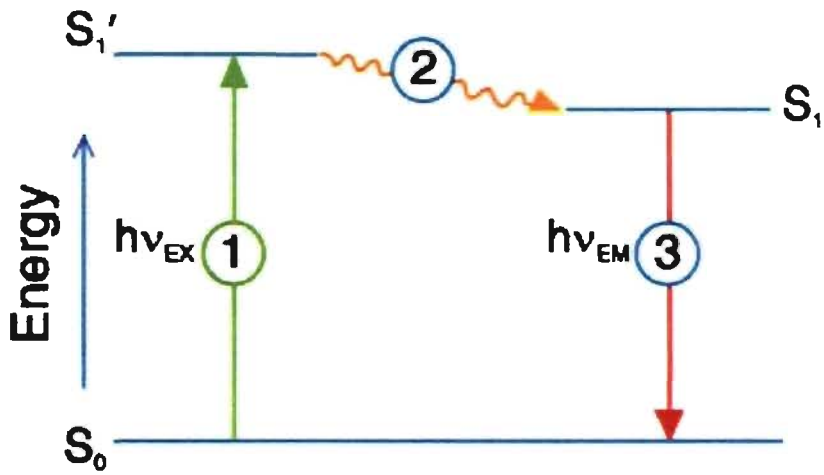

Figure 6: General scheme of the fluorescence process. Fluorophore absorbs a photon, which goes into an excited state (S_1) from a ground state (S_0) (process 1). It can then return to the ground state either by the emission of the photon (process 3), by internal conversion (process 2), or by transferring the energy to the environment. $h\nu_{EX}$, energy of the absorbed photon; $h\nu_{EM}$, energy of the emitted photon. (Adapted from Subcellular Biochemistry) [97]

When an ensemble of fluorophores are excited by a pulsed laser, their fluorescence returns to S_0 state with a characteristic kinetics that can be defined as an exponential decay (equation 9) and described by parameter of fluorescence lifetime, which therefore reflect the characteristic time that molecules spend in the excited state before emission of photon, which is specific for different molecular conformations.

Fluorescence typically follows first-order kinetics as:

$$[S_1] = [S_1]_0 e^{-\tau t} \qquad (9)$$

where $[S_1]$ is the concentration of excited molecules at time t, $[S_1]_0$ is the initial concentration and "τ" is the decay rate or the inverse of the fluorescence lifetime.

1.2.2. Endogenous fluorescence of living cells

Endogenous fluorescence means that the cells contain intrinsic fluorescent molecules, namely reduced NAD(P)H and/or oxidized flavins, which naturally emit fluorescence when excited by UV, or visible light. This intrinsic property of the cells is also called autofluorescence (AF) to be distinguished from fluorescent signals obtained by adding exogenous probe. Bulk of endogenous fluorescence emitted after excitation with UV or visible light in living cardiomyocytes originates from NAD(P)H and/or flavins, about 80% of AF measured after UV light excitation that originates from NADH [98-103]. Fluorescence spectroscopy has been proven to be a powerful tool with high sensitivity to study the distribution and function of biological endogenous fluorophores. Changes occurring in the cells and tissues during physiological and/or pathological processes result in modifications of the mitochondrial state, in combination with the amount and distribution of endogenous fluorophores and chemico-physical properties of their microenvironment. Therefore, analytical techniques based on AF monitoring can be applied in order to obtain information about physiological metabolic state of cells and tissues. Moreover, AF analysis can be performed in real-time because it does not require any treatment, fixing or staining of the specimens. As a results, in the past few years, numerous spectroscopic and imaging

techniques have been developed for different applications in both basic research and diagnostics [104].

AF is not only characterized by emission spectrum, but also by characteristic lifetime, as discussed in the previous section 1.2.1 and equation 9. Fluorescent lifetime is particularly useful to distinguish fluorescence components of endogenous fluorophore mixture in cells, or to monitor changes of the same fluorophore in different environments. Indeed, distinct fluorescence components have often poorly distinguishable spectra but clearly distinguishable lifetimes [105] [106]. Besides, natural fluorophores have often several decay components in different molecular states and variable local environments may therefore change the lifetime of these states in a specific way. As a result, there can be several fluorophore components in the same part of a cell, a single component being quenched with non-uniform efficiency, or there can be quenched and unquenched molecules in the same part of the cell [107]. Thus, in multi-compartment, complex systems (such as cells) the observed fluorescence is often described by multi-exponential decays, even if in *in vitro* conditions, the studied molecule is expected to have single-exponential characteristics. As a result, time-resolved fluorescence spectra give unique precise insight into the real behavior of fluorescing molecules. Moreover, the fluorescence lifetimes can also be a direct indicator of the energy transfer rate from the excited molecules to the local environment or to other fluorophores. An efficient energy transfer process is Förster resonant energy transfer (FRET). FRET occurs if two different fluorophores are present with the emission band of one fluorophore overlapping the absorption band of the other; the donor fluorophore is able to transfer its excited-state energy to the acceptor fluorophore[108-112]. When the energy is transferred, the actual fluorescence lifetime is less than in the natural state. Taking in consideration that in cell, endogenous fluorescence reflects their metabolic states, multi-parametric AF assays could, therefore, provide rapid and non-invasive measurement of the metabolic state directly in living cells.

1.2.3. Spectral characteristics of NAD(P)H fluorescence

Since the discovery of optical properties of NADH early in the 1950s [65, 113, 114], a lot of research has been carried out in organs, such as the liver, heart, brain, and kidneys, from animal models to human studies [115]. The pioneering work of Chance and collaborators [65, 113] led to development and establishment of unique measurement technology and theoretical conceptualization of mitochondrial function based on NADH redox state monitoring *in vitro* as well as *in vivo*. Endogenous fluorescence of NADH, induced following excitation with the UV light, has long been used for non-invasive fluorescent probing of oxidative phosphorylation changes [46] and has been an extremely useful tool for monitoring of energy metabolism in heart [116]. The absorption and fluorescence spectra of NAD(P)H have been well characterized at different levels of organization, namely, in solutions [117, 118], in the mitochondria [65, 116, 119], in the cell suspensions [38], in the surface of intact blood perfused myocardium [103, 120,40], and in the organs *in vitro* and *in vivo* [41, 117, 119, 121-124]. According to these results, the spectra of this molecule in most tissues are considered the same, although there are some small changes in the shape and maxima of the spectra in different environments and measurement conditions [125]. In the heart, the intrinsic NAD(P)H fluorophore absorbs UV light at 320-380nm and emits a broad-band blue fluorescence at 420-480nm range. Spectra analysis showed that there is a ~ 20nm blue-shift for the protein-bound coenzyme (400-460nm) in cells [38, 103, 119]. AF intensity is proportional to the concentration of mitochondrial NAD(P)H; an increase in the fluorescence intensity indicates a more reduced state of NAD(P)H and of the rest of the mitochondrial ETC [115]. After donation of electrons to the ETC, the oxidized $NAD(P)^+$molecule does not absorb or emit significant fluorescence at these wavelengths range.

In living cardiac cells, the fluorescence signals from cytosolic and mitochondrial NAD(P)H can not be distinguished. However, previous biochemical studies have estimated that the blue fluorescence observed in the heart originates predominantly from NAD(P)H in mitochondria, but with a negligible contribution of cytoplasm [38, 41, 120]. NADH is expected

to have as much as a four-fold greater fluorescence yield than NADPH in isolated heart mitochondria, at least 80% of the AF is essentially considered from NADH alone [38, 39, 116, 126-128]. Besides, the fluorescence profile of NADPH is practically indistinguishable from that of NADH [32, 33]. As there is no photophysical means to discriminate NADH from NADPH in living cells, we defined AF measured following UV excitation as that of NAD(P)H, a combined effect of both nucleotides.

Estimation of NAD(P)H concentration and their redox ratio in the tissues, whole cells and/or its subcellular compartments is rather complicated, depending on the species, tissue (brain, heart, liver etc.), enzymatic pathways involved, calculation chosen, as well as patho-physiological. Condition in rat liver, the total amount of NADH is approximately 1μmol per gram of wet weight, about 10 times the concentration of NADPH in the same cells [129]. The actual concentration of NADH in cell cytosol is harder to measure, with recent estimates in animal cells of about 0.3mmol/L [130, 131]. Over 80% of NADH corresponds to molecules bound to proteins, the concentration of free NADH in cell therefore is much lower [132]. Data for other compartments in the cells are limited: one study showed that in the mitochondrion, the concentration of NADH is similar to that in the cytosol [130]. Since the NADH cannot diffuse across membranes, it is carried into the mitochondrion by a specific membrane transport protein[133]. Other study identified NADH concentration ranging from 1-100μmol/L in mitochondria isolated from rat liver [126]. A measurement of NADH/NAD^+ ratio that reflects both the metabolic activities and the pathophysiological state of cells [134]. The effects of the NADH/NAD^+ ratio are complex, controling the activity of several key enzymes, including glyceraldehyde 3-phosphate dehydrogenase and pyruvate dehydrogenase [43]. In healthy mammalian tissues, estimates of the NAD^+/NADH ratio range from 0.05 (rat heart) to 4 (mice liver) [43, 134, 135]. In contrast, the $NADP^+$/NADPH ratio is normally about 0.005, around 200 times lower than the NAD^+/NADH ratio, indicating that NADPH is the dominant form of this coenzyme in cells [42, 134].

Endogenous flavins are also significant contributor to cellular AF [99, 102], which emits AF at maximum 520nm, but after excitation with visible light (450-488nm). FAD is almost

exclusively bound, as FAD-dependent dehydrogenase enzymes use a system of molecules (electron transport flavoprotein (ETF) and ETF dehydrogenase) to transport hydrogen atoms to Complex II of the respiratory chain. Flavins are involved in oxidation-reduction reactions with NAD(P)H. Both reduced NADH and oxidized FAD are significantly fluorescent molecules in cardiomyocyte mitochondria and these two signals respond oppositely to changes in mitochondrial metabolic state. The redox state of its FAD cofactor is in direct equilibrium with the mitochondrial NADH/NAD^+ pool, as indicated by the simplified reaction mechanism below:

$$\text{LipDH } (FADH_2) + NAD^+ \leftrightarrow \text{LipDH (FAD)} + NADH + H^+ \qquad (10)$$

1.2.4. NAD(P)H fluorescence lifetime pools in mitochondria

In heart tissue, a substantial fraction of the cellular NAD(P)H/$NAD(P)^+$ pool (about 75% in cardiomyocytes) is compartmentalized within the mitochondria [136,36]. Mitochondrial NADH levels and NADH/NAD^+ ratio were described to be much higher than NADPH ones and, therefore, the fluorescence signal in cells is considered to be essentially resulting from mitochondrial NADH [38, 39, 116, 126-128]. The NAD(P)H/$NAD(P)^+$ ratio reflects the balance between oxidative and reductive processes within the mitochondria: oxidation of NAD(P)H is leading to reduced mitochondrial NAD(P)H/$NAD(P)^+$ ratio. The total NAD(P)H pool in the matrix is constant due to its compartmentation in the matrix. Physiological perturbations are usually due to changes in the NAD(P)H/$NAD(P)^+$ ratio rather than changes in the total concentration of either [NAD(P)H] or [$NAD(P)^+$].

The blue AF is dependent on the mitochondrial redox state, on the conformation of molecule, and on the environment of the coenzyme [40]. Fluorescence lifetime is specific for different molecular conformations and is also sensitive to interactions of the fluorescing molecule with its surroundings. It can therefore be used as a sensitive probe to detect NAD(P)H binding. NAD(P)H binds to protein cofactors resulting in enhancement of fluorescence decay time and/or alteration of the maximal emission wavelength [40, 132]. Furthermore, NAD(P)H fluorescence lifetime was shown to be strongly dependent on the microenvironment [45, 103, 127], spanning from 0.3-0.5 ns in distilled water to 3-8 ns in viscous

and non-polar solutions [137]. The pronounced dependence of NAD(P)H fluorescence on microenvironment leads to multi-exponential fluorescence decay kinetics in most solvents, due to the effect of dynamic quenching related to the formation of non-fluorescent transient species from the first excited state [137, 138]. In addition, NAD(P)H forms complexes with several enzymes, which makes the interpretation of the NAD(P)H signals from intact tissues particularly difficult in living cells. Thus, any change in molecular conformation, binding to surrounding molecules and/or change of chemical compartments results in modification of lifetimes of the observed multi-component fluorescence decays.

Previous studies confirmed the existence of different pools of NADH in the mitochondrial matrix, which are distinguished by based on their characteristic fluorescence lifetimes [126, 132, 139]. To evaluate the contribution of different compartments to the overall cellular NAD(P)H fluorescence signals, a number of methodologies have been used, including spectra analysis [38, 140, 45, 128], microimaging [38, 141, 142], and fluorescence lifetime measurement [126, 139]. Out of all of these methods, the fluorescence lifetime provides the best quantitative measurement to distinguish between different NAD(P)H fluorescence pools. The steady-state kinetics of NADH fluorescence study by Blinova *et al.*[132] identified three pools of NADH fluorescence in isolated porcine heart intact mitochondria: a pool with a short lifetime of 0.4 ns, this component was consistent with free NADH, the intermediate (1.8 ns) and a long (5.7 ns) lifetime pools have a blue-shifted emission spectra, proposed to result from protein binding of NADH. The intermediate and long lifetime pools make up □ 35% of the total NADH contributing to almost 80% of the fluorescence emission. The steady-state kinetics for the NADH interaction with these sites results in an essentially linear relationship between NADH fluorescence and matrix [NADH]. The relative size of these pools also suggested that the majority of the steady-state fluorescence collected is dominated by the immobilized pool, due to the bound form of NADH, which contributes to major fluorescence emission [139]. As a general approach, most authors used 2- to 4-exponential decay models to describe the NADH fluorescence kinetics in mitochondria or in cells, ascribing different lifetime pools to bound forms of NADH in subcellular

compartments. Vishwasrao used a 4-exponential decay model to question the rotational mobility of free vs. bound NADH populations in neuronal tissues [40], two short lifetime pool have been referred to free form of NADH, other two pools have been used to describe bound forms of NADH.

1.2.5. Latest experimental approaches for monitoring cellular autofluorescence

Recently, promising new fluorescence techniques have been implemented in combination with light microscopy for biological research, such as spectrally-resolved and time-resolved fluorescence microscopy with either single-photon or two-photon excitation [99, 143, 144]. while spectrally-resolved confocal microscopy is used together fluorescence spectra images [99], time–resolved microscopy is also capable of identifying fluorescence lifetimes [143-145]. The advantages of two-photon microscopy are deep and continuous imaging of live cells for several minutes with no effect on cell viability or function.

The advanced time-correlated single photon counting (TCSPC) is used to study fluorescence lifetime characteristics [146]. This technique is based on the detection of single photons of a periodical light signal. The measurement of the detection times of the individual photons allows reconstruction of the waveform from the individual time measurements [147]. The spectrally-resolved fluorescence lifetime detection technique was already achieved on the basis of multi-dimensional TCSPC, with either single-photon or two-photon excitation [106, 107, 148]. This approach allows fast and reproducible measurement of complex patterns of spectrally and time-resolved fluorescence decay directly in living cardiac cells. It provides a promising tool with necessary sensitivity to detect the low-intensity intrinsic fluorescence signals, as well as the temporal and spectral resolution that can lead to identification of the individual fluorescence components in living cardiac cells. This technique, in combination of 2-photon confocal microscopy, allows spectral and fluorescence lifetimes to be resolved [106, 108, 148]. However, this approach requires high fluorescent yield from studied fluorophores. Classic TCSPC has been recently improved to multi-detector TCSPC [106]. This more advanced technology is an expansion of classic TCSPC for operation with several detectors. The photons of all detectors are combined into

a common timing pulse line. Simultaneously, a detector number signal is generated that indicates in which of the detectors a particular photon was detected. The combined photon pulses are sent through the normal time-measurement procedure of the TCSPC device. The detector numbers are used as a channel (or routing) signal for multi-dimensional TCSPC, routing the photons from the individual detectors into different waveform memory sections. Multi-detector TCSPC can be used to simultaneously obtain time- and wavelength resolution, or record photons from different locations of a sample.

1.3. Aim of present study

The aim of our study is to apply spectrally-resolved TCSPC to simultaneously measure NAD(P)H fluorescence spectra and lifetimes in living cardiac cells. Presently, there is a lack of precise knowledge of NAD(P)H fluorescence kinetic properties in intact living cardiomyocytes and their sensitivity to changes following metabolic modulation by TCSPC. Our aim is therefore to evaluate the feasibility and advantages of this new approach, to achieve efficient fingerprinting of metabolic oxidative state and its changes in pathophysiological state at the level of living cardiomyocytes, as well as early and sensitive detection of changes in cardiomyocytes mitochondrial metabolic oxidative state relevant to pathophysiological conditions. To achieve this goal, we propose

1. To study the dynamic characteristics of NADH fluorescence including concentration-dependence of NADH fluorescence decay kinetics, pH-dependence of NADH fluorescence decay kinetics, and changes of NADH fluorescence decay kinetics following binding of NADH to its enzymes such as LipDH *in vitro*.
2. To determine kinetics of NAD(P)H fluorescence with spectral and temporal characteristics directly in rat living left ventricular cardiomyocytes, an ideal model to study the heart metabolic modification. More specifically, NAD(P)H fingerprinting by spectrally-resolved lifetime spectroscopy will be investigated together with changes of the AF intensity and its lifetimes following the modulation of NAD(P)H production

and/or the respiratory chain, which may reflect the early and subtle change of mitochondrial dysfunction.

3. To examine effects of NAD(P)H fluorescence decay kinetics in ischemia-mimetic conditions studied in rat living cardiomyocytes.
4. To investigate possible applications of spectrally-resolved TCSPC technique to study NAD(P)H fluorescence in human living cardiomyocytes obtained from one additional biopsy samples of pediatric heart transplant patients. Endomyocardial biopsy (EMB) with cardiac catheterization is currently accepted as the "gold standard" for the diagnosis of rejection [149]. Using this method, an international grading system has been established for cardiac allograft rejection by International Society for Heart and Lung transplantation (ISHLT) [93, 150]. However, this approach does not always have the sufficient sensitivity to detect mild cases of the rejection at their early stages. Application of latest fluorescence technique therefore represents a new method with higher sensitivity for early detection of cardiac allograft rejection is a new challenge, at the present state of lack of relevant knowledge and reports in this area. As mentioned in the section 1.1.7., cardiac cells can be in a state of hypoxia or ischemia following rejection of transplanted heart, suggesting possible changes in mitochondrial respiration and oxidative metabolic state. We will therefore employ AF and examine spectral and lifetime NAD(P)H kinetics in human cells, which will be compared 1) to rat cardiac cells isolated in same conditions, 2) and with different rejection grades. In this way will be able to test our hypothesis: metabolic oxidative state changes in mitochondria occur at different level of the cardiac allograft rejection.
5. Complementary analytical approaches, namely decay-associated spectra (DAS) and the time-resolved emission spectra (TRES), will be tested to precisely separate individual components of NAD(P)H related to specific conformational state.

2. MATERIAL AND METHODS

2.1. Material

2.1.1. Isolation of left ventricular myocytes from rat hearts

The work was done on living cardiac cells, isolated from 13-14 week old adult Sprague-Dawley female rats (Charles River, St. Constant, Qc, Canada). Rats were sacrificed by decapitation. All procedures were performed in accordance with the Canadian Council on Animal Care (CCAC) guidelines and were evaluated by the local committee, "Comité Institutionnel des Bonnes Pratiques sur les Animaux en Recherche" (CIBPAR), accredited by the CCAC.

Left ventricular myocytes were isolated following retrograde perfusion of the heart with proteolytic enzymes by Langendorff instrumentation [82, 99]. Briefly, the heart was removed from body and cleared of blood by perfusion with Hepes-buffered physiological salt solution containing 0.75mmol/L $CaCl_2$ (see 2.1.3. for description of solution). This was followed by 5min perfusion with Ca^{2+}-free Hepes-buffered physiological salt solution containing 0.1mmol/L EGTA and then with the enzyme solution containing 0.5mg/ml collagenase type II (Worthington) and 0.03mg/ml protease type XXIV (Sigma) in 50µmol/L of $CaCl_2$. The left ventricle was dissected free, sliced into smaller fragments and agitated in the enzyme solution supplemented with 1.0% bovine serum albumin (BSA, Sigma). Aliquots of myocytes were harvested at 5-min intervals by filtration of the digest through 250µm monofilament nylon cloth followed by gentle centrifugation of the filtrate (100 x g for 2min). The pellets of myocytes were re-suspended in enzyme-free isolation solution containing 0.75mmol/L $CaCl_2$. Cardiomyocytes were maintained in a storage solution at 4°C until used. Only cells that showed clearly defined striations (Fig. 7A) were used in up to 10 hours following isolation.

Fragments of cardiac tissues were also used to isolate ventricular myocytes by the same approach as described for human myocytes (see 2.1.2. for the description of isolation and Fig. 7B for examination of isolated cell).

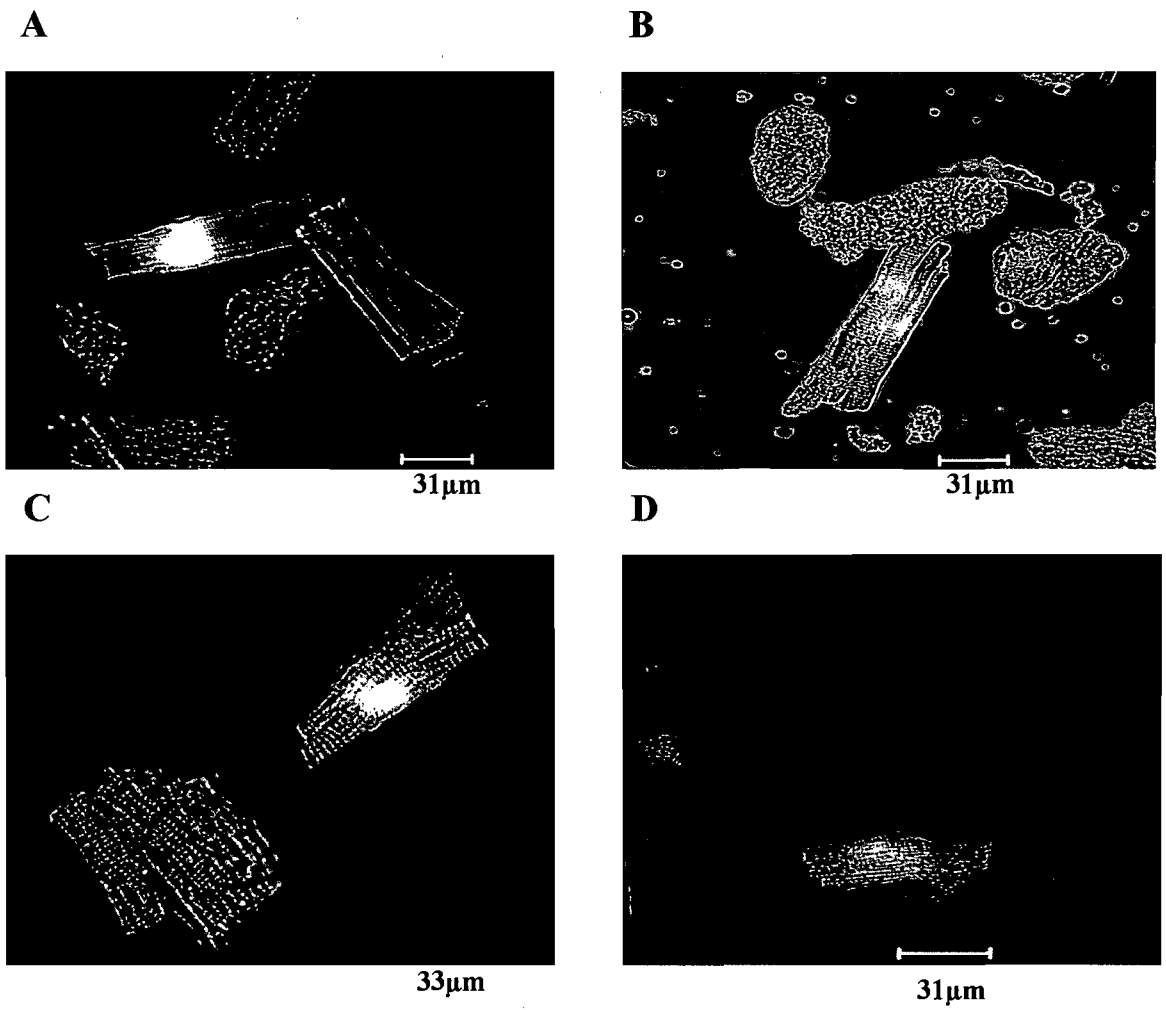

Figure 7: Transmission images of living cardiomyocytes. A: Cardiomyocytes isolated from left ventricular of rats by Langendorff instrumentation, B: cardiomyocyte isolated from fragments of rat cardiac tissues by the same approach as described for human myocytes (Isolation Approch I), C: cardiomyocyte isolated from an additional EMB of pediatric heart transplanted patients by Isolation Approach I, D: cardiomyocyte isolated from an additional EMB of pediatric heart transplanted patients by Isolation Approach II. Illuminated spot corresponds to defocused laser illumination.

2.1.2. Isolation of cardiomyocytes from endomyocardial biopsies of pediatric heart transplanted patients

Pediatric heart transplanted patients for 2 to 12 years, aged from several months to 18 years (mean age of 10 years) has been chosen in the present studies. All procedures were performed in accordance with Institutional Ethical Committee. Parental consent was obtained from subjects aged 2-12 years. Additionally, informed consent was obtained from older children who could understand the nature of the procedure. Cardiomyocytes were isolated from one additional biopsy sample of pediatric heart transplanted patients (when biopsy was performed because of clinical suspicion of rejection) at Cardiac Sciences Service of CHU Sainte-Justine during the regular rejection surveillance, cardiac tissue was taken from the right ventricle using cardiac catheterization, performed by pediatric cardiologist (Dahdah D., Poirier N. and Miro J., Department of Pediatrics Cardiac Sciences Service, CHU Sainte-Justine, Université de Montréal). Isolated cardiomyocytes were used within 2-5 hours after isolation.

To achieve appropriate isolation of cardiomyocytes from human biopsies, the isolation method has been tested and finally performed in two ways using different solutions. First, we have used Isolation Approach I; cardiac cells were isolated using a procedure adapted from Guinamard *et al.* [151]. Briefly, one biopsy sample weighting 1 to 5 mg, bulk of 1 to 2 mm^3 piece, was taken from right ventricle of patient, then promptly immersed into the isolation solution A (Krebs buffer, see section 2.1.3.) under oxygenation with 5% CO_2 and 95% O_2 (using a portable device) and taken to the lab (in the same building), where the tissue was washed and finely minced with a scalpel. Cardiomyocytes were then isolated by enzymatic digestion with collagenase Type V (Sigma) and protease type XXIV (Sigma). Tissue was digested by 4IU/ml protease and 160IU/ml collagenase for 15min. A further two to four 10 min steps in the presence of 320IU/ml collagenase alone were then performed. The cell suspension was filtered with 250µm pore size and centrifuged for 2 minutes at 100 x g. The pellet were gradually rinsed and resuspended in solution A. All processes were done in the presence of 30mmol/L 2,3-butanedione monoxime (BDM) and

in the absence of calcium in order to prevent all contractions. Isolated cardiac cells were identified by their rod-like shape and clear cross-striations (Fig. 7C).

Second, we have applied Isolation Approach II, the method adapted from Peeters *et a.l*[152]. This approach was comparable to Isolation Approch I, but the solution was modified to the solution B (Tyrode solution, see section 2.1.3.). Furthermore, the first digestion was performed with 3IU/ml protease type XXIV alone for 15min, while the second digestion was performed with 1.5IU/ml protease type XXIV and 0.5mg/ml (200IU/ml) collagenase type V for 10min. The process of digestion was done in the presence of 50μmol/L of calcium. A further three 6min steps were performed in the presence of 1.0mg/ml (400IU/ml) collagenase type V alone. 30mmol/L of BDM was present the whole process to prevent all contraction of cells. An example of isolated cell is at Fig. 7D.

2.1.3. Solutions

1. The isolation and storage solution (Hepes-buffered physiological salt solution) for rat cardiomyocytes isolation contained (in mmol/L): NaCl, 130.0; KCl, 5.4; $MgCl_2.6H_2O$, 1.4; NaH_2PO_4, 0.4; creatine, 10.0; taurine, 20.0; glucose, 10.0; and HEPES, 10.0; titrated to pH 7.30 with NaOH.
2. Basic external solution for study of cardiomyocyte AF contained (in mmol/L): NaCl, 140.0; KCl, 5.4; $CaCl_2$, 2.0; $MgCl_2$, 1.0; glucose, 10.0; HEPES, 10.0; adjusted to pH 7.35 with NaOH.
3. Basic intracellular solution for study of free NADH fluorescence *in vitro* contained (in mmol/L): KCl, 140.0; NaCl, 10; glucose, 10.0; HEPES, 10.0; adjusted to pH 5.40, 7.25 or 9.80 with NaOH.
4. Ischemia-mimetic solution contained (in mmol/L): NaCl, 135.0; KCl, 8.0; $MgCl_2.6H_2O$, 0.5; $CaCl_2$, 1.8; NaH_2PO_4, 0.33; Na^+-lactate, 20.0; HEPES, 5.0; titrated to pH 6.8 with NaOH and deoxygenated with 100% N_2 for 5 min.
5. Two solutions for isolation of human cardiac cells:

(1) Isolation solution A (Krebs buffer) contained (in mmol/L): NaCl, 35.0; KCl, 7.7; Na_2HPO_4, 16; $NaHCO_3$, 25; KH_2PO_4, 1.2; sucrose, 134.0; glucose, 10.0; and HEPES, 10.0; titrated to pH 7.30 with NaOH.

(2) Isolation solution B (Tyrode solution) contained (in mmol/L): NaCl, 120; KCl, 5.0; Na_2HPO_4, 5.0; KH_2PO_4, 0.5; $MgCl_2$, 0.5; taurine, 20.0; sodium pyruvate, 5.0; glucose, 20.0; and HEPES, 10.0; titrated to pH 7.25 with NaOH.

2.1.4. Reagents

1. *In vitro* reagents: NADH, NADPH and lipoamide dehydrogenase (LipDH) (from porcine) were purchased from Sigma-Aldrich (Canada) and used as such without further purification. NADH was added to basic internal solution in concentrations ranging from 1 to 40μmol/L, while LipDH was added to this solution in the concentration of 1 to 2 IU/μL, and NADPH was used at 20μmol/L, respectively.
2. Modulators of AF in living cardiac cells: 1μmol/L of Rotenone, 4mmol/L of cyanide and 50 μmol/L of 9,10-dinitrophenol (DNP) were added to cells in basic external solution for 5-25 min prior recording. 3mmol/L of 3-β-hydroxybutyrate (BHB) and 100 μmol/L of pyruvate were prepared freshly, while 150μmol/L or 1.5mmol/L of acetoacetate (AcAc) was added from 250mmol/L stock solution. 1mmol/L of Lactate and 1mmol/L of Octanoate were each added to the basic external solution from the 100mmol/L stock-solution, where pH was carefully adjusted to 7.25 [82]. 9,10-diphenylanthracene (DPA) was studied at 10^{-8}mol/L in ethanol (stock solution at 10^{-2} mol/l in cyclohexane), while 1,1'-diethyl-2,2'-carbocyanine iodide (DCI) was used at 10^{-4}mol/L in ethanol. 30mmol/L of 2,3-butanedione monoxime (BDM) was used in human cardiomyocytes isolation. All chemicals were from Sigma-Aldrich (Canada), except DPA, which was from Fluka (Canada).

2.2. Methods

2.2.1. Confocal microscopy

Confocal microscopy is an optical imaging technique used to increase micrograph contrast and/or to reconstruct three-dimensional images by using a spatial pinhole to eliminate out-of-focus light or flare in specimens that are thicker than the focal plane [153]. Only the light within the focal plane can be detected, the image quality is therefore much better than that of wide-field images. In laser-scanning confocal microscopy only one point is illuminated at a time so that, 2D or 3D imaging requires scanning over a regular raster (i.e. a rectangular pattern of parallel scanning lines) in the specimen. The thickness of the focal plane in confocal microscopy is defined mostly by the wavelength of light, index of refraction and confocal pinhole diameter, and is inversely proportional to the square of the numerical aperture of the objective lens. In the present study, images of NAD(P)H AF were taken by confocal laser scanning head LSM-510 Meta on Axiovert 200 inverted microscope (both Zeiss, Canada) and recorded with a PlanNeofluar 63x /1.3 oil objective, using tunable femtosecond oscillator (Coherent Chameleon) at 777 nm excitation (two-photon excitation), HFT KP 700/488 dichroic filter and 435-485 nm spectral range for emission detection. To avoid alteration of the AF spectral shape by photobleaching, spectral data were always recorded from the first scan of each cell.

2.2.2. Spectrally-resolved time-correlated single photon counting

TCSPC is based on the detection of single photons of fluorescence, excited by a periodical light signal. The measurement of the time delay between excitation and detection of the individual photons allows reconstruction of the waveform from the individual time measurements [147]. The principle of the classic TCSPC is shown in Fig. 8. The detector signal consists of a train of randomly distributed pulses due to the detection of the individual photons. There are many signal periods without photon, other signal periods contain one photon, periods with more than one photons are very rare. When a photon is detected, the time delay between the detector pulse and the corresponding detector pulse

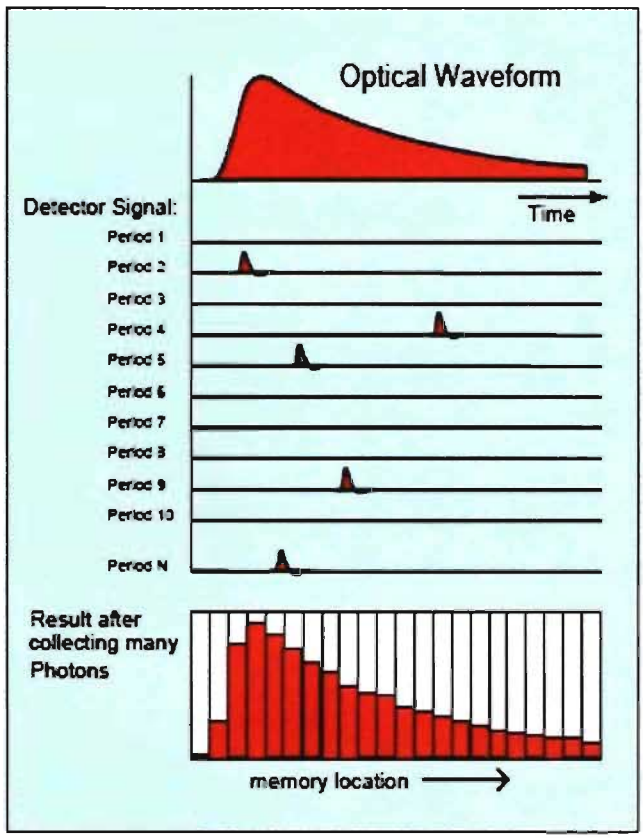

Figure 8: Principle of classic TCSPC measurement. Upper: the reconstruction of the original optical waveform from the individual time measurements. Middle: detector signal in periods from 1 to N. Lower: histogram of the detection time after accumulation of many photons detection event in the memory (Adapted from Advanced Time-Correlated Single Photon Counting techniques) [106].

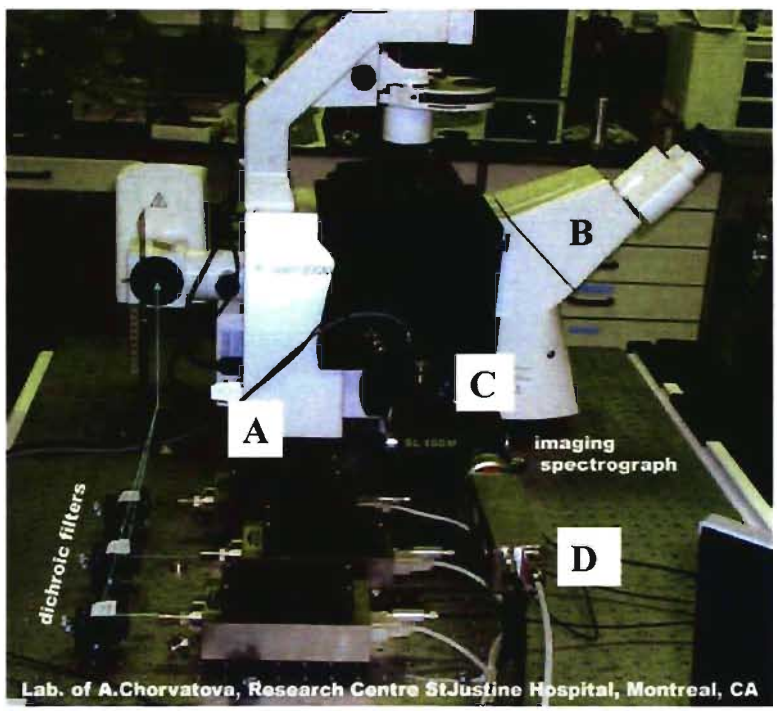

Figure 9: The spectrally-resolved time-correlated single photon counting (TCSPC) instrumentation. A: Picosecond laser diode with emission of 375 nm, B: Axiovert 200M inverted fluorescence microscope, C: imaging spectrograph, D: 16-channel photomultiplier.

that is measured. The measured times are used to address a histogram memory in which the events are accumulated. After acquiring a large number of photons the intensity distribution versus time builds up in the memory [106].

Multi-dimensional TCSPC which includes spectral detection is based on the excitation of the sample by a high-repetition rate laser and the detection of single photons of the fluorescence signal in one or several detection channels in the sample located on an inverted microscope. In this approach, each photon can be characterized by several parameters, such as its average time within the laser period, its number of detector channel, its wavelength and its time from the start of the experiment. This approach is simultaneous recording of time-resolved fluorescence in several wavelength channels that allows increased resolution of complex multi-exponential decays due to additional spectral coordinate, and capability to detect fast transient effects such as changes in the fluorescence lifetime, spectra and intensity in living cells. In addition to multi-wavelength detection capability, spectrally resolved TCSPC provides near-ideal counting efficiency and picosecond (ps) time resolution [106, 145].

Measurement of the NAD(P)H fluorescence that are presented in this thesis are carried out using a newly-designed experimental spectrally-resolved TCSPC setup (Fig. 9), which is based on combination of inverted microscope with single-photon excitation by a picosecond diode laser and multi-dimensional TCSPC instrumentation. This approach allows fast and reproducible measurement of complex patterns of spectrally and time-resolved fluorescence decay directly in living cardiac cells (see original recording at Fig. 10). It provides an extremely promising tool with necessary sensitivity to detect the low-intensity intrinsic fluorescence signals, as well as the temporal and spectral resolution allowing identification of the individual fluorescence components in living cardiac cells [148].

2.2.3. Recording of spectrally-resolved autofluorescence data in living cardiac cells

Cells and/or solutions of NADH molecules were mounted on an inverted microscope (Axiovert 200M, Zeiss, Canada) and studied at room temperature in 4-well chambers with UV-proof coverslip-based slides (LabTech, Canada). Background was monitored at the

blank area next to the cells. Picosecond laser diode with emission of 375 nm (BDL-375, Becker&Hickl, Boston Electronics, U.S.A.) was used as an excitation source with output power ~1 mW. Its pulse width was typically 60 ps at 20 MHz repetition frequency rate.

The laser beams were combined by dichroic filters and reflected to the sample through epifluorescence path of inverted microscope to create slightly defocused elliptical spot at the objective focus, reaching typically 10x20 μm (inset in Fig. 11C). The size of the spot was chosen in regard to the average width (20-30 μm) of one rat cardiomyocyte [82]. The emitted fluorescence was spectrally separated from the laser excitation using standard dichroic filter cubes (395 nm dichroic and 397 nm long-pass filters for excitation at 375 nm) located in the microscope filter turret. A polarizer in a "magic-angle" orientation was fitted in front of the detection system at the microscope output port, to avoid distortions of decay kinetics due to depolarization effects in the microscope optics. Data were acquired by a 16-channel multi-anode photomultiplier array (PML-16, Becker&Hickl, Boston Electronics, U.S.A), after spectral decomposition via a 100 mm imaging spectrograph (Solar 100, Proscan, Germany). The PML-16 detector was running in the photon-counting regime and fed the TCSPC interface card SPC 830 (Becker&Hickl, Boston Electronics, U.S.A) comprising of the discriminators, pulse-formation electronics, time-to amplitude converter (TCA), and analogue-to-digital converter, all driven by SPCM_95 software (Becker&Hickl, Boston Electronics, U.S.A). The card was synchronized-electrically by the laser diode driver in the reversed regime. To ensure a sufficient time-window (50ns) for observed fluorescence kinetics, 20 MHz pulse repetition rate of the excitation laser was selected. Fluorescence decays were measured simultaneously at 16 spectral channels with 25 ns TAC time-base sampled by 1024 points, leading to the temporal resolution of 24 ps/channel. Decay kinetics were measured for 30 s, with the number of photon counts at each channel reaching maximum intensity of about 500-5000 counts and the typical background noise of 10-100 counts per channel, present mostly due to ambient light.

To image the whole visible emission spectrum to the PMT array, the spectrometer was fitted with a grating (600 line-pairs/mm), providing the dispersion of 18 nm/mm. Since

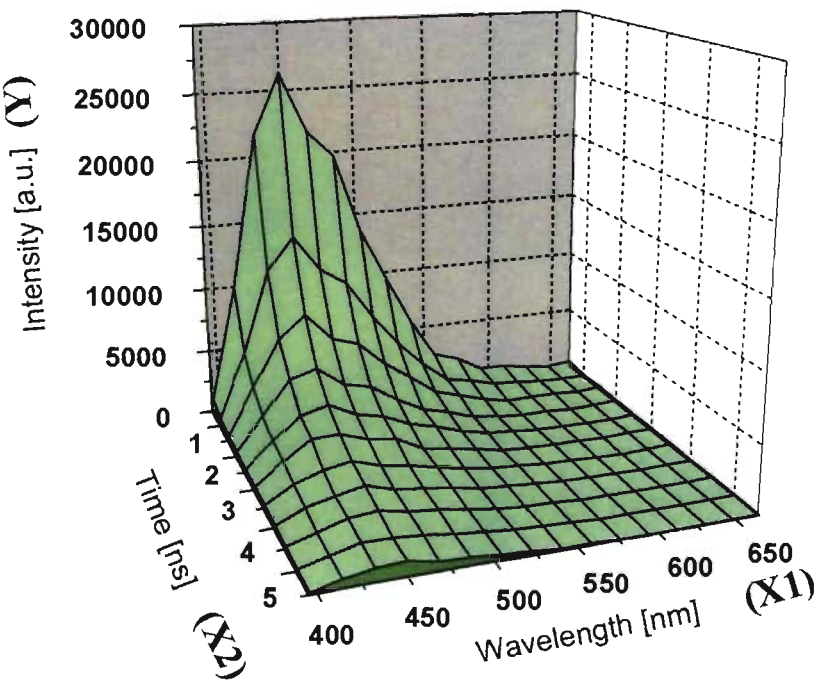

Figure 10: Original recording of spectrally and time-resolved fluorescence decay. X1-axis: spectrally resolved fluorescence decay, X2-axis: time-resolved fluorescence decay, Y-axis: fluorescence intensity.

the channel width of the used PMT array was 1 mm, the value of 18 nm also corresponds to the rough spectral resolution of our system. The spectrometer was calibrated using the emission maxima of known reference dyes, such as DPA and the water Raman peak [148]. After calibration, we estimated the spectral range of our system to ~390–680 nm (channel mid-point values), with 16 equidistantly spaced spectral intervals 18 nm wide. The influence of higher orders of diffraction on the spectrograph linear dispersion was minimized using the dichroic and long-pass emission filters in the microscope, blocking completely the wavelengths below 400 nm from entering the spectrograph and the detector. Thus, we avoided the physical overlay of the signal from higher-order responses (<350 nm) over the first-order wavelength detection range (385–675 nm). We have not corrected our data for spectral sensitivity of the detector, nor for the spectral properties of the grating or dichroic filters. Therefore, the spectral profiles presented hereafter should be regarded as uncorrected emission spectra.

The half-width of instrument response function (IRF) of our setup was 0.2-0.25 ns, according to the measurement of the Raman scattering peak of water [148]. Due to the absorption characteristics of the microscope filter cubes, the IRF of our setup could not be measured directly by laser-light scattering. For the estimation of instrument response profile colleagues in the lab have therefore used the fluorescence of DCI at 10^{-4}mol/L in ethanol. This dye has reported a short excited state-lifetime of ~10 ps [154], with the emission peak at 625 nm. The typical width of the IRF using the 375 nm laser and the PML detector (Fig. 12A) was ~200 ps full width in half-maximum (FWHM), slightly exceeding the typical specifications of the convolved response functions of the detector itself (180 ps), the laser (60 ps) and the TCSPC electronics (8 ps). A mono-exponential fluorescence decay with a lifetime of 40-60 ps after deconvolution was assigned to the DCI probe at 440 nm following 375 nm excitation (Fig. 12A) [148], which is in good agreement with other authors [155]. To test the precision of the setup in measurements at the ns scale, fluorescence kinetics

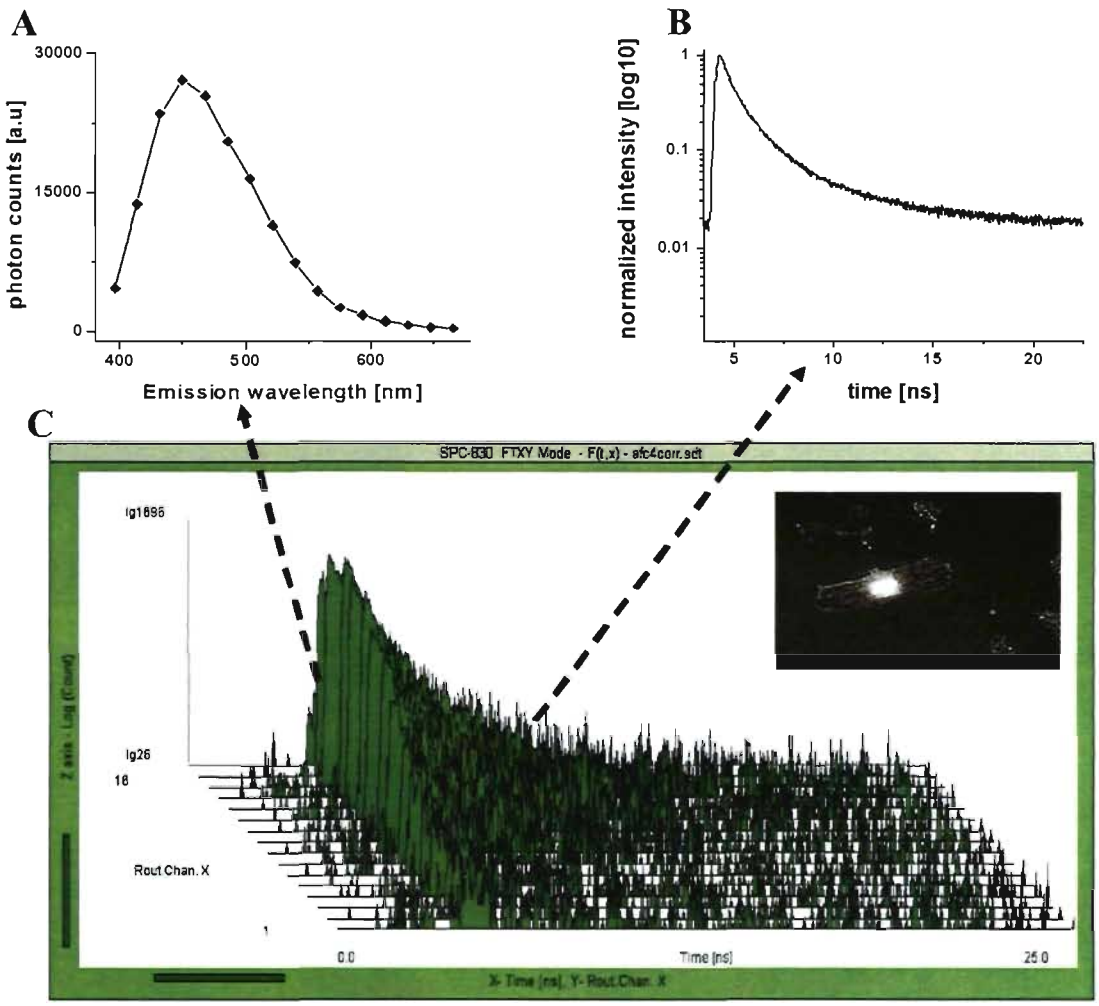

Figure 11: Original recording of AF decay. A: Background-corrected fluorescence spectrum, B: fluorescence decay, C: original recording of spectrally-resolved decay of AF gathered at 16 channels. In inset: laser excitation of elliptical spot in a single emitting cardiomyocyte, typically 10x20 μm.

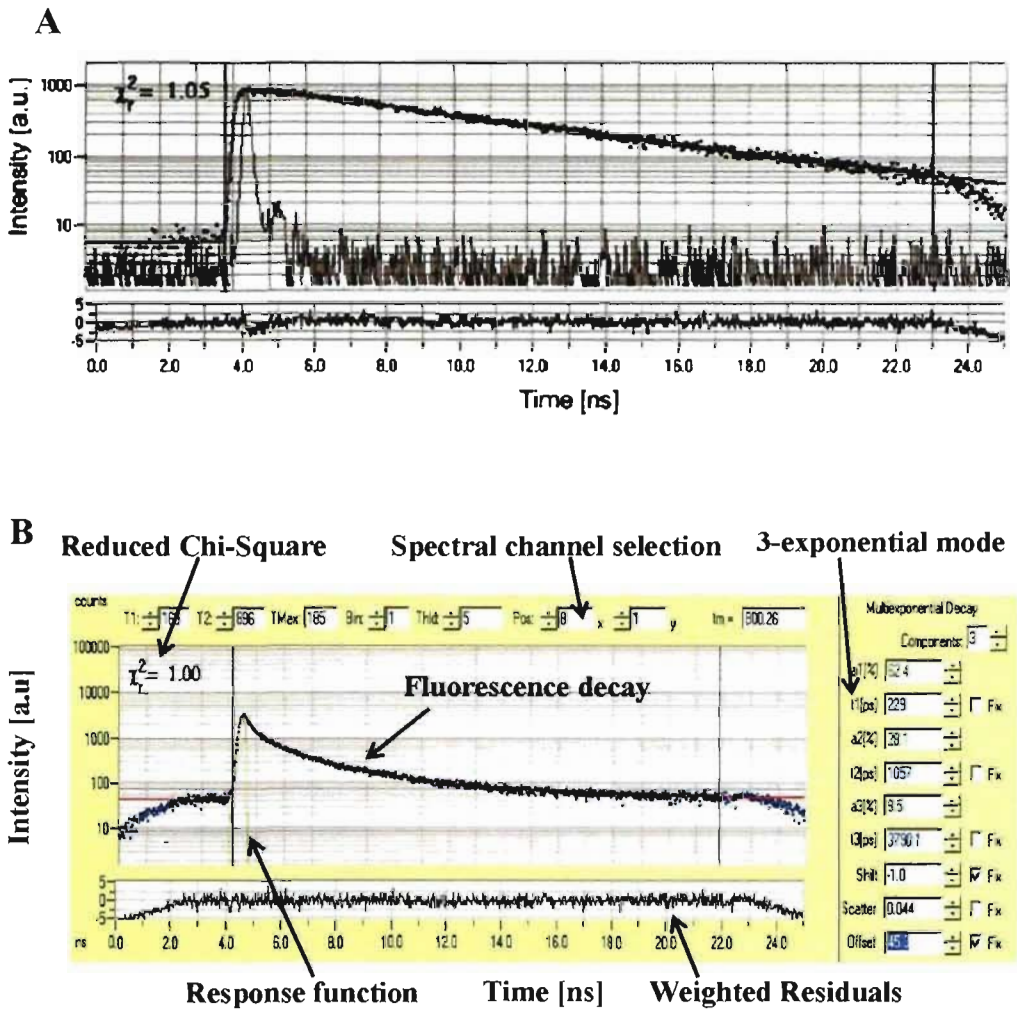

Figure 12: Analysis of fluorescence decay. A: single-exponential fluorescence decay of DPA in ethanol in one selected spectral channel detected by the PML-16 detector after excitation with 375 nm pico-second laser [148]. Instrument response function (*grey lineon A and green line on B*) was estimated using DCI. B: 3-exponential mode for analysis of fluorescence decays in living cardomyocyte (Adapted from D. Chorvat Jr *et al.*) [148].

of the fluorescence lifetime standard DPA in ethanol (10^{-8} mol/L) have been recorded in the lab following 375 nm excitation. The observed decay was single exponential, with the estimated value of the fluorescence lifetime of 6.42 ± 0.12 ns, corresponding to the reported values of DPA lifetime ~ 6.1 ns [156]. This result suggests that rapid lifetime kinetics can be conveniently recorded by our setup.

2.2.4. Definitions of terms and derived quantities

Spectrally and time-resolved TCSPC data were recorded from each cell (Fig. 11A, B and C). Steady-state AF spectra were evaluated as total photon counts for each spectral channel (see equation 11). Each lifetime pool was assessed by examining its fluorescent lifetime (τ_i) and relative amplitude (a_i), accordingly to equation 12. At least a 3-exponential model was used for analysis of exponential decay of NADH AF, chi-square values (χ^2) <1.2 was considered as acceptable (Fig.12B). In our experiments, we typically collected a photon-counting histogram of spectrally-resolved AF decay $P(\lambda_j, t_k)$. The histogram was measured simultaneously on 16 spectral channels (18 nm wide) denoted as λ_j, and on 1024 temporal channels denoted t_k, equidistantly spaced by 24.4 ps. The steady-state AF spectra $S(\lambda_j)$ were calculated as a total photon count for each spectral channel:

$$S(\lambda_j) = \sum_{k=1}^{1024} P(\lambda_j, t_k) \qquad (11)$$

The fluorescence decay kinetics were analyzed using a sum of three exponential terms, according to the model I (λ_j, t) with the functional form:

$$I(\lambda_j, t) = I_{baseline} + \sum_{i\ 1=}^{3} a_{i,j} \times \exp(-(t - t_0)/\tau_{i,j}) \qquad (12)$$

where (t_0) is the variable zero-time shift, $I_{baseline}$ fits the background intensity, and the amplitude (a_i) represents the fractional population of molecules associated with each decay component *i*. The sum of these fractional populations for each selected wavelength equals 100%:

$$\sum_{i\ 1=}^{3} a_{i,j} = 100 \qquad (13)$$

In the fitting procedure (nonlinear least-squares minimization routine implemented in SPCImage by Becker&Hickl), the parameters of the model function $I(\lambda_j, t)$ were iteratively changed, while being convolved with the IRF to best fit the measured photon histogram $P(\lambda_j, t_k)$. Thus, each lifetime component *i* was assessed by examining its estimated fluorescent lifetime $\tau_{i,j}$ and relative amplitude $a_{i,j}$, both being dependent on the emission wavelength λ_j. For simplicity, we provide the results either in the form where these parameters are plotted against wavelength coordinate, or we specify the particular emission wavelength used, omitting the second index (j).

Once the fitting parameters have been obtained, the following derived quantities were calculated:

1) the average fluorescence lifetime $\langle\tau\rangle$;

$$\langle\tau\rangle = \sum_{i=1}^{3}(a_i \times \tau_i)\Big/\sum_{i=1}^{3} a_i = \sum_{i=1}^{3}(a_i \times \tau_i)/100 \qquad (14)$$

2) the relative intensity of each species $a_i\tau_i$;

3) the relative fraction r_i of the fluorescence generated by each species *i*, with respect to the total fluorescence;

$$r_i = (a_i \times \tau_i)\Big/\sum_{i=1}^{3}(a_i \times \tau_i) \qquad (15)$$

Furthermore, the decay associated spectra (DAS) were computed as a fraction of the total fluorescence emission for each lifetime pool, using the quantities r_i and S defined above:

$$DAS_i(\lambda_j) = r_i(\lambda_j) \times S(\lambda_j) \qquad (16)$$

The time-resolved emission spectra (TRES) were constructed as described previously [148] by summing the photons registered over a chosen number of consecutive time channels t_k after a temporal delay Δt:

$$TRES(\lambda_j) = \sum_{k=(k_{max}+\Delta t)}^{(k_{max}+\Delta t+\delta t)} P(\lambda_j, t_k) \qquad (17)$$

where k_{max} corresponds to channel with maximal detected photon counts, i.e. the peak of the excitation impulse, λ_j to emission wavelength, $P(\lambda_j, t_k)$ to the photon-counting histogram of spectrally-resolved AF decay. We have used the TRES interval width δt of 1ns (in regard to the instrument response width) leading to the time interval expressed in channel numbers as $k \in (\Delta t, \Delta t + \delta t)$, where 1 channel ~ 24 ps.

2.2.5. Data analysis

Data were analyzed using SPCImage software (Becker&Hickl, Boston Electronics, U.S.A). All data were corrected for the systematic wobble of the temporal-shift in the detected photon histogram at different channels of the PMT array [106] using custom procedures for data correction and analysis written in C^{++}. A home-made database was used for appropriate data management. Data are shown as mean ± standard error of the mean (SEM), as our main focus was to compare different populations of cells in specific experimental conditions. However, we are aware that this is not sufficient to reflect variations around an average value. Standard deviation (SD), which is a measurement of dispersion in original units, reflects more precisely a natural accuracy of the measuring system rather than SEM, and can be calculated from equation 18:

$$SEM = \frac{SD}{\sqrt{n}} \text{ or } SD = SEM \times \sqrt{n} \qquad (18)$$

where n is the number of experiments. For example, in the case of cardiomyocyte AF in control condition (discussed in Table 4), its fluorescence can be described as follow (means ± SD): photon counts = 23200 ± 6600; Pmax =1550 ± 570; a1 = 69.3 ± 8.4, τ1 = 690 ± 92; a2 = 27.6 ± 8.4, τ2 = 2030 ± 440; a3 = 3.1 ± 1.7, τ3 = 12700 ± 6500.

Data analysis was performed using Origin7.0. Comparison between means was made at spectral maximum of 450 nm and at 504 nm (to account for observed red-spectral shift), using one-way analysis of variance (ANOVA), followed by Tukey post-test.

3. RESULTS

3.1. Recording of NADH flurescence *in vitro*

Part of this study has been published in ANEBA S., CHENG Y., MATEASIK A., COMTE B., CHORVAT D. JR, CHORVATOVA A., 2007: Probing of cardiomyocyte metabolism by spectrally-resolved lifetime detection of NAD(P)H fluorescence. ***The Computers in Cardiology.*** 39:349-352. See attached Appendix I.

3.1.1. Kinetics of free NADH fluorescence decay

To understand the characteristics of free NADH endogenous fluorescence, we have studied steady-state spectra and lifetimes of intrinsic NADH fluorescence *in vitro* in intracellular media-mimicking solutions (pH 7.25). Steady-state spectra measured simultaneously at 16 acquisition channels were determined as the total photon counts on each spectral channel. Fluorescence lifetime pools were assessed by examining their fluorescent lifetimes (τ_i) and relative amplitudes (a_i) by 3-exponential decay (see methods 2.2.4.for detail). The results showed that NADH AF had (1) spectral patterns with maximum emission between 450-470 nm after UV light excitation (Fig. 13A). (2) At the maximum emission wavelength of 450 nm, we resolved (20μmol/L, n=10) fluorescence lifetimes $\tau 1$ = 0.4±0.1 ns (with relative amplitude of 69.9±1.0 %), $\tau 2$ = 1.5±0.1 ns (20.5±0.8 %) and $\tau 3$ = 8.1±0.1 ns (9.8±0.2 %) (See Table 3 for number of experiments).

3.1.2. Concentration-dependence of NADH fluorescence decay kinetics

To understand changes of NADH fluorescence decay kinetics with its concentration, we studied concentration-dependence of NADH fluorescence kinetics *in vitro*. These experiments are important to comprehend changes of NADH kinetics resulting from modification in $NADH/NAD^+$ ratio (in response to demand for ATP production) in different workloads of the heart, and/or in pathological condition. Concentrations ranging from 1 to 40μmol/L were used to question the dose dependence of spectral and lifetime properties of the NADH fluorescence. Spectrally- resolved free NADH fluorescence intensity was concentration-dependent with a linear correlation between the numbers of

photon counts and NADH concentration (Fig. 13A and C), as described previously [132]. Normalized spectra superimposed perfectly for NADH concentrations between 1 to 40μmol/L (Fig. 13B), confirming the same molecular origin. Neither resolved lifetimes, nor their relative amplitudes were dependent on the NADH concentration at spectral maximum (see examples for 450 nm fluorescence decay at Fig. 13D, Table 3 for number of experiments) or in the range of emission wavelength (between 420 and 560 nm; Fig. 14A-F). These results suggest that a change of the fluorescence intensity correlates with modification of free NADH concentration. In addition, we also found 20μmol/L of NADH, with its appropriate fluorescence yield an ideal concentration for further study of free NADH kinetics.

3.1.3. pH-dependence of NADH fluorescence decay kinetics

Next, we questioned whether intracellular solutions with modified pH are able to affect the kinetics of free NADH fluorescence decay. Since metabolic acidosis or alkalosis may occur in many pathological conditions, such as ischemia, these experiments help to understand potential changes of NADH fluorescence kinetics with pH. Fluorescence characteristics of free NADH recorded in intracellular solution with modified pH (5.4, 7.25, or 9.8) showed slightly increased intensity of NADH in the presence of pH 5.40, but no change in the presence of pH 9.80, when compared to pH 7.25 ones. Fluorescence spectral shape, resolved lifetimes and their relative amplitudes were not significantly different (Fig. 15A-H, table 3 for number of experiments). These results indicated that free NADH in different pH alone is not likely to significant affect the intrinsic NADH fluorescence decay kinetics.

3.1.4. Binding of NADH to lipoamide dehydrogenase

We then tested changes in kinetics of NADH fluorescence decay in the presence of lipoamide dehydrogenase (LipDH) *in vitro* in intracellular media-mimicking solutions (pH 7.25). LipDH was found in several 2-oxo acid dehydrogenase multi-enzyme complexes [157]. It is a disulfide oxidoreductase, comparably to the first protein of multi-enzyme Complex I

of the mitochondrial respiratory chain. The experiment was designed to understand changes of NADH fluorescence kinetics by binding, dehydrogenation of NADH to NAD^+ by LipDH can mimic binding of NADH to enzymes of the Complex I. LipDH in the concentration of 2 U/μL but not in the1 U/μl was capable of decreasing NADH fluoresence (20μmol/L), while LipDH itself did not present any background AF (Fig. 16A). The decrease in the fluorescence intensity of NADH in the presence of 2 U/μL LipDH was accompanied by a slight spectral broadening of about 10 nm towards red spectral region, as demonstrated by normalized emission spectra (Fig. 16B). Resolved fluorescence lifetime pools and their relative amplitudes showed tendency to decrease in the 1st lifetime pool and increase in the 2nd and 3rd lifetime pools after binding (Fig. 17A, B and C, Table 3 for the number of performed experiments). NADH fluorescence decays were prolonged by binding to LipDH (as illustrated at Fig. 16C and D) due to a significantly increased 2nd lifetime pools (at 504 nm wavelength, $\tau 2$ was prolonged from 1.8±0.1 ns to 2.7±0.2 ns, $p<0.05$. See Table 3 for number of experiments), leading to increased average lifetime. Interestingly, the fluorescence lifetime of the intermediate pool increased in a spectrally-dependent manner; the lifetime prolongation was mainly observable at emission wavelengths that were longer than the emission spectral maximum of NADH (>450 nm) (Fig. 17D). These data demonstrate sensitivity of the 2nd fluorescence lifetime pool to change in NADH binding to LipDH enzyme.

Fluorescence characteristics of binding of NADH (20μmol/L) to LipDH (2 U/μl) recorded in intracellular solution with modified pH (5.4, 7.25, or 9.8) gone similar results as observed from free NADH molecule (Fig. 18A-H), indicating that no significant changes in NADH fluorescence kinetics can be attributable to change in pH.

Our data demonstrated that the NADH content is principally correlated with the overall fluorescence intensity at 450 nm (spectral maximum), while average fluorescence lifetime is more sensitive parameter to change in NADH binding to its enzymes. Surprisingly, NADH fluorescence was not significantly affected in intracellular solution with different physiological pH.

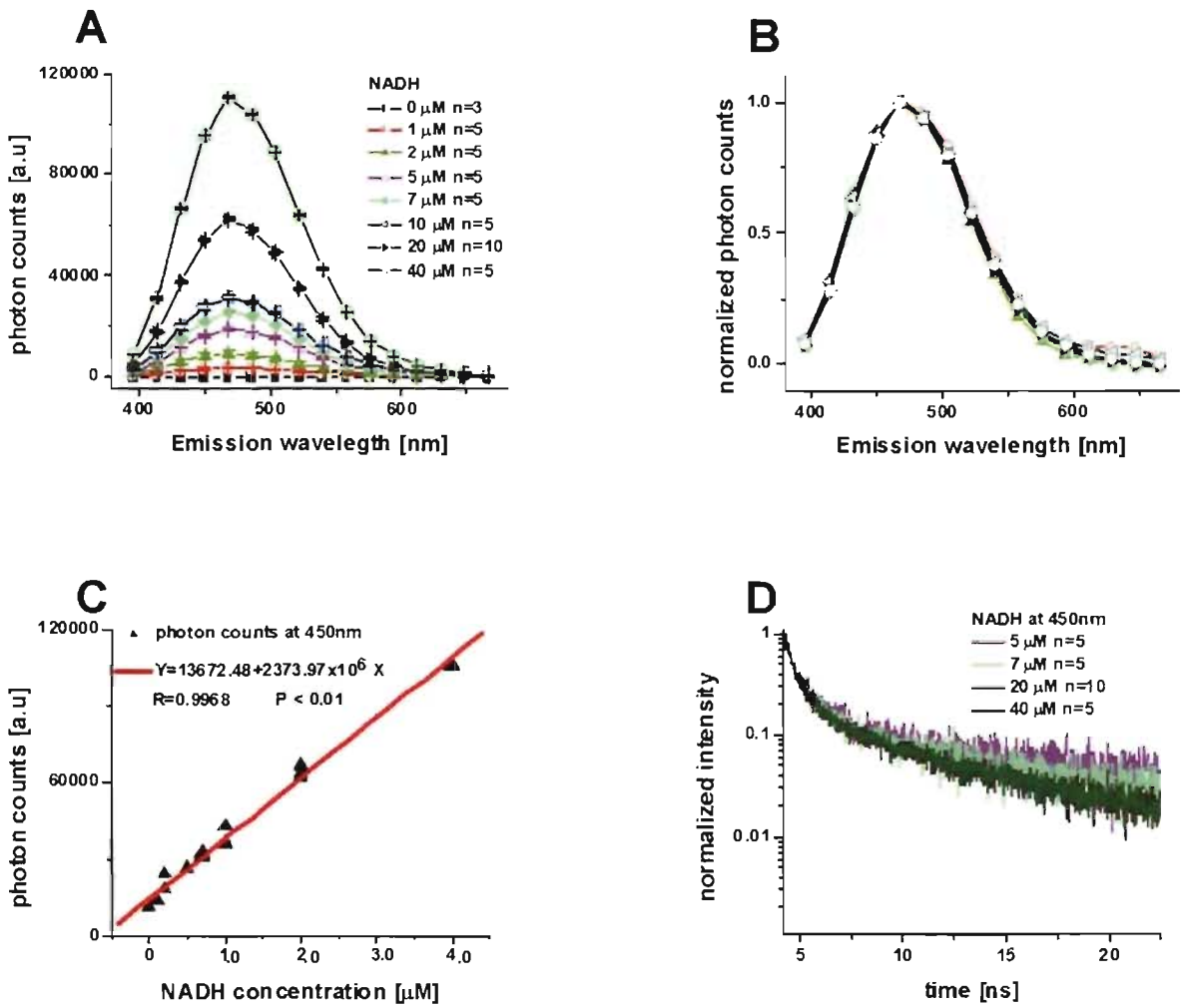

Figure 13: NADH fluorescence spectra and lifetimes *in vitro*. A: NADH fluorescence spectra at concentrations ranging from 1 to 40μmol/L. B: Normalized background-corrected NADH fluorescence spectra. C: A linear correlation between the number of photon counts and NADH concentration at spectral maximum of 450nm. D: NADH fluorescence decays in concentrations ranging from 5 to 40μmol/L at 450nm.

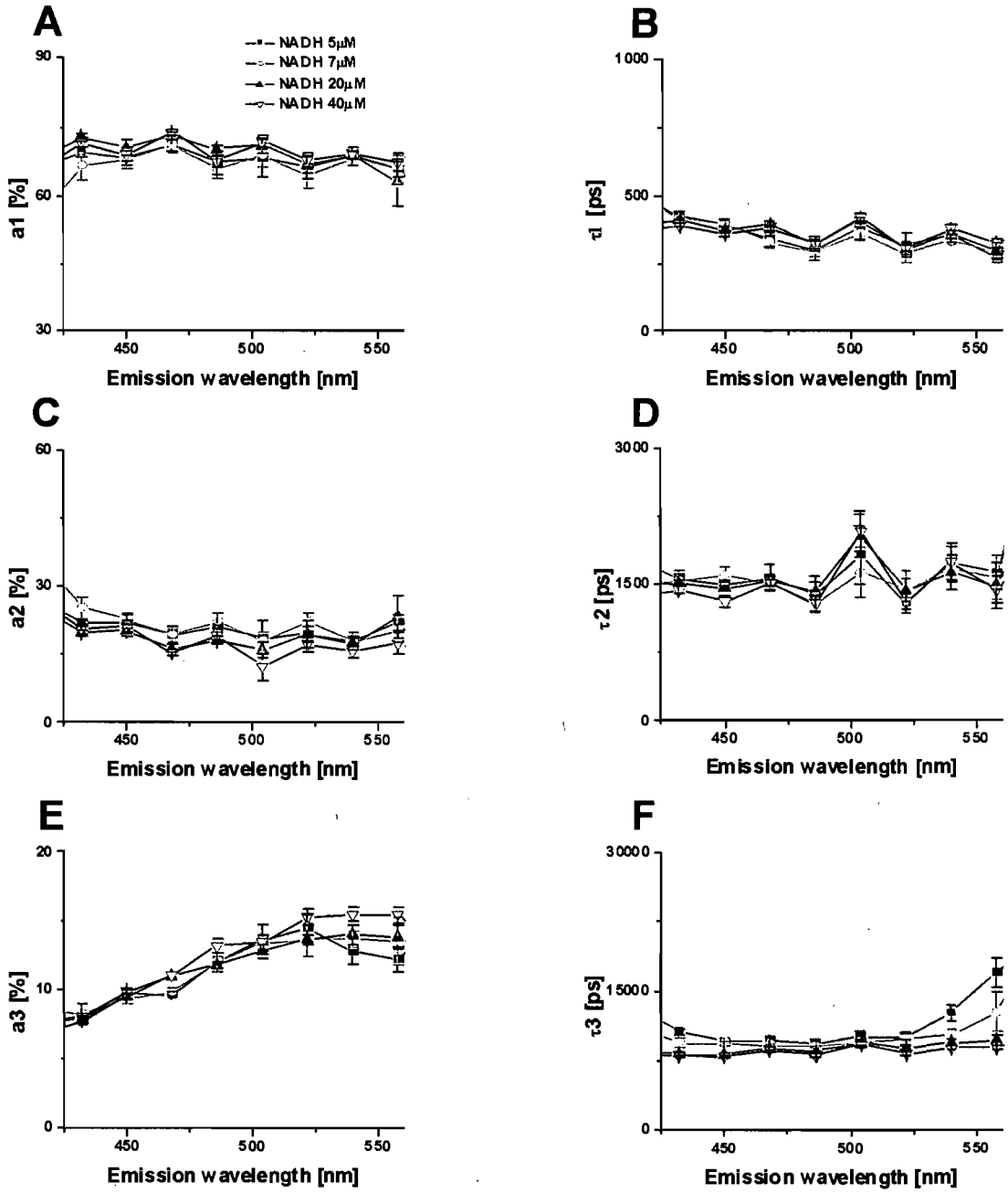

Figure 14: Concentration-dependence of NADH fluorescence lifetimes and their relative amplitudes *in vitro*. [NADH] ranging from 5 to 40μmol/L was recorded on emission wavelength from 420 to 560 nm. A, C; and E: lifetime pool relative amplitudes (a1, a2, and a3, respectively). B, D and F: fluorescence lifetimes (τ1, τ2 and τ3, respectively).

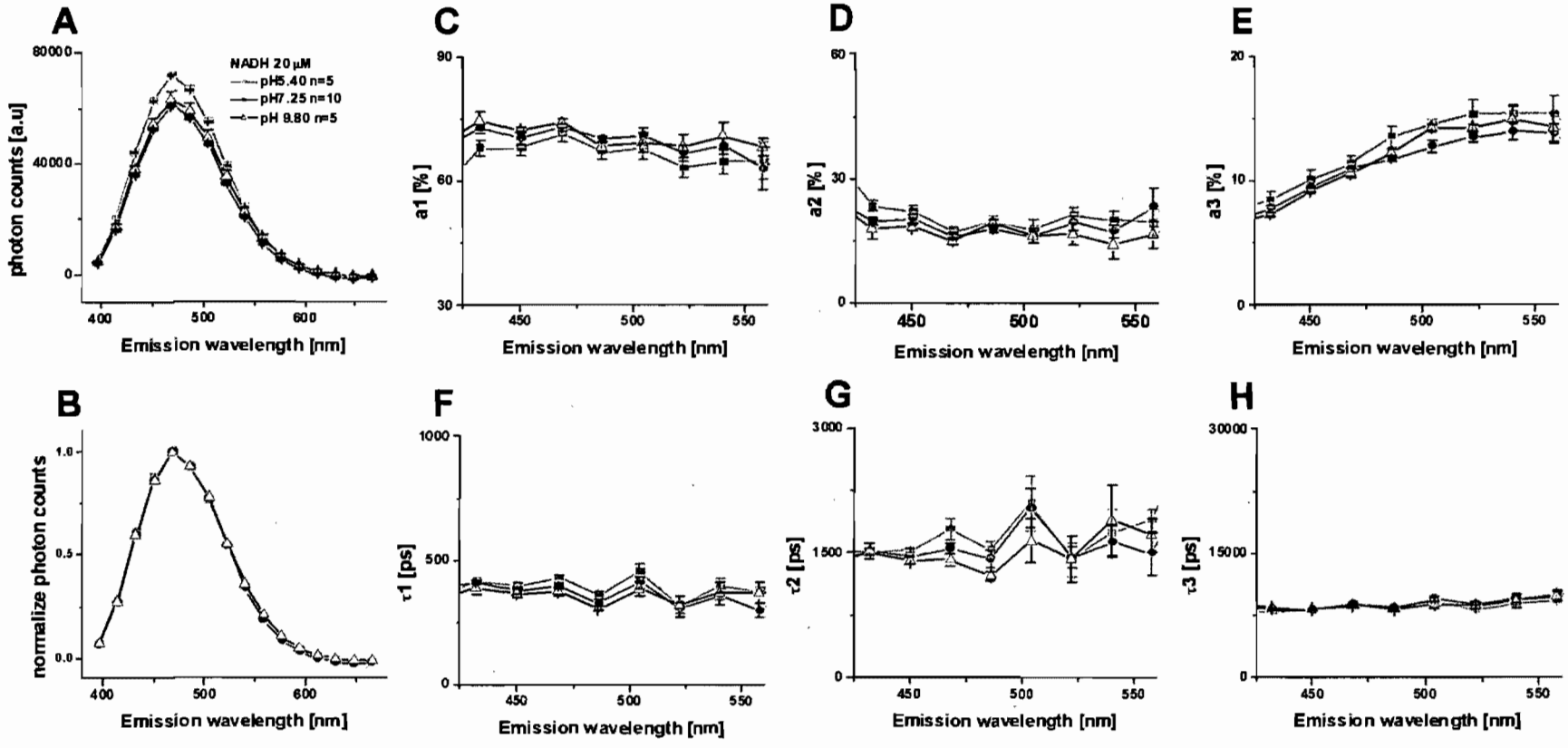

Figure 15: pH-dependence of NADH fluorescence decay kinetics *in vitro*. Spectrally-resolved fluorescence lifetime pool characteristics of NADH recorded in intracellular solution with modified pH (5.40, 7.25, or 9.80) on emission wavelength from 420 to 560 nm. A: Steady-state fluorescence spectra, B: Normalized spectra. C, D and E: lifetime pool relative amplitudes (a1, a2, and a3, respectively), F, G, and H: fluorescence lifetimes (τ1, τ2 and τ3, respectively).

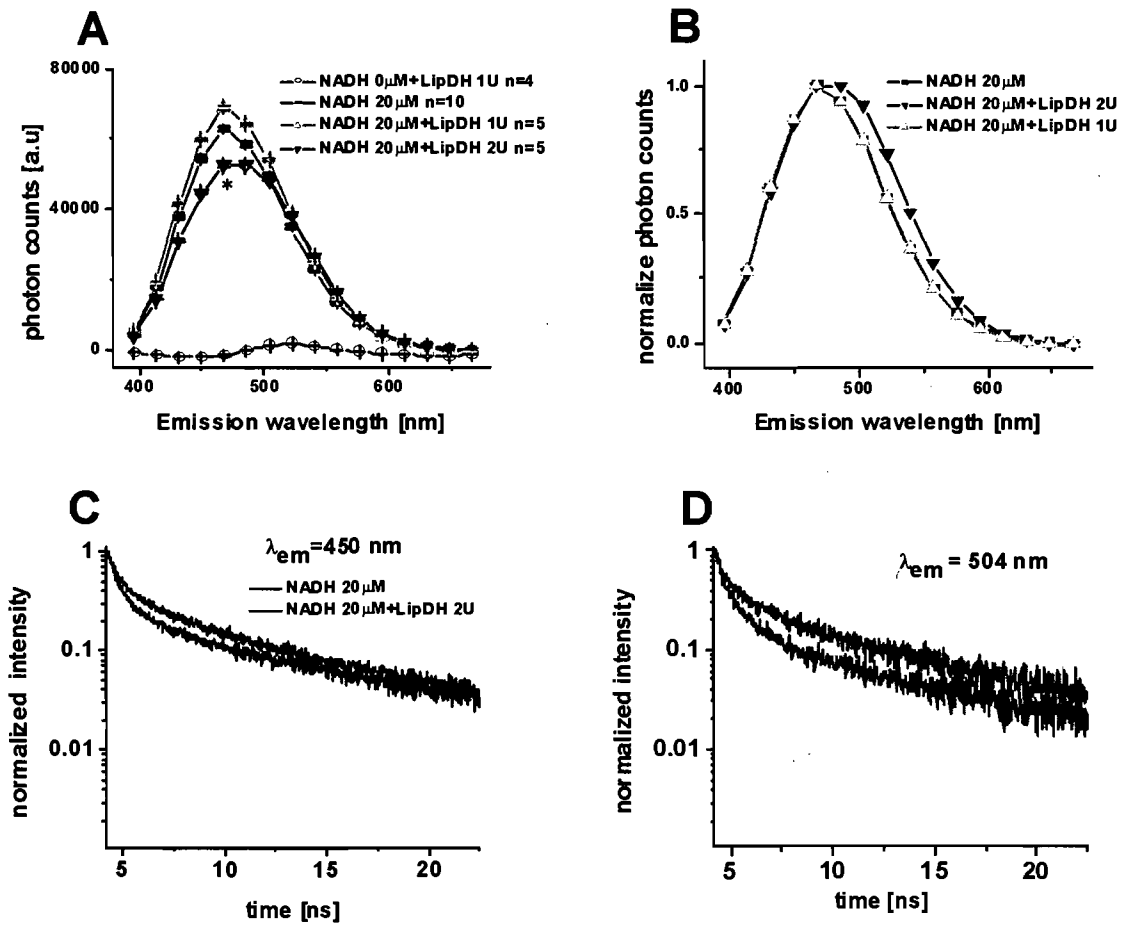

Figure 16: Spectral and fluorescence lifetime characteristics of NADH after binding to LipDH *in vitro*. LipDH (1 U/μl or 2 U/μl) in the absence or presence of NADH (20μmol/L). A: Steady-state fluorescence spectra. B: Normalized spectra. C: NADH fluorescence decay at 450 nm of emission wavelength. D: NADH fluorescence decay at 504 nm of emission wavelength. *$p<0.05$ vs. NADH 20μmol/L.

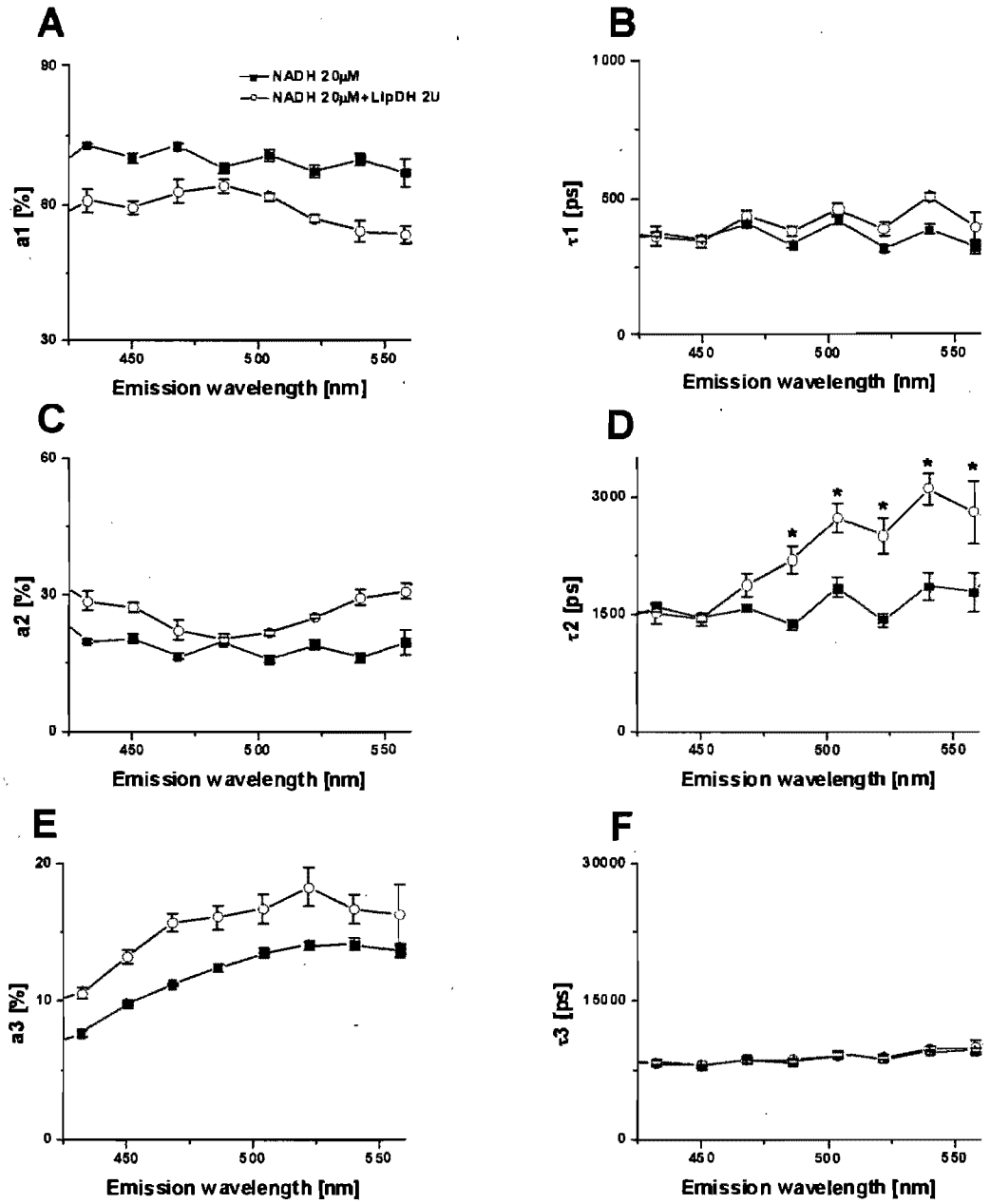

Figure 17: Fluorescence lifetimes and their relative amplitudes after binding of NADH to LipDH *in vitro*. LipDH (2 U/µL) in the presence of NADH (20µmol/L) compared to NADH alone on emission wavelength from 420 to 560 nm. A, C, and E: component amplitudes (a1, a2, and a3, respectively). B, D and F: fluorescence lifetime (τ1, τ2 and τ3, respectively). * $p<0.05$ vs. NADH 20µmol/L.

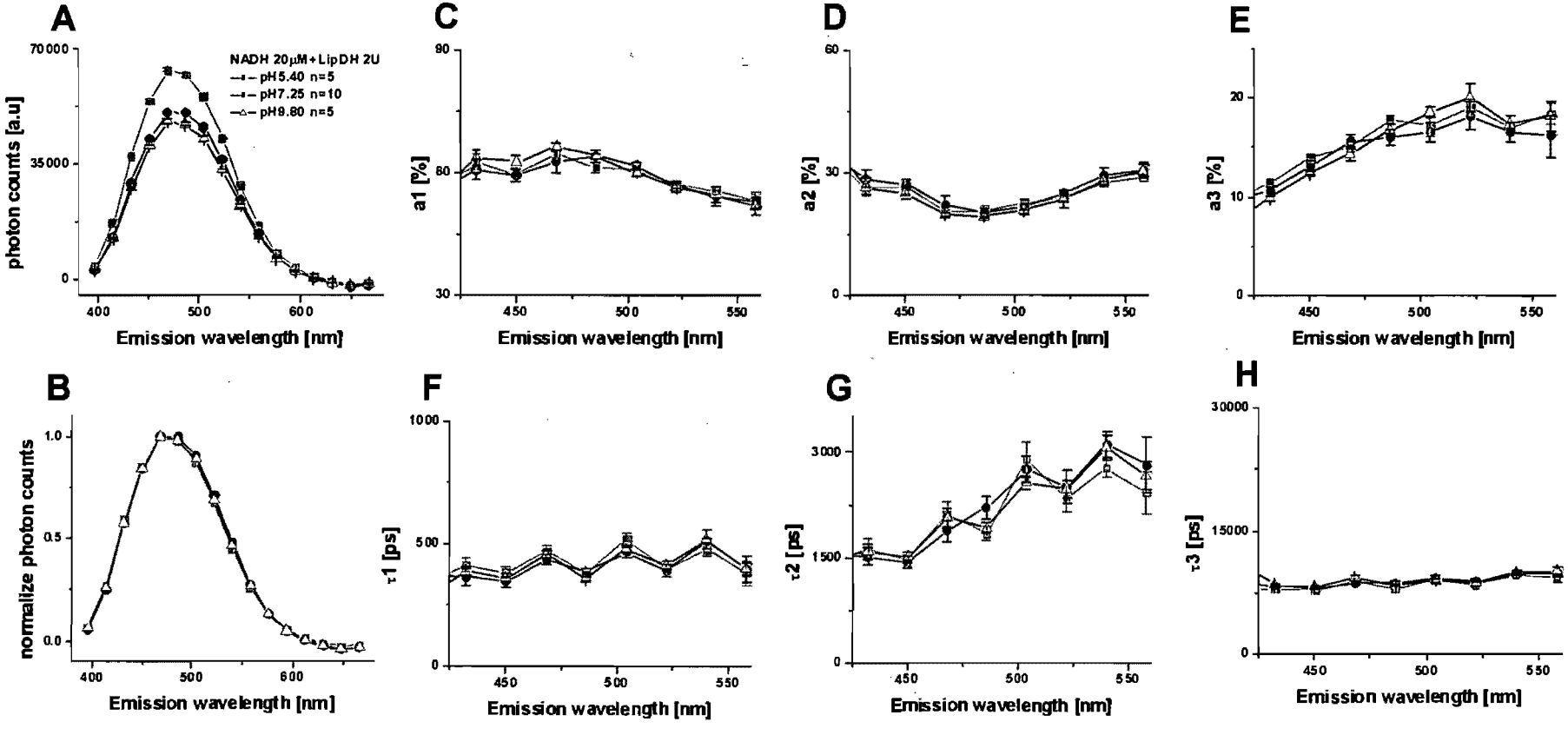

Figure 18: pH-dependence of NADH fluorescence decay kinetics after binding to LipDH *in vitro*. LipDH (2 U/µL) in the presence of NADH (20µmol/L) and 20µmol/L of NADH were compared in intracellular solution with modified pH (5.40, 7.25, or 9.80) on emission wavelength from 420 to 560 nm. A: NADH fluorescence spectra. B: Normalized spectra. C, D and E: component amplitudes (a1, a2, and a3, respectively). F, G and H: fluorescence lifetime (τ1, τ2 and τ3, respectively).

	Photon counts [a.u]	a_1	τ_1 [ps]	a_2	τ_2 [ps]	a_3	τ_3 [ps]	χ^2
	F_{max} [a.u.]	$a_1\tau_1$ [ns]	r_1	$a_2\tau_2$ [ns]	r_2	$a_3\tau_3$ [ns]	r_3	$<\tau>$ [ns] [ ]
NADH 5μM (5)	25900±130$^+$	68.4±1.6	398±32	22.0±1.5	1490±40	9.6±0.1	9630±55	1.00
	980±13$^+$	27.2±1.0	0.18±0.01	32.6±1.4	0.21±0.01	92.8±1.7	0.61±0.00	1.53±0.03
NADH 7μM (5)	31300±360$^+$	68.0±2.1	397±8.6	22.6±1.7	1600±103	9.4±0.5	9420±260	1.01±0.01
	1270±17$^+$	27.0±1.5	0.18±0.01	35.6±1.3	0.24±0.01	88.2±3.5	0.58±0.01	1.51±0.04
NADH 10μM (5)	37600±1300$^+$	73.8±1.1	443±25	17.4±1.1	1760±89	8.8±0.4	9700±340	1.01±0.01
	1520±69	32.7±2.0	0.22±0.01	30.3±1.7	0.21±0.01	84.6±2.2	0.57±0.02	1.48±0.02
NADH 20μM pH 5.4 (5)	73800±310	68.0±2.1	396±28	22.2±1.3	1520±41	10.0±0.7	8100±110	1.03±0.02
	3460±32	27.0±1.5	0.19±0.02	33.3±1.7	0.24±0.00	81.8±5.8	0.57±0.01	1.42±0.06
NADH 20μM (10)	63400±570	69.9±1.0	389±9.0	20.5±0.8	1460±54	9.8±0.2	8120±73	1.03±0.01
	2920±45	27.2±1.0	0.20±0.01	29.6±0.5	0.22±0.00	79.3±1.3	0.58±0.01	1.36±0.02
NADH 20μM pH 9.8 (5)	63400±1700	70.9±1.1	373±7.7	19.6±1.0	1390±52	9.2±0.2	8240±84	1.02±0.01
	3010±92	26.5±0.9	0.20±0.01	26.9±0.5	0.21±0.00	76.1±1.7	0.59±0.01	1.30±0.01
NADH 40μM (5)	106100±180$^+$	69.0±1.4	360±11	21.2±1.2	1310±64	9.8±0.1	7960±110	1.09±0.02
	5130±32$^+$	25.0±1.3	0.19±0.01	27.5±0.5	0.21±0.00	78.3±0.6	0.60±0.00	1.31±0.01
NADH20μM +LipDH 2u pH 5.4 (5)	65300±420	59.6±1.6	382±27	26.6±1.1	1480±98	14.0±0.5+	7780±130	1.02±0.01
	2410±34	23.0±2.2	0.13±0.01	38.7±0.5	0.23±0.01	110.0±2.9	0.64±0.01	1.71±0.04
NADH 20μM +LipDH 2u (5)	53800±320$^+$	59.4±1.6	345±22	27.2±1.2	1430±82	13.2±0.5+	8050±210	1.01±0.01
	2040±35	20.6±1.8	0.12±0.01	38.7±1.4	0.23±0.01	110.0±1.9+	0.64±0.01	1.65±0.032
NADH 20μM +LipDH 2u pH 9.8 (5)	51600±540$^+$	62.6±1.5	361±15	25.0±1.5	1500±77	12.4±0.2	8260±36	1.00
	1970±42	22.7±1.5	0.14±0.01	37.2±0.8	0.23±0.01	102.9±2.2	0.63±0.01	1.62±0.02
NADH 20μM +LipDH 1u (5)	69600±520	66.8±0.8	374±13	22.2±0.6	1470±22	11.1±0.4	8100±62	1.01±0.00
	3010±83	32.7±2.0	0.17±0.01	32.5±0.4	0.22±0.01	90.0±3.5	0.61±0.01	1.48±0.04

Table 3: Fluorescence parameters of NADH in the absence and in the presence of LipDH in intracellular solutions (λex/λem = 375 nm/450 nm). Total photon counts, fluorescence lifetimes (τ1 to τ3) and their relative amplitudes (a1 to a3) of free NADH in the absence and in the presence of 1U/μL to 2 U/μL LipDH, or in intracellular solution with modified pH (5.40, 7.25, or 9.80). In grey, maximum AF emission (P_{max}; time-resolved at $\Delta t = 0$ ns), calculated relative intensities and relative fractions for each component, as well as average lifetime. Data are shown as mean ± SEM, the number of experiments shown as (number of samples); $P < 0.05$: $^{+}$ vs NADH 20 μmol/L.

Definitions of Terms and Derived Quantities (See methods, section 2.2.4. for details)

3.2. Study of NAD(P)H fluorescence in living cardiomyocytes

This work is a part of study, which is a subject of paper in preparation by CHORVAT JR. D., CHENG Y., MATEASIK, A., BASSIEN-CAPSA V., ZANG W-J., AND CHORVATOVA A. entitled: Component analysis of NAD(P)H autofluorescence resolved by multi-wavelength fluorescence lifetime spectroscopy in living rat cardiomyocytes.

3.2.1. Distribution of NAD(P)H fluorescence

We studied endogenous NAD(P)H fluorescence directly in living cardiomyocytes. Mitochondrial distribution of the AF in myocytes was first verified by confocal microscopy. Images of NAD(P)H fluorescence were recorded by confocal laser scanning microscope (See methods. section 2.2.1. for details.) using excitation at 777 nm and 435-485 nm spectral range for emission detection. We observed that the emission AF of cardiomyocyte was principally distributed in stripes (Fig. 19), corresponding to cardiomyocyte mitochondria [99]. This result suggests that NAD(P)H fluorescence recorded in living cardiac cells has mainly mitochondrial origin.

3.2.2. Spectral and lifetime characteristics of NAD(P)H fluorescence

Spectrally and time-resolved NAD(P)H fluorescence decays were then recorded by TCSPC in living left ventricular cardiomyocytes bathed in basic external solutions (see an original recording at Fig. 11), following excitation of an elliptical spot (20 x 10 μm) of the cell (inset of Fig. 12C) by the 375 nm picosecond laser diode. Steady-state spectra of the cardiomyocyte AF, determined from the total photon counts on each spectral channel, had spectral maximum at 450 nm (Fig. 21A control). Gathered data were comparable to our previously published observations of NADH and /or NADPH fluorescence in intracellular solutions (see section 3.1.1 and Appendix I) [33]. Normalized emission spectra of the cardiomyocytes showed a ~20nm blue-spectral shift when compared to NADH *in vitro* (Fig. 20A), while being closer to those of NADPH (Fig. 20B). Analysis of exponential decay of cardiac myocytes AF for different lifetime pools showed acceptable chi-square values

(χ^2<1.2) and flat plot of weighted residuals when using at least a 3-exponential model. Three fluorescence lifetime pools were resolved at 450 nm: $\tau 1$ = 0.7±0.1 ns (69.3±1.0%), $\tau 2$ = 2.0±0.1 ns (27.6±0.9%) and $\tau 3$ = 12.7±0.1 ns (3.1±0.2%) (See Table 4 for data at λ_{em}= 450 nm, and for number of experiments). Maximum AF emission (Pmax), calculated the average lifetime (τ), relative intensity ($a_i\tau_i$) and relative fraction (r_i) for each lifetime pools were also assessed using mathematical analysis (see methods, section 2.2.4. for details, and Table 4 for calculated values). The gathered values were comparable to previous study of the steady-state kinetics of NADH fluorescence lifetime pools in cardiac mitochondria by Blinova et al. [132]

Estimated lifetimes were dependent on emission wavelength within the 420-560 nm spectral range (Fig. 22). Both, the 1st the 2nd lifetime pool exhibited a slight decrease, while that of the 3rd one presented a slight increase at longer wavelengths (Fig.22 B, D and F, control). Besides, all three lifetime pools and their relative amplitudes were prolonged at spectral channels with low intensity of detected light (data not shown). Therefore, we evaluated data only for spectral channels which intensity reached threshold of 500 counts in maximum, i.e. within the spectral range of 420 nm to 560 nm. In control conditions, the relative amplitudes of all three lifetime pools changed only slightly in the analyzed spectral region (within 10 % fraction of the total population, Fig. 22A, C and E, and Table 4).

3.2.3. Inhibition of the mitochondrial respiratory chain

We next tested spectral and lifetime characteristics of cardiomyocyte AF following inhibition of the mitochondrial respiratory chain activity. NADH is the main electron donor necessary for creation of the electrochemical gradient in cardiac mitochondria, used in the process of oxidative phosphorylation for ATP formation. As this process is initiated by dehydrogenation of NADH at the Complex I of the mitochondrial respiratory chain, we have therefore analyzed whether inhibition of Complex I activity is capable of affecting fluorescence spectral and/or lifetime characteristics of steady-state NAD(P)H fluorescence in cardiomyocytes. Application of Rotenone (1μmol/L for 5-20 min), the inhibitor of the

Complex I of the mitochondrial respiratory chain [51, 59, 158], induced a significant increase in the steady-state cardiomyocyte AF intensity (Fig. 21A), in accordance with the rise in free mitochondrial NADH content following restriction of the respiratory chain. Normalized AF spectra in control conditions and in the presence of Rotenone were identical (Fig. 21B), suggesting same molecular contributors. Rotenone significantly shortened fluorescence lifetimes of the 1st and 2nd lifetime pool in living cardiomyocytes (See original recording at Fig. 21C and D, 22B and D, as well as assessed values in Table 4), while having tendency to increase the relative amplitude of the 1st and lowering the one of the 2nd lifetime pool (not significant) (Fig.22A and C, Table 4). Each lifetime pool was also assessed by examining its relative intensity, as well as relative fraction (gray in Table 4, see Methods, section 2.2.4. for details). This assessment revealed a significant decrease in the relative intensity of the 2nd lifetime pool in the presence of Rotenone, leading to reduced average lifetime (see Table 4, τ and $a_2\tau_2$ for Rotenone). However, relative fractions of all three components remained unchanged.

To insure that NAD(P)H, accumulated after application of Rotenone, is not used by other dehydrogenases of the respiratory chain, we have also questioned the effect of Na-cyanide, an inhibitor of the complex IV of the respiratory chain [49]. Both Rotenone and cyanide are inhibitors of respiratory chain. But while Rotenone inhibits NADH dehydrogenase at Complex I, cyanide, on the other hand, blocks cytochrome oxidase at Complex IV. This prevents both coupled and uncoupled respiration with all substrates, including NADH and succinate that can reduce the FAD fluorescence, induced in living cardiomyocyte by visible light [99]. Addition of Na-cyanide (4mmol/L) to cells alone, or in the presence of Rotenone, had no significant effect on the AF dynamics when compared to Rotenone (Fig. 21E and F, Table 4). This result indicates that accumulation of NADH following inhibition of Complex I by Rotenone is not significantly affected by other dehydrogenases of the respiratory chain. The effect of Rotenone in cardiomyocytes was comparable to that observed in the presence of cyanide by other authors[38]. This effect is in agreement with the shortening of fluorescence lifetimes identified in adipocytes [159],

although no change in fluorescence decays was found in liver mitochondria [126] following application of the inhibitor. Therefore, the application of Rotenone is an appropriate means to isolate events related to the Complex I activity in cardiomyocytes.

3.2.4. Stimulation of NADH dehydrogenation by uncoupling of ATP synthesis

To promote NADH dehydrogenation to NAD^+ by the Complex I, we have used DNP. DNP is an uncoupling agent, which uncouples oxidative phosphorylation by carrying protons across the mitochondrial membrane, thereby destroying the proton gradient that drives oxidative phosphorylation. This leads to rapid consumption of energy without generation of ATP [50, 98]. Application of DNP (50μmol/L) was intended to stimulate NADH dehydrogenation to NAD^+ by Complex I of the respiratory chain. As expected, DNP significantly decreased the steady-state AF intensity in cardiomyocyte (Fig. 21A), in accordance with higher NADH dehydrogenation rate. Interestingly, after normalization, spectral broadening towards red spectral region of about 20 nm was observed in the presence of the uncoupler (Fig. 21B). The spectral broadening recorded in cardiomyocytes after application of DNP was comparable, but broader than the one observed for NADH in the presence of LipDH *in vitro* (Fig. 16B). At spectral maximum of 450 nm, both the value of 1st fluorescence lifetime pool and the relative amplitude of the 3rd one were significantly increased in the presence of the DNP when compared to control conditions or the presence of Rotenone, leading to significantly increased relative intensities and average lifetime (Fig. 21C, 22Band E, Table 4). Furthermore, the relative fractions of the 2nd and 3rd lifetime pools were also modified by DNP (Table 4). At 504 nm, we have also found significantly increased fluorescence lifetime of the 2nd pool (Fig. 22D). When compared to Rotenone, all fluorescence lifetimes were prolonged, resulting in higher relative intensities and thus increased average lifetime (Figures 22B, D and F, Table 4).

Effects of DNP on spectral amplitude, determined as total photon counts, was comparable to that of FCCP, an uncoupling agent, described previously in cardiac tissue [38]. Both of DNP, CCCP or FCCP are uncoupling agents. CCCP and FCCP are very powerful mitochondrial uncoupling agent, a tiny amount of them can catalyze the movement of huge

numbers of protons, and short-circuit the respiratory chain, leading to lower fluorescence signals, and decreased in the signal/noise ratio [38]. We have opted for DNP in the present studies, but recording of changes following application of FCCP or CCCP should be also tested in future.

3.2.5. Modulation of NADH production in living cardiomyocytes

As mentioned in previous chapters (see section 1.1.2.), substrates availability is able to modulate the rate of acetyl-CoA production in TCA cycle, leading to change in the production of mitochondrial and/or cytosolic NADH. Fatty acid β-oxidation and pyruvate oxidation are two major sources of acetyl-CoA formation in TCA cycle. Modulation of these two control points therefore alters the NADH/NAD^+ ratio in the cells.

NADH is known to be produced by mitochondria in the TCA cycle. To promote NADH production in cardiomyocytes, we have administered BHB (3mmol/L) in basic extracellular solution in the presence of different concentrations of AcAc: 150μmol/L (ratio 20:1) to favor NADH production and 1.5mmol/L (ratio 2:1), closer to physiological conditions [29]. In cardiac tissue, NADH used by the respiratory chain is produced from the acetyl-CoA formed by the fatty acid oxidation entering the citric acid cycle and is strongly dependent on appropriate balance of fatty acids, carbohydrates and ketone bodies utilization [17]. BHB oxidized into AcAc is producing NADH dependently on the BHB/AcAc ratio [29]. As expected, the BHB/AcAc ratio of 2:1 induced no significant change in AF of cardiomyocytes when compared to control conditions (Fig.23A). However, increasing the ratio to 20:1, condition favorable to NADH production, led to significant rise in the cardiomyocyte AF intensity (Fig. 23A), in accordance with the higher in free NADH concentration in cardiomyocyte mitochondria. This effect did not affect the emission spectral shape (Fig. 23B), or fluorescence lifetime pools (Fig. 24 A-F and Table 4).

We have also tested effect of NADH utilization by promoting fatty acid β-oxidation. Octanoate (4mmol/L), a medium chain fatty acid is completely oxidized through the mitochondrial β-oxidation and respiration pathways [25, 26]. Surprising, application of

Octanoate did not significantly affect the steady-state emission spectra or the lifetimes of cardiomyocyte AF (Fig. 23C and D, Table 4).

Application of lactate and pyruvate, which activate PDH activity by rising acetyl-CoA production in TCA cycle, are capable of inducing cytosolic NAD(P)H redox changes, hence elevating cytosolic NADH level, as well as cytosolic NADH/NAD^+ ratio. This experiment was designed to confirm preferential mitochondrial contribution of AF. Addition of lactate (1mmol/L) in the presence of pyruvate (100μmol/L), should therefore not significantly affect the steady-state emission spectra or the lifetimes of cardiomyocyte AF. Indeed, these were exactly gathered results (Fig.23E and F, table 4), indicating that the cytosolic NADH is not likely to significantly contribute to the recorded fluorescence signal. Instead, the observed AF signal is primarily resulting from mitochondrial NAD(P)H.

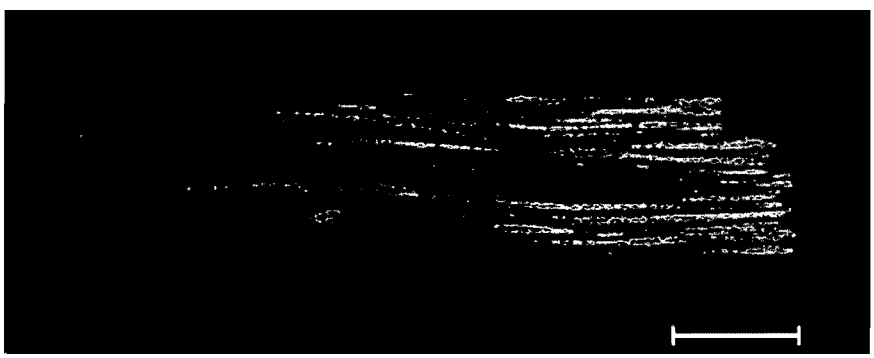

Figure 19: Confocal image of NAD(P)H fluorescence in one cardiac cell. Two-photon excitation with 777 nm emission laser, HFT KP 700/488 dichroic filter and 450-470 nm spectral range for emission detection.

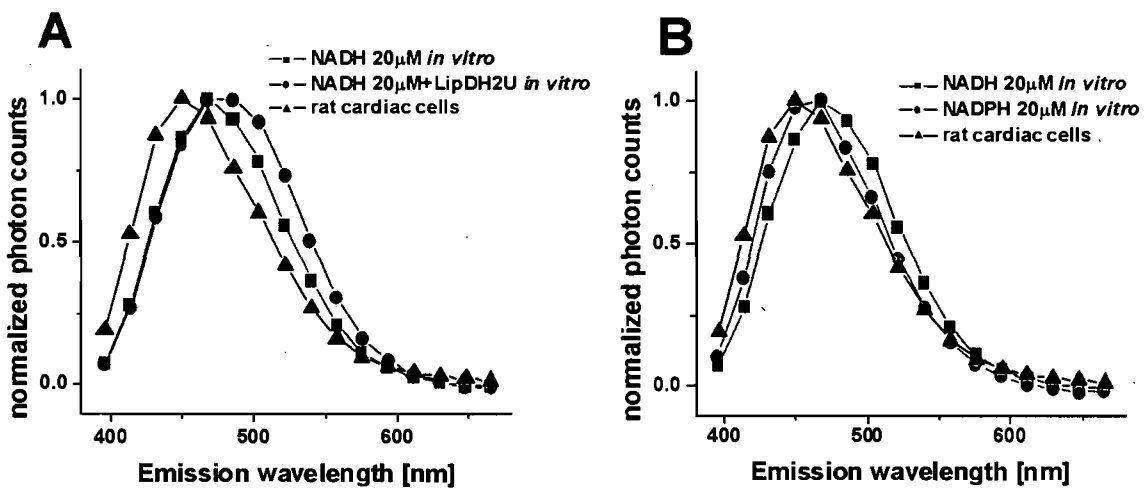

Fig. 20: NAD(P)H fluorescence spectral characteristics in living cardiomyocytes. A: Normalized emission spectra of cardiac cells compared to NADH (20µmol/L) in the absence and in the presence of LipDH (2U/ml) *in vitro.* B: Normalized emission spectra of cardiac cells compared to NADH (20µmol/L) and NADPH (20µmol/L) *in vitro.*

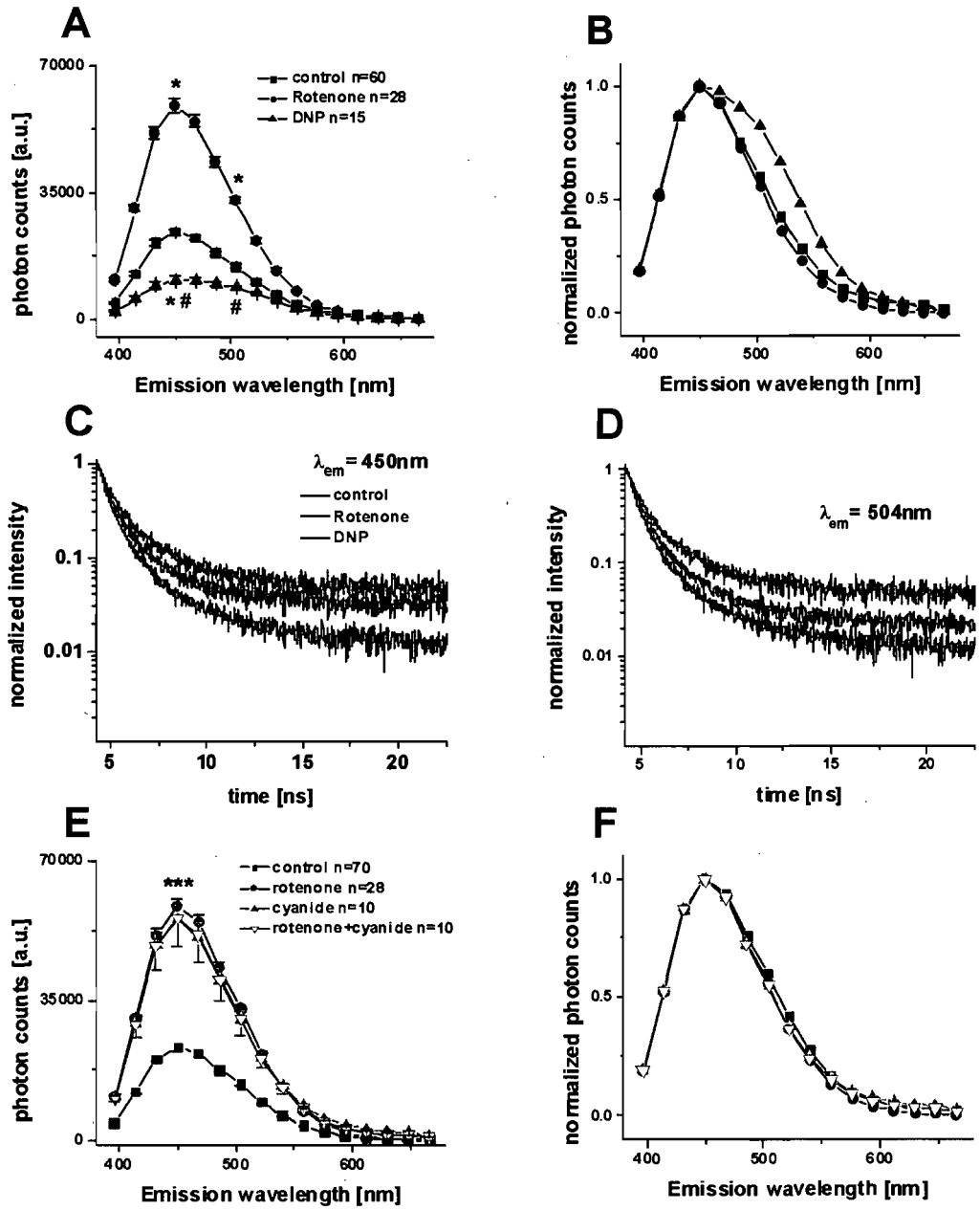

Figure 21: Steady-state NAD(P)H fluorescence in living cardiomyocytes following application of the modulators of respiratory chain. Steady-state (A) and normalized (B) fluorescence spectra and fluorescence decay (C: λ = 450 nm, D: λ = 504 nm) following application of Rotenone (1µmol/L) or DNP (50µmol/L), respectively. E-F: Steady-state and normalized AF spectra following application of Na-cyanide (5mmol/L) alone, or in the presence of Rotenone (1µmol/L), *p< 0.05 vs. control, #p<0.05 vs. Rotenone.

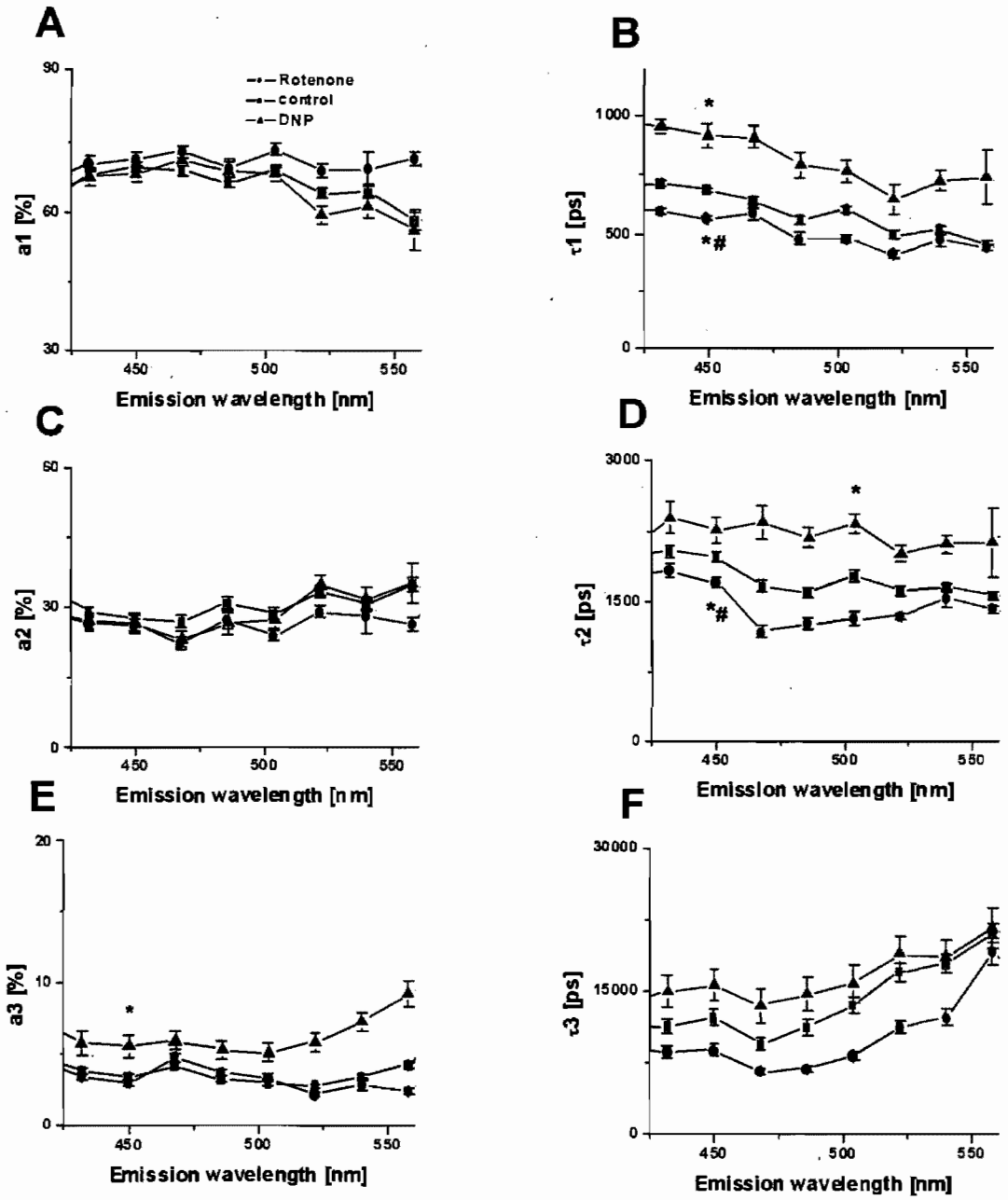

Figure 22: NAD(P)H fluorescence lifetimes and their relative amplitudes following application of Rotenone and DNP. A, B and C: Lifetime pool relative amplitudes (a1, a2 and a3, respectively), D, E and F: fluorescence lifetimes (τ1, τ2 and τ3, respectively) estimated in control condition and in the presence of Rotenone (1μmol/L) or DNP (50μmol/L), *p< 0.05 vs. control, #p<0.05 vs. Rotenone.

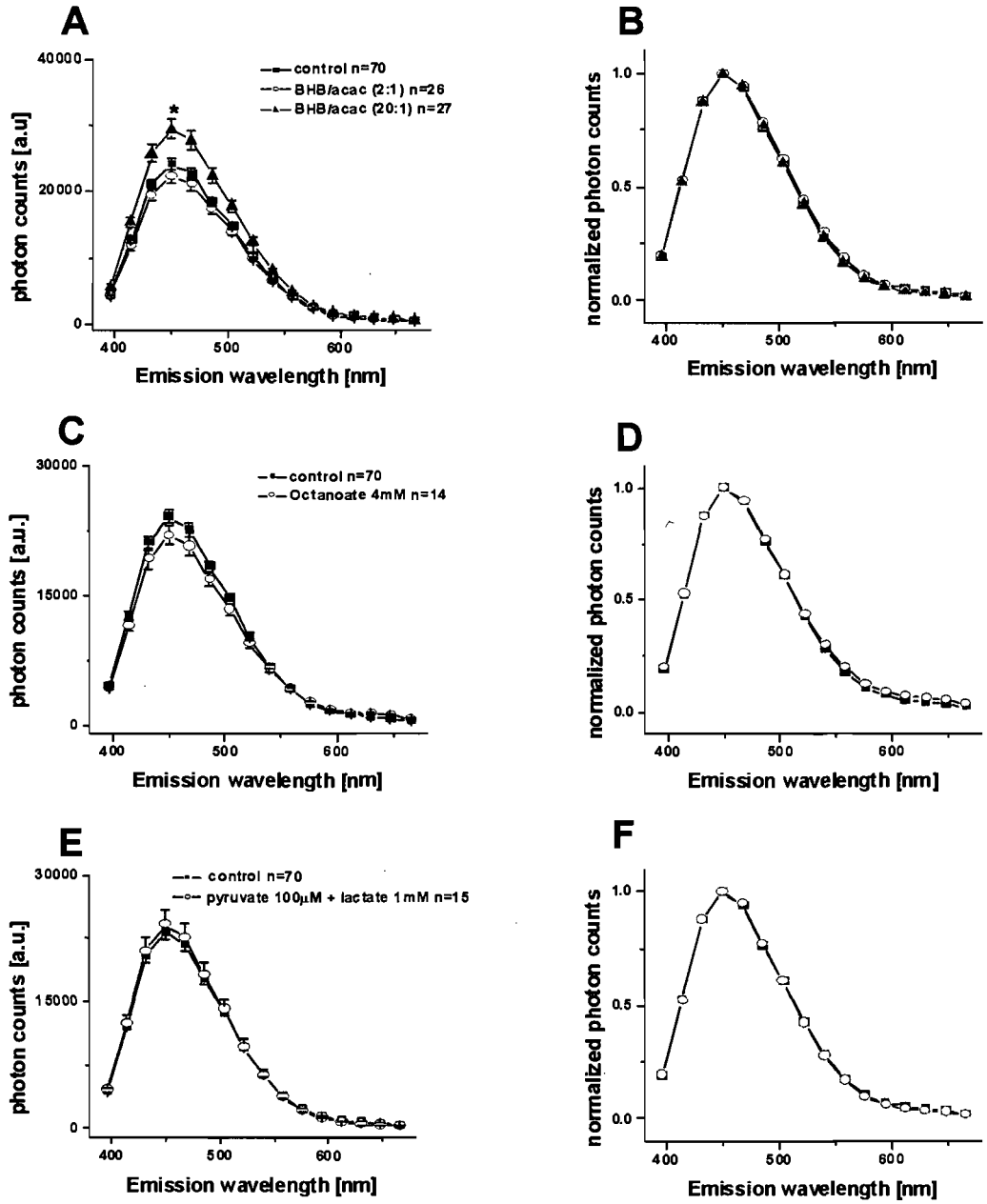

Figure 23: Steady-state NADH fluorescence spectra in living cardiomyocytes following application of metabolic substrates. A-B: Steady-state and normalized spectra following application of BHB/AcAc (2:1) and BHB/AcAc (20:1). C-D: Steady-state and normalized spectra following application of Octanoate(4mmol/L). E-F: Steady-state and normalized spectra following application of pyruvate (100µmol/L) and lactate (1mmol/L), *$p<0.05$ vs. control.

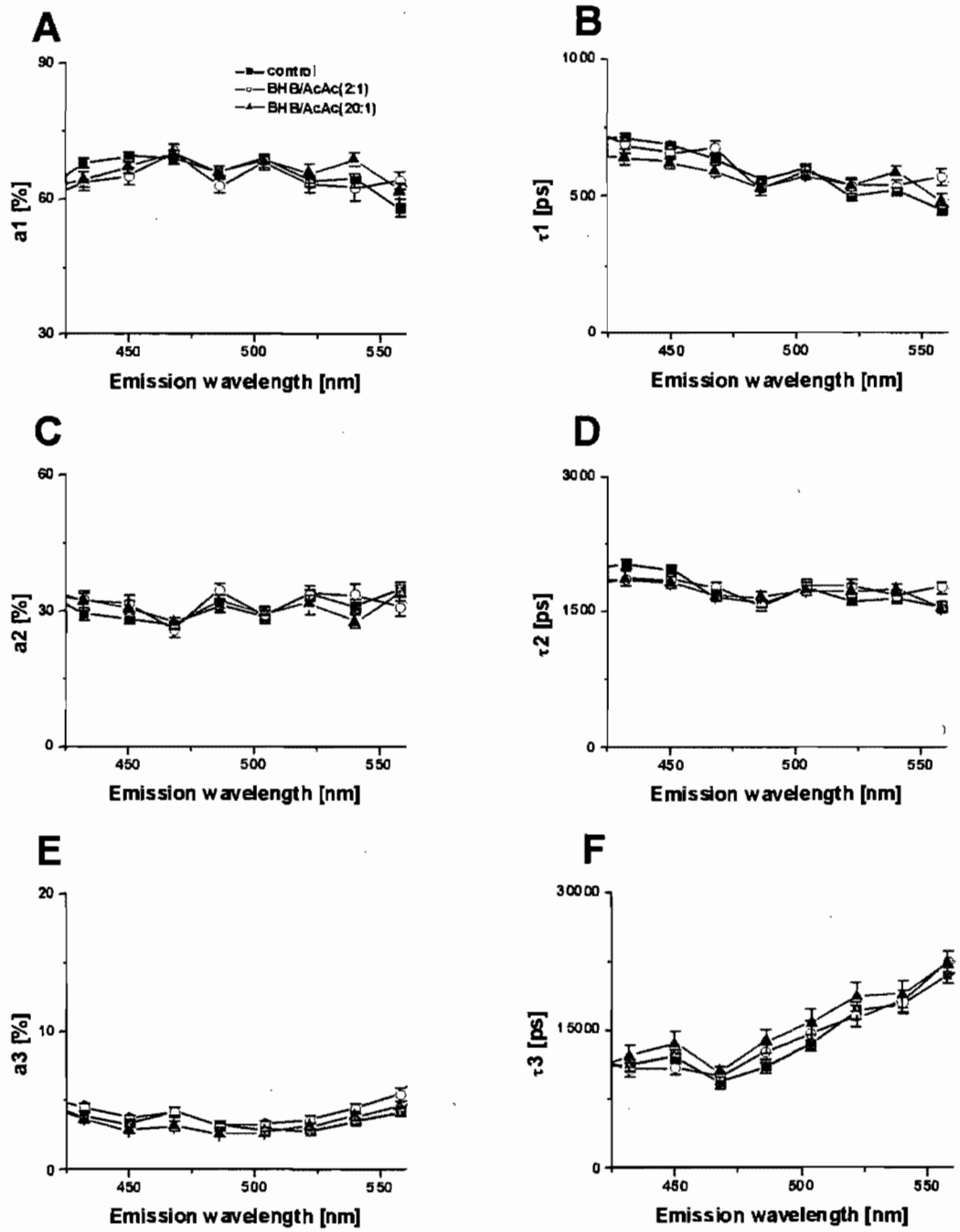

Figure 24: NAD(P)H fluorescence lifetimes and their relative amplitudes following application of BHB/AcAc (2:1) and BHB/AcAc (20:1). A, C and E: Lifetime pools relative amplitudes (a1, a2 and a3, respectively), B, D and F: fluorescence lifetimes (τ1, τ2 and τ3, respectively).

	Photon counts [a.u.]	a_1	τ_1 [ps]	a_2	τ_2 [ps]	a_3	τ_3 [ps]	χ^2
	P_{max} [a.u.]	$a_1\tau_1$ [a.u.] [*10^3]	r_1	$a_2\tau_2$ [a.u.] [*10^3]	r_2	$a_3\tau_3$ [a.u.] [*10^3]	r_3	$\langle\tau\rangle$ [ns]
Control (70/13)	23200±790	69.3±1.0	690±11	27.6±1.0	2030±52	3.1±0.2	12700 ±780	1.02±0.01
	1550±68	48.0±1.3	0.36±0.01	53.6±1.0	0.40±0.01	32.7±1.7	0.24±0.01	1.34±0.03
Rotenone (28/6)	58900±1800*	71.0±1.6	560±10*+	26.3±1.5	1700±57*	3.0±0.2+	8800±650	1.05±0.01
	3570±160*	40.5±1.5	0.36±0.02	42.5±1.0*+	0.40±0.01	23.1±1.1	0.22±0.01	1.06±0.01*
Cyanide (10/2)	55400±7000*	68.8±1.3	486±13*+	28.8±1.2	1600±55*+	2.5±0.2+	9400±1300	1.01±0.01
	3640±470*	33.6±1.4*	0.33±0.01	45.2±1.3	0.45±0.01	21.7±1.0+	0.22±0.01	1.00±0.02*
Rotenone/cyanide (10/2)	55600±3600*	72.3±1.8	556±16	25.0±1.6	1690±91	2.7±0.3	8500±700	1.05±0.02
	3760±230*	40.4±2.1	0.39±0.02	41.0±0.7*	0.40±0.01	21.2±1.4	0.21±0.02	1.03±0.01*
DNP (15/3)	10800±990*#	67.3±1.7	901±55*#	27.1±1.7	2160±120#	5.6±0.8*#	15800±1800#	1.01±0.01
	770±95*#	60.5±3.7*#	0.32±0.02	59.1±5.2#	0.31±0.02*#	74.6±7.2*#	0.38±0.02*#	1.94±0.12*#
BHB (9/1)	32000±3100*$^{\&}$	64.0±4.2	526±78*	33.0±3.5	1580±200*	3.2±0.9	10100±2700	1.00±0.01
	1970±550$^{\$}$	33.7±6.0*	0.29±0.04	51.8±5.2	0.45±0.03	30.5±7.1	0.26±0.04	1.16±0.04
BHB/AcAc (20:1) (27/4)	29300±1600*$^{\&}$	66.3±1.6	598±22	31.1±1.5	1800±65	2.8±0.3	12600±1400	1.01±0.01
	1980±95$^{\$}$	40.1±2.20	0.32±0.02	54.4±1.3	0.44±0.01	30.1±1.2	0.24±0.01	1.24±0.02
BHB/AcAc (2:1) (26/4)	21500±1100	65.0±2.0	658±22	31.4±1.9	1860±65	3.7±0.3	10900±680	1.00
	1390±74	43.6±2.6	0.32±0.02	55.7±2.1	0.41±0.02	37.5±1.8	0.27±0.01	1.37±0.02
Lactate/pyruvate (15/3)	24100±1900	65.7±2.7	656±24	30.9±2.3	1890±120	3.6±0.5	10400±2000	1.01±0.00
	1480±93	43.8±3.0	0.34±0.02	55.2±1.5	0.43±0.01	30.5±2.7	0.23±0.02	1.29±0.02
Octanoate (14/3)	22600±4400	68.8±1.7	649±21	28.1±1.8	1910±71	3.2±0.4	14400±1700	1.00
	1400±71	45.0±2.4	0.33±0.02	53.1±3.2	0.39±0.02	37.7±1.4	0.28±0.01	1.36±0

Table 4: Fluorescence parameters of rat cardiomyocytes AF (λex/λem = 375 nm/450 nm). Total photon counts, fluorescence lifetimes (τ1 to τ3) and their relative amplitudes (a1 to a3) of single cardiomyocytes in control conditions and in the presence of 1µmol/L Rotenone, 4mmol/L cyanide, 50µmol/L DNP, 3mmol/L BHB with 150µmol/L or 1.5mmol/L AcAc (ratio 20:1 and 2:1 respectively), lactate (1 mmol/L) in the presence of pyruvate (100µmol/L) or Octanoate (1mmol/L). In grey, maximum AF emission (P_{max}; time-resolved at $\Delta t = 0$ ns), calculated relative intensities and relative fractions for each component, as well as average lifetime. Data are shown as mean ± SEM, the number of experiments shown as (number of cells/number of animals); *$p<0.05$ vs. control, $^{\#}p<0.05$ vs. Rotenone, $^{\&}p<0.05$ vs. BHB/AcAc (ratio 2:1)

3.2.6. NAD(P)H fluorescence in cardiomyocytes under ischemia-mimicking conditions

As mentioned in introduction (section 1.1.7.), myocardial ischemia is a pathological condition resulting in reduced ATP formation from oxidative phosphorylation, and alternatively promotes the production of anaerobic ATP and lactic acid by glycolysis to maintain ATP level. This leads to accumulation of cytoplasmic NADH with the $NADH/NAD^+$ ratio increasing several-fold, accompanied by accumulation of lactate and H^+ in the cell [72-74]. Ischemia is also known to induce a rise in NADH fluorescence in cardiac tissue [160] at a rapid (minute-based) scale. To test the sensitivity of cardiomyocyte AF parameters to ischemia-like metabolic changes, we have therefore compared kinetics of NAD(P)H fluorescence in living cardiomyocytes in normoxic conditions (control) to ischemia-mimicking ones, induced at physiological temperatures by reducing cell pH and oxygen content (see 2.1.3. ischemia-mimetic solutions for details) [161]. After exposure of cardiomyocytes to these conditions for 5-10 min, steady-state AF was significantly increased (Fig. 25A), while no change was observed in normalized spectral shape (Fig. 25B). Fluorescence lifetimes and their relative amplitudes were not significantly affected (Table 5) when compared to control normoxic conditions.

Inhibition of the mitochondrial respiratory chain with Rotenone induced comparable changes of AF in ischemia-mimicking conditions as in normoxia (Fig. 25C and D, 26A-F), except that it failed to significantly modify the fluorescence lifetimes (Fig.25B, D and F, Table 4). This result can be also related to lower number of experiments performed in control vs. ischemia-mimicking conditions. Despite this fact, the average fluorescence lifetime was significantly decreased as a result of concerted changes of several parameters (Table 5). In the presence of DNP, the fluorescence intensity failed to decrease (Fig. 25E) and the spectral broadening was no longer present (Fig. 25F). This result can be due to modification in the mitochondrial membrane structure during ischemia, preventing the binding of the uncoupler. 1^{st} and 3^{rd} fluorescence lifetimes were significantly prolonged in ischemia-mimetic solution in the presence of DNP, leading to a significant increase in average lifetime (Fig. B and F, Table 5).

Furthermore, we have estimated the percentage of nucleotides that have capacity to be oxidized in cardiac cells using the effect of modulators of mitochondrial respiratory chain described in chapter 1.1.4. Considering that the cell is working in fully-reduced conditions in the presence of Rotenone and in fully-oxidized ones in the presence of DNP, or in other words that cardiomyocyte is working close to its maximum (100%) capacity in the presence of DNP and minimum (0%) capacity in the presence of Rotenone, we have estimated the percentage in the nucleotides that have capacity to be oxidized at a specific moment of time from the total photon count as:

$$S_{oxidized} = (S_{fully\_reduced} - S)/(S_{fully\_reduced} - S_{fully\_oxidized}) = (S_{rotenone} - S_{control})/S_{rotenone} - S_{DNP}) \quad (19)$$

Using this equation at spectral maximum of 450 nm, our data indicate that in control, normoxic conditions, the mitochondrial respiratory chain oxidizes about 82 % of total available NADH, while this activity is lowered to about 43 % in ischemia-mimetic solutions, in agreement with expected inhibition of the respiratory activity in this condition.

Our results indicate, in accordance with observations in hypoxic neuronal tissues [40], that increase in the NADH concentration inside mitochondria, rather than modification in the dehydrogenation rate is responsible for higher fluorescence values under ischemia-mimicking conditions. However, the limit of this experiment is that used solutions do not completely mimic the ischemia condition in the heart. To improve this experiment in the future, we need to expose cells to ischemia condition at different time-scale (extending to an hour-exposure, for example) induce ischemia using external perfusion at physiological temperatures and/or provoke ischemic insult directly in the whole heart.

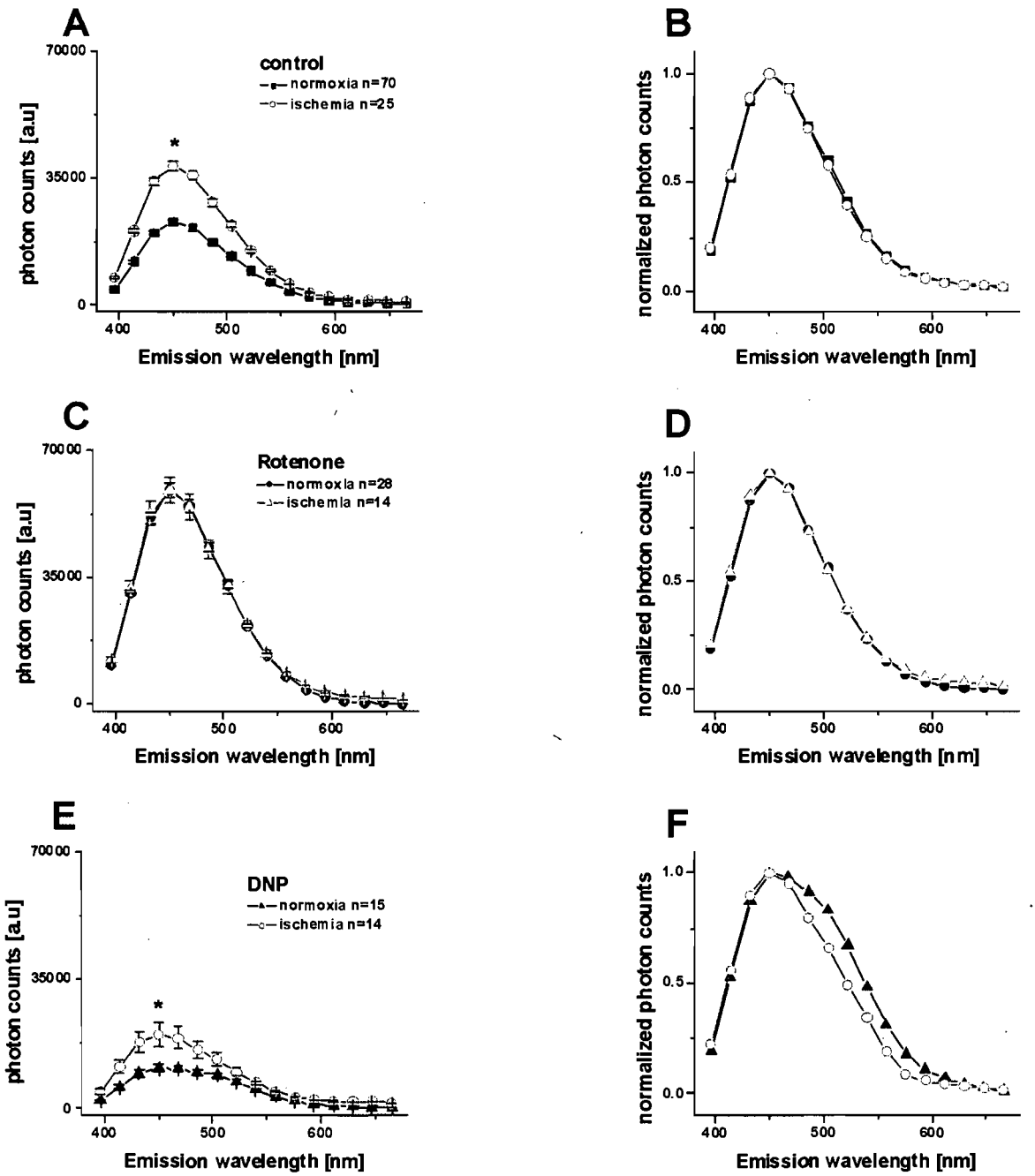

Figure 25: Steady-state NAD(P)H fluorescence spectra of cardiomyocytes under ischemia-mimicking condition. A, C and E: Steady-state emission spectra compared between normoxic and ischemic conditions in control, and in the presence of Rotenone (1μmol/L) or DNP (50μmol/L), respectively. B, D and F: normalized spectra in the studied condition. * $p<0.05$ vs. normoxia.

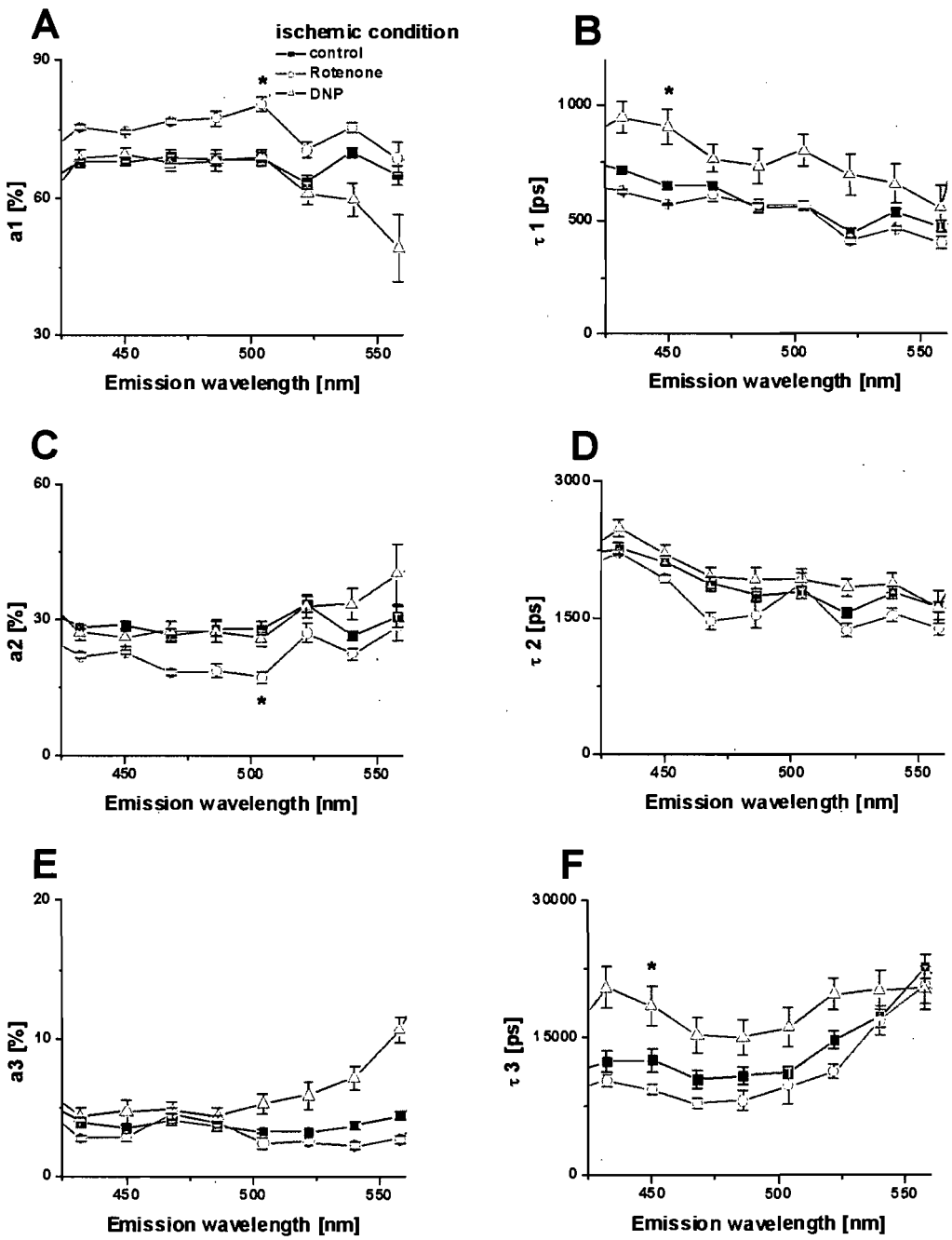

Figure 26: NAD(P)H fluorescence lifetimes and their relative amplitudes in ischemia-mimicking conditions. A, C and E: Relative amplitude (a1, a2 and a3, respectively). B, D and F: Fluorescent lifetimes (τ1, τ2 and τ3, respectively) following application of Rotenone (1μM) or DNP (1μM). * $p<0.05$ vs. control.

	Total photon counts [a.u.]	a_1	τ_1 [ps]	a_2	τ_2 [ps]	a_3	τ_3 [ps]	χ^2
	P_{max} [a.u.]	$a_1\tau_1$ [a.u.] [*10^3]	r_1	$a_2\tau_2$ [a.u.] [*10^3]	r_2	$a_3\tau_3$ [a.u.] [*10^3]	r_3	$<\tau>$ [ns]
Control (25/4)	49500±1400*	68.0±0.9	651±17	28.7±0.8	2120±55	3.4±0.3	12500±1300	1.01±0.01
	2010±81	44.5±1.6	0.31±0.01	60.1±1.4	0.42±0.01	40.0±4.9	0.26±0.02	1.45±0.05
Rotenone (14/3)	70000±3700$	74.4±0.5	570±6	22.8±0.3	1930±44	2.9±0.3	9300±560	1.09±0.04
	3800±1200$	42.4±0.6	0.38±0.00	43.8±0.9$	0.39±0.01$	25.3±0.9	0.23±0.01	1.12±0.01$
DNP (11/3)	25100±1300$	69.2±1.4	979±85$	25.6±2.0	2220±140	5.4±1.0	19600±2600$	1.03±0.02
	743±69$	68.5±6.7$	0.32±0.02	57.7±6.3	0.29±0.04$	86.3±13$	0.39±0.03$	2.12±0.16$

Table 5: Fluorescence parameters of cardiomyocytes AF in ischemia-mimetic solutions (λex/λem = 375 nm/450 nm). Total photon counts, fluorescence lifetimes (τ1 to τ3) and their relative amplitudes (a1 to a3) of single cardiomyocytes in control conditions and in the presence of 1 µmol/L Rotenone, or 50µmol/L DNP. In grey, maximum AF emission (P_{max}; time-resolved at $\Delta t = 0$ ns), calculated relative intensities and relative fractions for each component, as well as average lifetime. Data are shown as mean ± SEM, the number of experiments shown as (number of cells/number of animals); **$p<0.05$ vs. control in normoxia (Table 4), $^{\#}p<0.05$ vs. Rotenone, $^{\$}p<0.05$ vs. control in ischemia-mimetic conditions.

3.3. Investigation of NAD(P)H fluorescence in living cells from human endomyocardial biopsies

Parts of this study have been published in CHENG Y., DAHDAH N., POIRIER N., MIRO J., CHORVAT D. JR., CHORVATOVA A., 2007: Spectrally and time-resolved study of NADH autofluorescence in cardiomyocytes from human biopsies. ***Proceedings of SPIE, the International Society for Optical Engineering Vol. 6771,*** Advanced Photon Counting Techniques II: 677104-1 to 677104-13, see attached Appendix II.

3.3.1. Isolation of living cardiac cells from endomyocardial biopsies

Isolation of cardiac cell from living human tissue is still rather rare procedure. We therefore first needed to establish an appropriate isolation procedure to gather living human cardiomyocytes. We initially used modified procedure from Guinamard *et al.* [151](Approach I, see section 2.1.2 for details). However, using this approach, the yield of the isolated cardiomyocytes was not sufficient, about 2-10 cells/isolation, and sometimes the procedure failed completely. Cell morphology was not sustained, less than 5% rod-shaped and cross-striated cells were found. We believe that this can be due to the fact that this procedure was originally designed for electrophysiological measurements. In our experimental conditions, in the absence of voltage-clamp, the ionic strength applied to the cell is therefore likely to depolarize it. This may have resulted in hypercontraction, despite the presence of BDM in the external media. Furthermore, we also advance that lack of calcium in isolation solution hampered enzymatic activity of the collagenase. In order to increase cardiomyocyte yield and viability and minimize cell damage, and therefore improve the quantity and the quality of isolated cells, we have applied the Approach II, which was a modification of the procedure from Peeters *et al.* [152]. This solution is based on Tyrode solution which is designed for contraction studies. In this case, 50μmol/L of calcium was presented in the dissociation media to enhance the proteolytic activity of the enzyme. Using this method, we were capable to isolate 10-20 cardiomyocytes/isolation, which were rod-shaped and with clearer striations.

We noted following main factors due to which isolation of cardiomyocytes can lead

to low yield of isolated rod-shaped and cross-striated cells: (1) variability of the obtained biopsy fragment due to patient's condition variation. This was the case when the biopsy sample was taken from cardiac papillary muscles or tendons. It was also the case when the biopsy was not taken deep enough, in which case the color of the sample was white, meaning that not enough myocardium available in the specimen. However, this part of the procedure is fully dependent on the operation and on the surgeon, and constitutes therefore limitation of the study. (2) The severe cardiomyocytes damage that occurred during cell isolation process is thought to be caused by prolonged exposure of the cells to protease and lack of calcium for enzymatic activity of collagenase. However, collagenase itself caused minimal cell injury. Over-digestion decreases the yield of viable cells and increases the number of severely damaged cells. Choice of right protease and collagenase concentrations, slicing the biopsy fragment into thin sections, as well as presence of low concentration of calcium reduced over-digestion process of superficial myocardial and speeded the dissociation process, which resulted in minimization of cells damage. (3) Selection of medium was also crucial in the isolation of human cardiomyocytes. High potassium salt solution (Approach I) produced lesser yield of cardiomyocytes, in agreement with previous finding [152].

Interestingly, steady-state spectra of human cardiomyocytes AF (Fig. 27A), normalized spectral shape (Fig. 27B), as well as fluorescence lifetime (data not show) were not significantly different between the two cardiomyocyte isolating procedures, suggesting that cells isolated by both procedures are viable materials.

3.3.2. NAD(P)H fluorescence in human cells: comparison to rat

After gathering spectrally and time-resolved data of AF decay in human cells, we intended to make their comparison to models that are more commonly used for study of metabolic activity of cardiac cells, such as the rat one. When compared to ventricular cardiomyocytes of rats, which were isolated from fragments of heart tissue by the same experimental approach as used for human biopsy (see section 2.1.2.), we found significantly smaller total photon counts in human cardiomyocytes (Fig. 27C).

Fluorescence decay was slower in human than in rat cells. This result was accompanied by significantly smaller relative amplitude of the 1st lifetime pool, against significantly higher relative amplitude of the 2nd lifetime pool (Fig. 28A and C). We also noted that the 2nd and 3rd lifetimes have tendency to increase in human cells, but this change was not significant (Figs. 28D and F, Table 6). We hypothesize that this result can be related to lower amount of NAD(P)H present in human cells due to higher metabolic activity of mitochondrial respiration and thus to more substantial ATP production. As expected, application of Rotenone increased the total photon counts of the human cells (Fig. 27C), while modifying fluorescent decays (Fig. 27E) by significantly rising amplitude of 1st lifetime pool and decreasing the 2nd one. Rotenone had also tendency of decreasing the amplitude of 3rd lifetime pool (Figs. 28A, C and E, Table 6). These data point to possible higher metabolic activity in control conditions in human cells, when compared to commonly used rat model. However, a more profound study of human cardiomyocytes AF is needed in the future to avoid differences due to signal dependence on the cell size.

3.3.3. Study of NAD(P)H fluorescence in heart transplanted patients with different rejection grades

Once we recorded spectral and lifetime characteristics of human cardiomyocyte AF in control conditions, we wanted to estimate whether the developed method is also sensitive to its changes with different rejection stages. In accordance to classification of allograft rejection stages for heart transplantation (ISHLT) [93, 150], the allograft rejection of heart transplantation are classified on a scale of 4 histological grades, namely Grade 0R-no rejection; Grade 1R-mild rejection; Grade 2R-moderate rejection; and Grade 3R-severe rejection. Estimation of histological grade of rejection in our studies had been done using endomyocardial biopsy by pathologists at CHU Sainte-Justine. We have correlated gathered results with the rejection grade from total of 14 patients: 6 cases presented no rejection (R0), 4 cases showed mild rejection (R1), while grade of remaining 4 cases was not known. Therefore, NAD(P)H fluorescence of human cardiomyocytes was compared

between R0 and R1 grade. Comparison of human cardiomyocyte AF between R0 and R1 showed significantly increased fluorescence intensity (Fig. 29A), with no change in the spectra shape (Fig. 29B). Neither the fluorescence intensity, nor the normalized spectra shapes in responses to Rotenone were significantly modified between R0 and R1 (Figs. 29C and D). Fluorescence decays were not significantly changed between R0 and R1, or in response to Rotenone (Fig. 29E). Fluorescence lifetime pools and relative amplitudes of R1 when compared to R0, remained unchanged (Table 6). This result can be comparable to the effect of ischemia-mimic conditions, points to possible lesser metabolic activity in the presence of rejection. However, further study is needed to fully understand limits of this approach and it possible use for rejection diagnostics.

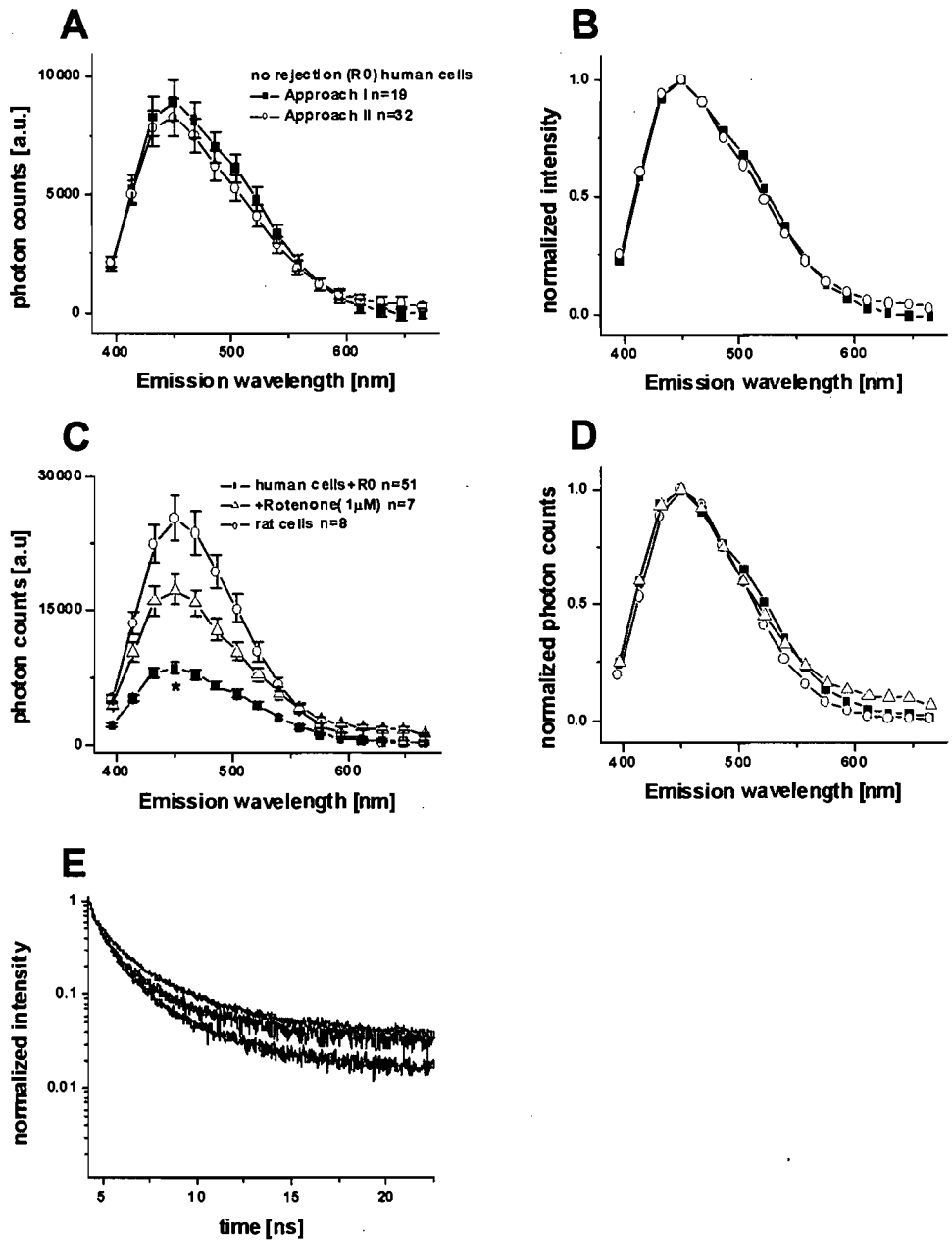

Figure 27: Steady-state NAD(P)H fluorescence of human cardiomyocytes isolated from EMB of pediatric heart transplanted patients. A-B: Steady-state and normalized spectra recorded in cardiomyocytes isolated by the two isolation methods, C, steady-state spectra, D, normalized spectra and E, fluorescence decays, recorded in human cells in control condition (R0) or in the presence of Rotenone (1µmol/L), and/or in rat cells isolated in the same conditions.*$p<0.05$ vs. rat cells.

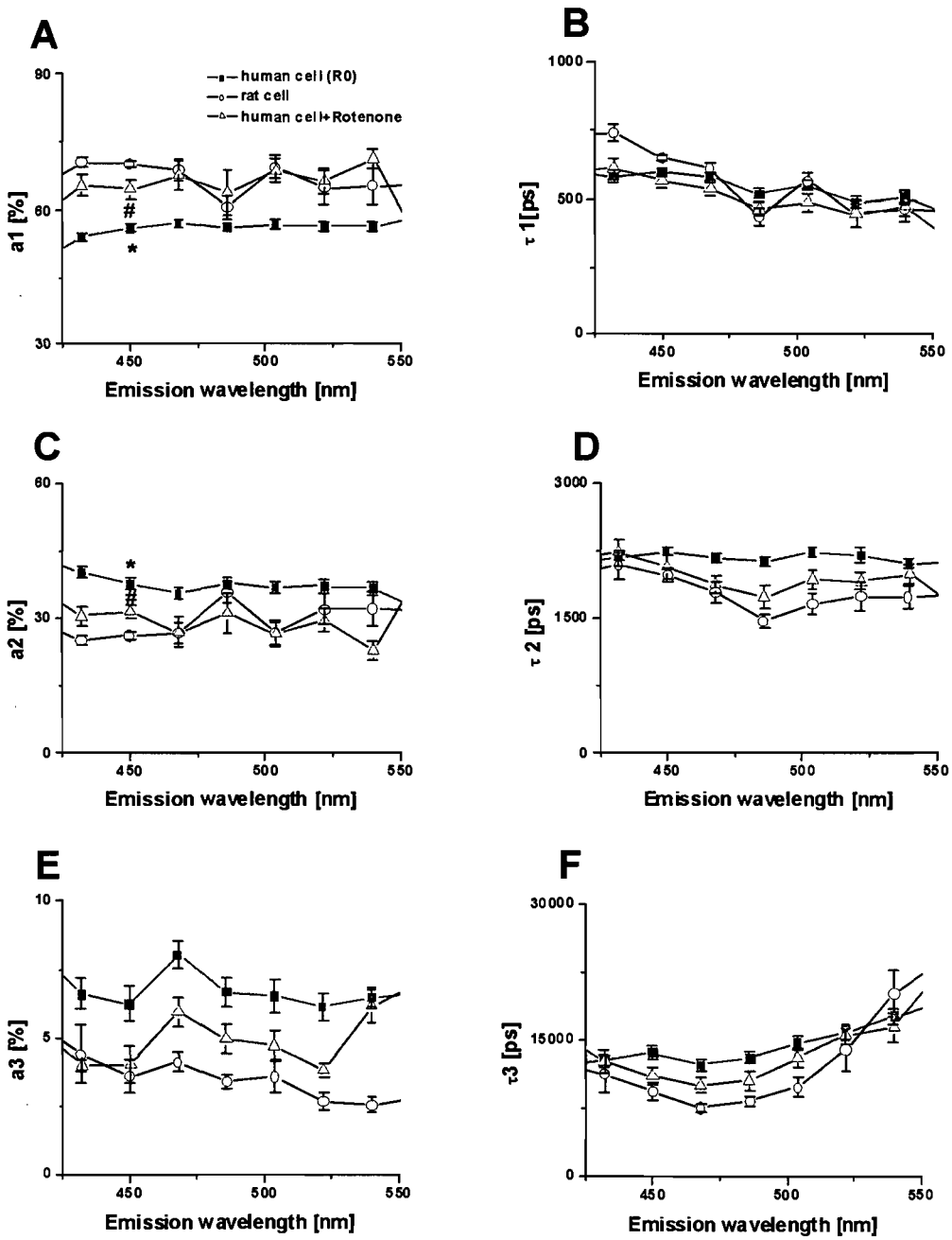

Figure 28: NAD(P)H fluorescence lifetimes and relative amplitudes in human cells. Human cells in control conditions (R0) or in the presence of Rotenone (1µmol/L) compared to rat cells isolated by the same approach. A, B and C: relative amplitudes (a1, a2 and a3), D, E and F: mean spectrally-resolved fluorescence lifetimes (τ1, τ2 and τ3), *$p < 0.05$ vs. rat cells, #$p < 0.05$ vs. human cells in control condition.

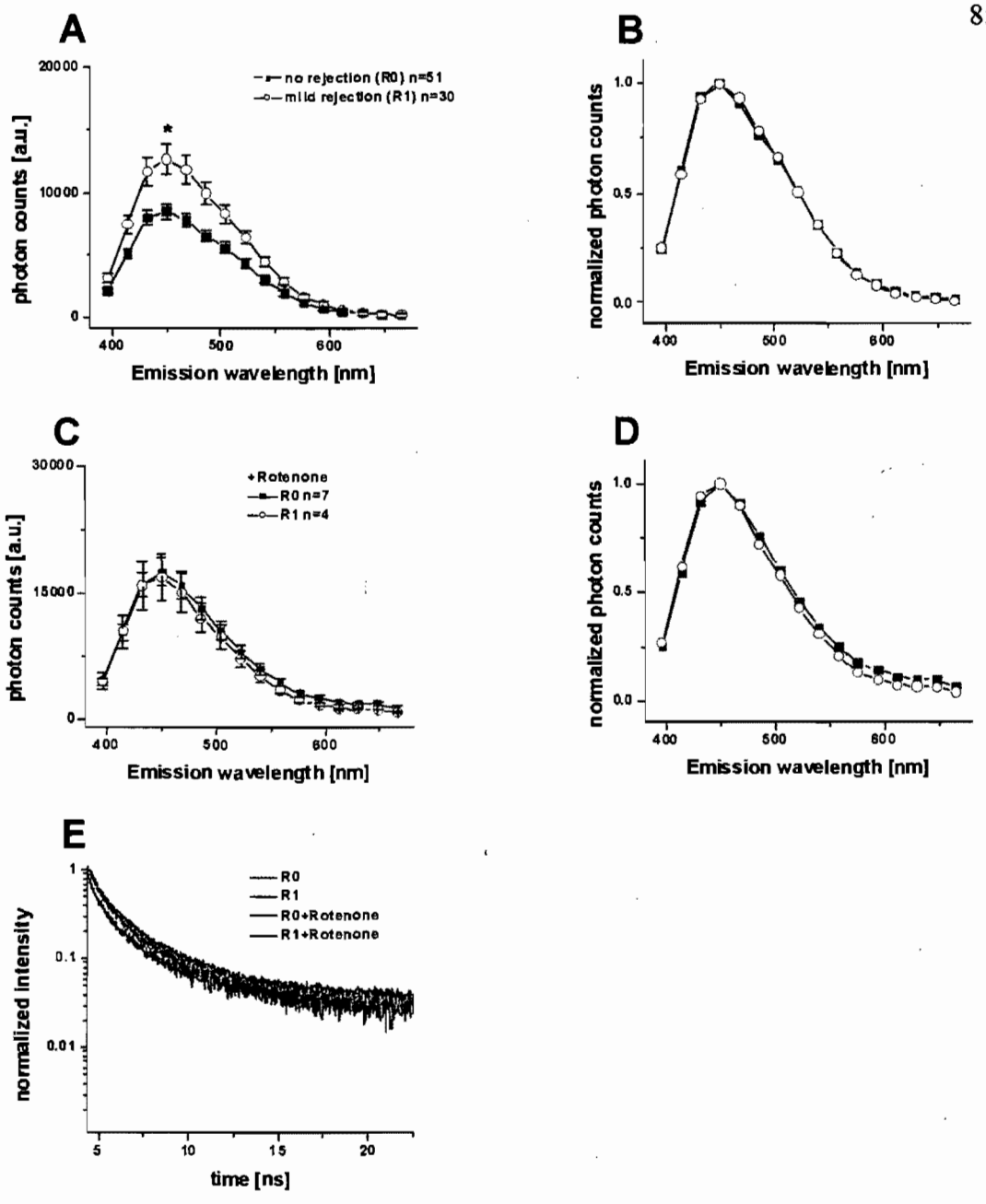

Figure 29: Steady-state NAD(P)H fluorescence of human cardiomyocytes with different grade of rejection (ISHLT). A) steady-state spectra and B) normalized spectra compared between R0 and R1. C: Steady-state and D) normalized spectra compared between R0 and R1 in the presence of Rotenone (1μmol/L). E: Fluorescence decays compared in different experimental conditions, *$p<0.05$ vs. R0 group.

	Total photon counts [a.u.]	P_{max} [a.u]	a_1	τ_1 [ps]	a_2	τ_2 [ps]	a_3	τ_3 [ps]
Human + R0 (control) (51/6)	**8500±590**	**680±29**	**58.1±0.7**	**621±17**	**35.8±0.9**	**2180±63**	**6.4±0.7**	**15900±960**
Human + R1 (30/4)	**12700±1200***	**850±39**	**55.9±0.7**	**589±16**	**39.7±0.9**	**2420±82**	**5.8±0.8**	**12100±840**
R0 + Rotenone (7/2)	**17400±1600*#**	**1040±110***	**65.4±0.9#**	**543±18**	**31.7±0.8*#**	**2130±150**	**3.6±0.8**	**12400±1000**
R1 + Rotenone (4/1)	**16800±2690***	**950±95**	**67.0±1.5*#**	**616±25**	**28.2±1.2*#**	**1990±200**	**5.2±0.7**	**10800±1400**
Rat cells (8/1)	**25200±2500*#**	**1650±370***	**70.4±0.6***	**649±13**	**26.3±0.8***	**1980±75**	**3.6±0.6***	**9300±930***

Table 6: Fluorescence parameters of human cardiomyocytes AF (λex/λem = 375 nm/450 nm). Total photon counts, fluorescence lifetimes (τ1 to τ3) and their relative amplitudes (a1 to a3) in human cardiomyocytes, or in the presence of Rotenone between rejection grade R0 and R1, and in the rat cardiomyocytes isolated using same approach as used in EMB. Data are shown as mean ± SEM; the number of experiments shown as (number of cells/ samples); *$p<0.05$ vs. human cells in control condition (R0), #$p<0.05$ vs. human cells present rejection R1.

3.4. Perspectives

Despite advantages of simultaneous recording of fluorescence spectra and lifetimes, the achieved work has a limitation that our current analysis of fluorescent decays is not able to precisely separate individual components in the recorded AF data. In perspective, to overcome this limit, we therefore propose to search for better separation of individual lifetime components (instead of lifetime pools), applying methods such as decay-associated spectra (DAS) and time-resolved emission spectra (TRES). In a prospective study, we have tested the feasibility of such analyses.

3.4.1. Decay associated spectra of NAD(P)H fluorescence

To precisely analyze spectra related to specific lifetime pools, decay associated spectra (DAS) can be estimated as a fraction of total fluorescence emission for each lifetime pool. These spectra serve to understand the relative contribution of the lifetime pools in studied experimental conditions. We attempted this approach and DAS were constructed for each lifetime pool as a product of wavelength-dependent fraction of the fluorescence emission of each lifetime pool with respect to the total fluorescence, multiplied by total photon counts (see section 2.2.4.) [132]. Constructed DAS data (Fig. 31) showed that, in control conditions, the 1st and 3rd lifetime pool had spectral amplitude around 470 nm, while the 2nd lifetime pool is comprised of a blue-shifted peak with the maximum around 450 nm and the red-shifted shoulder at 490 nm. This result suggests presence of spectrally-distinct populations of NADH molecules. Rotenone increased the intensity of all three DAS lifetime pools, while DNP mainly affected the DAS1 and the DAS2, as did the changes of BHB/AcAc ratio.

However, DAS analysis is only relevant when single fluorescence lifetime value can be assigned to specific lifetime component and when this value is constant, e.g. unchanged in studied experimental conditions. Apparently, this is not our case, as both the change in lifetimes of the fluorescence pools, as well as the mixed-character of the intermediate lifetime pool (likely involving the emission from various forms of NAD(P)H) point to non-specificity of identified lifetime pools and indicate that analysis of the fluorescence decays

alone is failing to assign estimated values to precise molecular states and/or conformations. Instead, additional analytical approaches such as TRES, are required to clearly distinguish between individual NAD(P)H states.

3.4.2. Analysis of time-resolved emission spectra of NAD(P)H fluorescence

To consolidate the analysis of the spectral and temporal distribution of AF intensity, a complementary approach to the exponential decay analysis by applying TRES representation [147] can be used. In brief, photons counted in several consecutive time channels were summed to minimize the inherent photon shot-noise and the spectra of NAD(P)H were constructed at different time intervals after the excitation by the laser pulse (Fig. 32A). We attempted this approach (see full description in section 2.2.4.) to resolve time-dependent changes in NAD(P)H spectra (Fig. 32B). TRES analysis revealed two peaks at 456 nm and 496 nm in control conditions. In contrast to the second peak, the first (456 nm) peak rapidly faded in the first couple of nanoseconds, suggesting a process with a corresponding lifetime of 1-2 ns or less. At $\Delta t = 0$ ns (Fig. 32C and D), we observed significant changes in spectral profiles with Rotenone and DNP, which were present, but less pronounced at $\Delta t = 4$ ns (Fig. 32E and F). Gathered data corroborated findings from the steady-state spectra (total photon counts in different spectral channels). This result suggests that the modulators of respiratory chain mainly affect the first, rapid-lifetime component.

This result showed the feasibility of future use of the TRES approach in the future for isolation of principal components of NAD(P)H fluorescence. In such context, TRES analysis can be employed, after estimation of reference spectra of principal NAD(P)H components by principal component analysis (PCA), followed by linear unmixing. This approach was already tested and achieved in the lab for spectral separation of flavin components in multispectral microscopy images [162] TCSPC data [143], as well as in separation of calcium-probes fluorescence signal from AF [144].

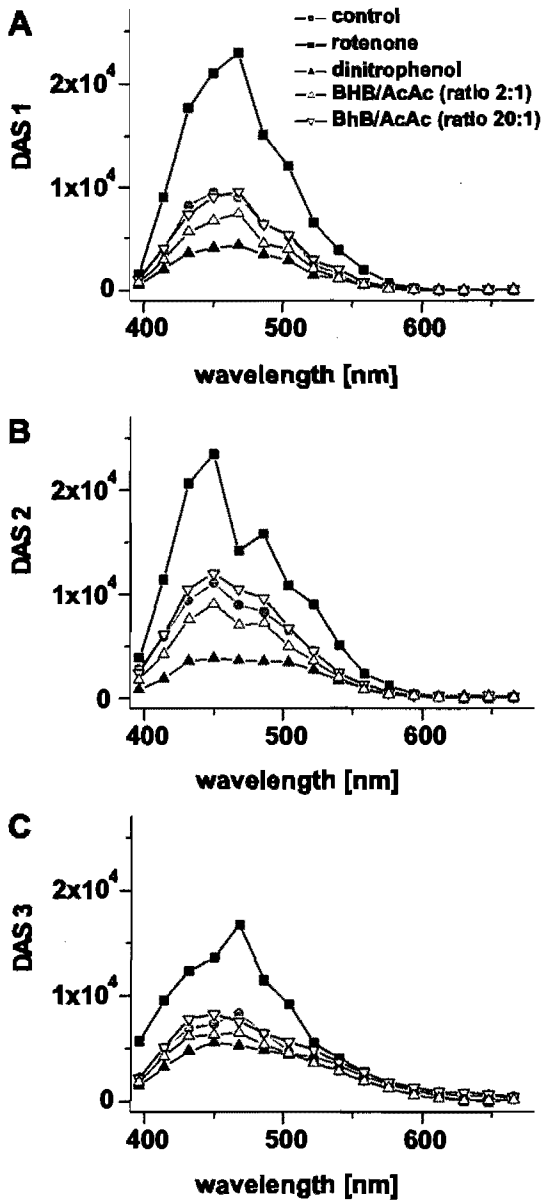

Figure 30: Decay-associated spectra (DAS) of NAD(P)H fluorescence in cardiomyocytes. A: DAS for the 1st lifetime pool, B: DAS for the 2nd lifetime pool, and C: DAS for the 3rd lifetime pool, in control conditions and in the presence of 1μmol/L Rotenone, 50μmol/L DNP, or following application of BHB/AcAc (ratio 20:1 or 2:1).

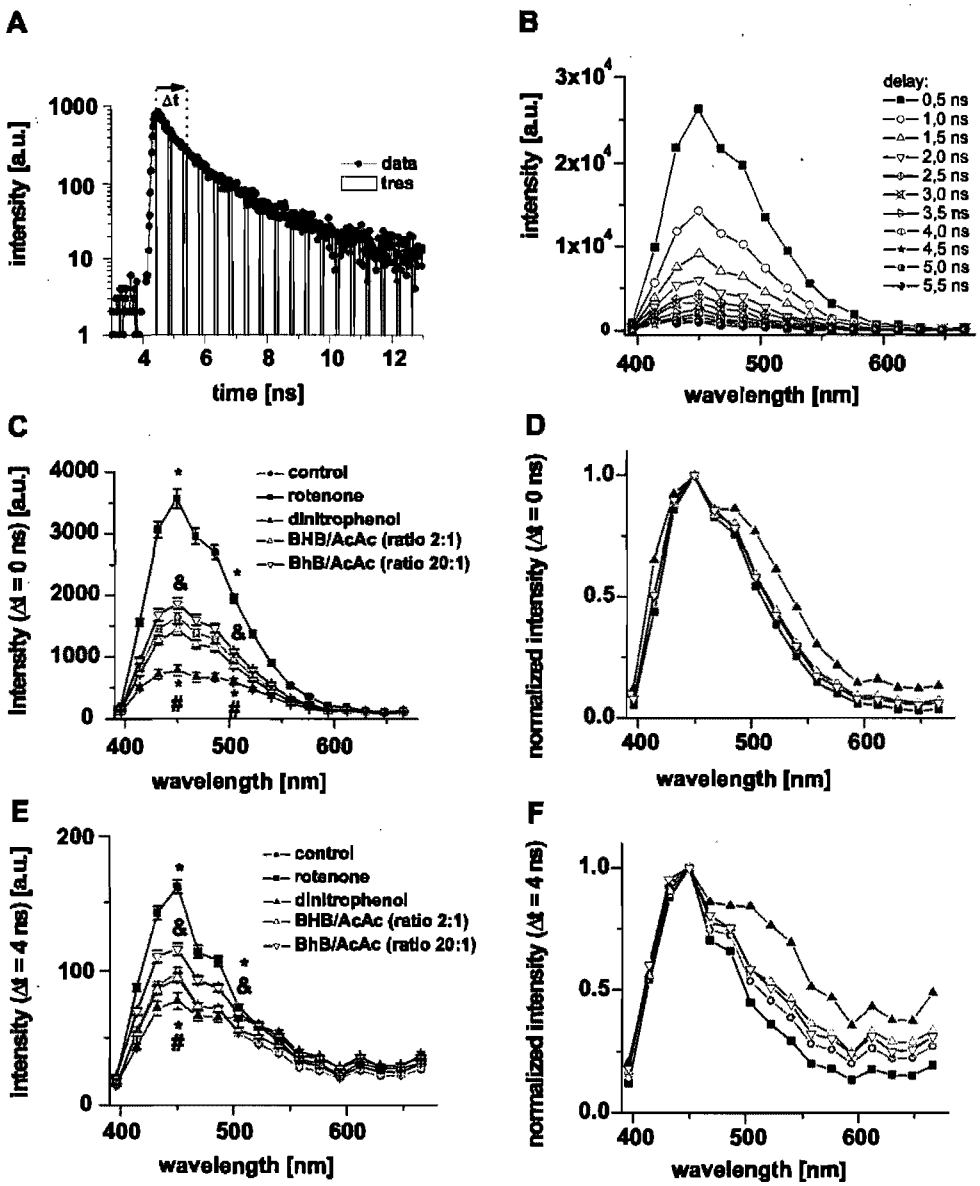

Figure 31: Time-resolved emission spectroscopy (TRES) of NAD(P)H fluorescence in cardiomyocytes. A. Construction of TRES from representative original recording. B. Example of TRES of cardiomyocyte AF resolved with 0.5 ns resolution (Δt = 0.5 ns) in control conditions. Emission spectra (C, E) and normalized spectra (D, F) resolved at $\Delta t = 0$ ns (C, D) and at Δt = 4 ns (E, F). Number of cells is as in Table 4; *$p<0.05$ vs. control, $^{\#}p<0.05$ vs. Rotenone, $^{\&}p<0.05$ vs BHB/AcAc (ratio 2:1).

4. Discussion

In the present contribution, we have demonstrated the following original findings:

(1) NAD(P)H fluorescence fingerprinting, achieved by spectrally-resolved lifetime spectrometry technique, is a useful tool for study of modifications in the mitochondrial oxidative metabolism in living cardiomyocytes.

(2) At least 3 different NAD(P)H fluorescence lifetime pools are present to describe its free and bound conformational states in living cardiac cells. Spectral and temporal characteristics of cardiomyocyte NAD(P)H fluorescence are sensitive to the modulation of NADH production and/or the respiratory chain. Steady-state fluorescence intensity of NAD(P)H is increased and fluorescence lifetimes and average fluorescence lifetimes are shortened in the presence of Rotenone, the inhibitor of the Complex I of the respiratory chain. On the other hand, the fluorescence intensity is significantly lowered and fluorescence lifetimes and average fluorescence lifetime prolonged after application of DNP, an uncoupler of ATP-synthesis. The stimulation of NADH production by modification of the BHB/AcAc ratio is correlated with a rise in fluorescence amplitude, without changes in fluorescence lifetimes. These effects corroborate our *in vitro* findings. Ischemia-mimicking conditions caused increase in the amount of NAD(P)H in cardiomyocytes, indicating altered mitochondrial energy balance.

(3) We also evaluated, for the first time, spectrally-resolved lifetime characteristics of NAD(P)H fluorescence in living cardiac cells isolated from human endomyocardial biopsies of pediatric heart transplanted patients with different rejection grades. NAD(P)H fluorescence was found significantly lower in human than in rat cardiomyocytes. Rotenone increased the fluorescence in human cardiac cells, making them more comparable to experimental rat model. Steady-state NAD(P)H fluorescence spectra were significantly increased in human hearts with rejection stage R1 when compared to healthy transplanted heart. These results suggest that human cardiac cells are more metabolically active than rat cells in the same conditions and this activity seems decreased during rejection process.

(4) In perspective, new analytical approaches were tested. DAS analysis revealed presence of 4 spectrally-distinct populations of NADH molecules in cardiomyocytes with spectral maximum at 470 nm for short-lifetime component, and emission peaks at 450, 470 nm and 490 nm for intermediate and long-lifetime components. TRES analysis revealed two peaks at 456 nm and 496 nm in control conditions. In contrast to the second peak, the first (456 nm) peak rapidly faded in the first couple of nanoseconds, suggesting the presence of the process with a corresponding lifetime of 1-2 ns or less. These findings corresponds conformational states of NADH molecule. Precise separation of these components of NADH fluorescence will be attempted in the future.

4.1. Fingerprinting of metabolic oxidative state in living cardiomyocytes

In the heart, endogenous blue fluorescence is well known to result from the reduced mitochondrial NAD(P)H following excitation with the UV light [98, 100, 103]. At fluorescence spectral emission wavelength of 450 nm, where the maximum fluorescence intensity was recorded, at least 3 exponential components were needed to achieve acceptable χ^2 values (<1.2) during analysis of cardiomyocyte AF decays [147]. As the fluorescence lifetimes indicate typical decay times of the excited state of the molecule, possibly in some conformation-specific state, the presence of three lifetime pools could indicate the existence of three different states of NAD(P)H molecules with distinct fluorescence kinetics in single cells. However, this is only true under the condition where each molecular conformation is linked to a single lifetime value, which is not the case for NAD(P)H in most physical and chemical conditions; instead the fluorescence decay of NADH is mostly bi-exponential with the lifetime values spanning from 1 ns (the short lifetime pool) to 7 ns (the long lifetime pool) [138]. Such simplification may therefore not be appropriate for NAD(P)H fluorescence emission in cardiac cells. The most relevant analysis of such complex system would be the spectrally-resolved lifetime distribution analysis by maximum entropy method, followed by spectral unmixing of the DAS. Nevertheless, as this procedure requires vast computational and experimental resources that are not readily available, we

have opted for its simplified variant, which involves the same formalism as used by Blinova *et al.* [132]. This approach defines three observable lifetime pools, covering the short, the intermediate and the long-lifetimes as representative intervals where several species can be observed simultaneously. To spectroscopically examine possible molecular origins of the fluorescence components, we analyzed their changes in response to modulation of cardiomyocyte metabolic state. Obviously, the chosen approach does not allow to separate the stacked vs. opened conformations of free NADH in solution, reported by other authors in solvents [137, 163], or in cells [40]. Nevertheless, fluorescence lifetimes resolved in multi-exponential analysis in single cardiomyocytes were well comparable to those gathered for NAD(P)H in isolated heart mitochondria by Blinova *et al.* [132], where three NAD(P)H fluorescence lifetime pools were found: the free pool (with a lifetime of 0.2-0.4 ns), the intermediate pool (1-2 ns) and the long lifetime pool (3-8 ns). The intermediate and the long lifetime pools were ascribed to protein binding of NAD(P)H, which make up □35% of the total NADH while contributing almost 80% of the fluorescence emission. Our analysis in single cardiac cells corroborated these findings in mitochondria, including the fact that the relative amplitude of the 1st lifetime pool is the most abundant.

We have also confirmed a blue-shift of the steady-state fluorescence spectral maximum of NAD(P)H in cardiomyocytes vs. free NADH *in vitro*, already reported in cardiomyocyte mitochondria [132]. The emission spectra of NAD(P)H in most tissues have been demonstrated to be blue-shifted by 10-20 nm as compared to free NADH in solution [38, 103, 164], or following binding to dehydrogenases [38]. According to the derived DAS, DAS2 of the cardiomyocyte AF was blue-shifted when compared to DAS1 in control conditions. Besides, rise in the NADH by increased BHB/AcAc ratio shifted the spectrum of the 3rd lifetime pool towards blue spectral region in cardiomyocytes (Fig. 31). These findings indicate that NADH binding to enzymes can underlie observed blue-shift, as proposed previously for cardiac tissue [38, 132]. Furthermore, our experiment with lactate and pyruvate corroborates findings by others [21, 38, 41, 120] that AF of cardiomyocytes results from mitochondrial, rather than cytosolic NADH as elevation of lactate and pyruvate

concentration greatly increased the cytosolic NADH/ NAD^+ ratio but had a lesser effect on the mitochondrial NADH/ NAD^+ ratio. These results indicate that processes described for cardiomyocyte AF in this contribution can be assigned primarily to sub-mitochondrial pools.

Free NADH in water solution was proposed to exist in two conformations: folded (NADH with stacked dinucleotide and adenine moiety) with the lifetime of 350 ps and extended (open form) with the lifetime of 760 ps. When existing as a mix in water solution, the average lifetime of the free NADH was described in the range of 400-500 ps [40, 126], which is in agreement with the lifetime resolved for the 1st lifetime pool, suggesting that it can be attributable to such free forms. In single cell, the NADH is generated in the process of Krebs' cycle, acetyl-CoA from fatty acid β-oxidation and from pyruvate oxidation are two major sources for NADH production by Krebs' cycle in the heart. Resolved components were therefore tested for higher levels of mitochondrial NADH in cardiomyocytes using BHB in the presence of AcAc [29]. Low concentrations of AcAc, the condition favorable to NADH production, led to an increase in the fluorescence intensity without change in fluorescence lifetimes (as defined using the lifetime-pool model) when compared to more physiological concentrations of AcAc. The effect of higher BHB/AcAc ratio in cardiomyocytes is in agreement with changes provoked by rise in NADH concentrations *in vitro*. Overall, no modification in the lifetime pools or in their relative amplitudes was observed in relation to increased NADH concentration *in vitro* (for the range of tested concentrations between 1 to 100 μmol/L). This is in agreement with previously published data [126], but in contrast with calculated estimations [40], which could be explained by smaller (μmol/L vs. mmol/L) concentrations tested. It is noteworthy that our results point to lower NADH concentrations in cardiomyocyte mitochondria (in order of 10 to 100μmol/L) than previously estimated in cardiac trabeculae [165]. This result is, however, strongly dependent on assumption that linear concentration-dependence of NADH fluorescence observed *in vitro* is applicable in the cellular environment. Our data indicate that rise in NADH concentration in cardiomyocytes is primarily translated into increased

amplitudes of DAS of all three lifetime components without modification in the average lifetime.

UV-excited AF in cardiac cells is considered originate primarily from the endogenous fluorescence of NADH, rather than NADPH, due to high mitochondrial NADH levels. At least 80% of the AF is essentially considered to be from NADH alone [38, 39, 116, 126-128]. Nevertheless, our studies of NADH and NADPH molecule fluorescence in intracellular media-mimicking solutions (see Appendix I) [33] demonstrated that NADH and NADPH had close spectral profiles, the spectral characteristics of NADH and NADPH make them indistinguishable from fluorescence signals in biological samples, such as cardiomyocytes. These results were in agreement with previously studies [117, 126, 132, 166]. Curiously, we have identified difference in their lifetimes. This can be due to distinct kinetics of the two molecules, or the presence of impurities; kinetics of further purified molecules needs to be done in the future. As there is no known photophysical means to discriminate NADH fluorescence signals from that of NADPH in living cells [126 32], we term the measured AF as that of NAD(P)H fluorescence.

In living cells, NAD(P)H forms complexes with several enzymes, which makes the interpretation of the NAD(P)H signals from intact tissues particularly difficult. We have applied modulators of the respiratory chain to further characterize fluorescence lifetime species related to NADH. Namely, we have used Rotenone, the specific inhibitor of the Complex I of the respiratory chain [59, 158] and DNP, an uncoupler of ATP synthesis [50, 167], stimulating NADH dehydrogenation. Effects of Rotenone and DNP on spectral amplitudes, determined by total photon counts, were comparable to those of cyanide and FCCP respectively, described previously in cardiac tissue [38]. Rotenone induced significant increase in the cardiomyocyte AF intensity, in accordance with the rise in NADH content inside mitochondria following inhibition of the mitochondrial respiration. The inhibitor also significantly decreased the average lifetime, but without affecting the relative fractions of the lifetime pools. The effect of the Rotenone in cardiomyocytes is in agreement with the shortening of fluorescence lifetimes identified in adipocytes[159], although no change in

fluorescence decays was found in liver mitochondria [126] following application of the inhibitor.

DNP uncouples oxidative phosphorylation by carrying protons across the mitochondrial membrane, thereby destroying the proton gradient that drives oxidative phosphorylation. This leads to stimulation of NADH dehydrogenation to NAD^+ by Complex I in mitochondrial respiration, and a rapid consumption of energy without generation of ATP [50, 98]. Application of DNP induced significant decrease in the steady-state AF intensity. This effect was accompanied by spectral broadening of emission wavelength by about 20 nm towards red region, as well as by an increase in the fluorescence lifetimes when compared to control conditions, which became even more pronounced when compared to Rotenone. Analysis of DAS pointed to the fact that the effect of DNP primarily results from the spectral change of the 1st and 2nd lifetime pools. Such behavior is in agreement with the one observed after NADH binding to LipDH *in vitro,* associated with the decrease of the emission amplitude, the red spectral shoulder, as well as the prolongation of the 2nd fluorescence lifetime. At low temperatures, NADH fluorescence decay in most solutions was reported to be two-exponential [137], depending upon solvent polarity and viscosity. The nature of the intermediate lifetime pool, although not interpreted with certainty, was mostly linked to some form of bound NADH [40, 132] and our experiments with DNP corroborate these findings. The two-exponential fluorescence kinetics of NADH were described to follow the dynamic quenching of NADH fluorescence via formation of non-fluorescent transient species from the first excited state [137, 138]. Therefore, the same pattern is likely to exist for the bound state of NADH in cellular environment, leading to the mixed-character of the intermediate lifetime pool involving the emission from various bound forms of NADH. This fact is supported by the character of the DAS2, where at least two distinct spectral peaks (450 and 490 nm) could be observed. In addition, TRES analysis of the long lifetime component revealed a new emission peak appearing at 470 nm after stimulation with Rotenone over the blue-shifted spectra of bound forms of NADH (440-470 nm). Whether this peak can be related to the increased NADH

production, manifested by the rise in the 470 nm-peak in the DAS of the short component, remains unclear.

The 3rd lifetime pool could not be associated with a single molecular species. The long lifetime pool covering the lifetimes of ~5-10 ns was described to be related to bound state of NADH, supported by the fluorescence anisotropy decay analysis, used as a complementary assay probing the rotational mobility of the resolved molecular populations [40]. NADH binding to enzymes mostly involves non-covalent electrostatic interactions between the protein and NADH, which adopts a rotationally immobile (at the nanosecond scale), "opened" conformation [40]. Thus, one can expect that the fluorescence kinetics of such a state would be similar to those of NADH in very viscous environments. Our data indicate that the 3rd fluorescence lifetime pool is sensitive to overall dynamics between NADH dehydrogenation and its production in cardiac cells. Indeed, upon metabolic modulation by DNP, the 3rd fluorescence lifetime was increased when compared to those by Rotenone and had also an increasing tendency with higher BHB/AcAc ratio. Furthermore, the 3rd lifetime pool was also enhanced after application of Octanoate (1mmol/L), a medium chain fatty acid that is not regulated by the carnitylpalmitoyl transport system in cardiomyocytes [22-24], but is completely oxidized through the mitochondrial β-oxidation and respiration pathways [25, 26]. Octanoate induces both, the NADH generation by the Krebs cycle following dehydrogenation of octanoyl-CoA [27] and an uncoupling effect [28], suggesting additive and/or multiple origins of the 3rd fluorescence lifetime pool, perhaps in a specific sub-mitochondrial environment.

Multiple efforts were made to distinguish free vs. bound states of NADH molecules in living tissues. Our observations suggest the presence of several populations of fluorescing molecules in cardiac mitochondria, excitable with UV light. We propose that the first lifetime species with 0.6 ns lifetime and spectral maximum around 470 nm seem to correlate with free (both folded and unfolded) conformations, whereas two other groups of species with the longer lifetimes and 450-490 nm spectral maxima rather correspond to enzyme-bound NADH conformations. Our data indicate that in living cardiomyocytes, the

modification in the mitochondrial NADH content is mainly correlated with the fluorescence intensity at 450 nm without changes in fluorescent lifetimes and that NADH binding to LipDH enzyme leads to significant modification of the average lifetime.

Altogether, our data point to the existence of at least 3 spectrally-distinct populations of NADH molecules in cardiomyocyte mitochondria, corresponding to both free and bound conformational states. In addition to relatively well-resolvable free NADH with short (sub-ns) fluorescence lifetimes and the ~470 nm emission peak, we provide evidence of species having nanosecond lifetimes and fluorescence spectra shifted towards blue, as well as to red wavelengths. Both, TRES and DAS analysis suggest that spectral broadening towards wavelengths longer than the emission maximum of NADH molecule in solution can be due to modification in the relative presence of these spectrally-different NADH populations in single cells. One of the candidates responsible for the change in the presence of distinct NADH populations is the LipDH. The LipDH flavoprotein served as example to investigate NADH dehydrogenation. Observed increase in the lifetime kinetics can be related to conformational changes of NADH induced by the enzyme. Indeed, upon dehydrogenation, the oxidized form of the protein promotes the binding of the neutral dihydro-nicotinamide moiety of NADH [168], in addition to the formation of negatively charged charge-transfer complexes between transiently bound NAD^+ and covalently bound FAD cofactor. In this reduced form, nicotinamide moiety is in a different conformation from uniformly ordered structure of NADH juxtaposing nicotinamide and isoalloxazine flavin ring systems and is not proximal to FAD [168], which can be reflected in the change of fluorescence kinetics. Overall, following the binding to LipDH, NADH molecule can therefore exist in at least two different conformational states. Our results are in favor for a possible switch from one NADH conformation to another.

In addition to this explanation, the decrease of the NADH intensity following binding of NADH to LipDH, the increase of the 2^{nd} fluorescence lifetime pool and the appearance of the red-spectral shoulder can also have another interpretation. The normalization of emission steady-state spectra of cardiomyocyte in the presence of DNP revealed the red-

spectral shoulder was broader than the one observed free NADH in the presence of LipDH *in vitro*. This may be due to part of the AF originate from endogenous flavins, which emits green FAD fluorescence with maximum around 500-520nm after visible light excitation (420-460 nm) [99, 102, 162, 169], and is involved in oxidation-reduction reactions with NADH. Possible contamination of our recordings with the fluorescence arising from LipDH-bound FAD following excitation at 375 nm is improbable, as no fluorescence additional to background could be identified *in vitro* for LipDH alone, in the absence of NADH. Decrease in the emission fluorescence at 450 nm, spectral broadening towards 520 nm, as well as spectrally-dependent change of the 2nd lifetime pool *in vitro* are all in favor with possible Förster resonant energy transfer (FRET) to LipDH-bound FAD. As the LipDH-binding domain for NADH is in close proximity to FAD^+-binding one[168, 170] and the 450 nm emission maximum of NADH corresponds exactly to an absorption peak of the FAD^+ moiety, this fulfils the prerequisites for the FRET between NADH and FAD^+ molecules. Considering that the C4 atom of the nicotinamide base is aligned for hydride transfer with N5 of the FAD at an average distance of 0.3 nm [168] and that the most efficient FRET is known to occur between two molecules which are closer than 2-7 nm [171], it is conceivable that excitation of NADH would induce a FRET with FAD^+ molecules. However, we previously discussed [33] (see Appendix I) the lack of FRET in enzyme-stimulated NADH dehydrogenation in intracellular solutions and, comparably, we found no proof of possible FRET between NAD(P)H and flavins in cells: namely lack of $\tau 1$ shortening of the NAD(P)H donor (see Table 4, conditions where dehydrogenation is affected such as application of DNP) is discussed in relation to condition where the rate of dehydrogenase is increased, such as application of DNP, is arguing against an eventual energy transfer. A further study is needed to fully understand significance of changes in NAD(P)H fluorescence following its binding to enzymes in living cells.

Nevertheless, precise distinction of individual NAD(P)H fluorescence component requires additional approaches. Use of the PCA followed by spectral linear unmixing techniques, which were already successfully attempted for free and bound flavin

fluorescence in the rat in cardiomyocytes [143, 162], is a suitable strategy to be employed in the future to clearly elucidate separate roles of individual lifetime species of NAD(P)H. This approach allows more advanced separation of the spectral and lifetime components in NAD(P)H fluorescence than previously achieved.

4.2. Changes of metabolic oxidative state in living cardiomyocytes under pathophysiological conditions

Our studies clearly demonstrated that metabolic state can be determined directly in living cardiac cells with good reproducibility via measuring their naturally occurring NAD(P)H fluorescence by spectrally and time–resolved emission spectroscopy approach. We have therefore tested use of this technique to study mitochondrial oxidative metabolism changes in pathophysiological conditions.

The heart is a pump converting chemical energy into mechanical work and the power for this work is gathered almost entirely from oxidation of carbon fuels and to a great extent these fuels are provided by coronary (myocardial) blood flow. Such oxidative metabolism is primarily the function of mitochondria in the process of oxidative phosphorylation. Because of the high oxidative metabolism, heart cells have elevated oxidative capacity, demonstrated by their ultrastructure: 25–35% of total cardiomyocyte volume is occupied by mitochondria [82]. Myocardial ischemia occurs following a reduction or restriction in coronary blood flow result in a series of biochemical reactions occurs in the cardiac cells. When oxygen delivery to the myocardium is abnormally low, the Krebs' cycle is blocked, the rate of oxygen consumption and aerobic ATP formation from oxidative phosphorylation are insufficient to support the required cardiac power for a given heart rate, arterial blood pressure, and inotropic state. The cell therefore turns to anaerobic metabolism and accelerates production of anaerobic ATP and lactic acid, in addition to suffering from oxygen deprivation [172] to maintain ATP level by glycolysis. This leads to accumulation of cytoplasmic NADH, with the NADH/NAD^+ ratio increasing several-fold, and accompanied accumulation of lactate and H^+ in the cell [72-74]. Many researchers have identified Complex I

as a major site of damage to the respiratory chain in ischemia [75, 76] and observed a reduction in oxidation rate for NADH-linked substrates by up to 60%. Oxidation rates with succinate were unchanged, suggesting that the damage was restricted to Complex I. Therefore, difference in redox states of NADH/NAD^+ pools during ischemia could reflect ATP generated by anaerobic metabolism.

NADH changes were proposed to play crucial role in ischemia/reperfusion injury [86]. Exposure of cardiomyocytes to ischemia-mimetic conditions, namely reducing cell pH (6.8) and oxygen content (deoxygenated with 100% N_2) for 5-10min, lead to significantly increased NAD(P)H fluorescence intensity, while fluorescence lifetime pools and their relative amplitudes were not significantly affected when compared to control normoxic conditions. As we have demonstrated no sensitivity of fluorescence kinetics to change in pH alone, this result is more likely to be related to lack of oxygenation and/or reduction in ATP production due to inhibition of respiratory chain during ischemia. Accumulation of the NADH content inside mitochondria, with increasing NADH/NAD^+ ratio under ischemia-mimicking conditions, is in agreement with biochemical changes in ischemia [13, 36, 72, 74]. In regard to the effect of the Rotenone and DNP on the steady-state AF, we have estimated percentage of oxidized nucleotides to about 82 % in control normoxic conditions. In ischemia-mimicking conditions, this percentage was lowered to 42%, while cardiomyocyte AF related to NADH was increased. This effect was comparable to the one observed in neuronal tissues following hypoxia [40] and suggests that changes in ischemia-mimicking conditions are rather related to modifications of NADH content than to change in the NADH binding to enzymes of the respiratory chain. Our data gathered in ischemia-mimic condition therefore point to modification in the NAD(P)H content rather than binding to enzymes of the respiratory chain.

We then evaluated, for the first time, spectrally-resolved lifetime characteristics of NAD(P)H fluorescence in living cardiac cells isolated from human endomyocardial biopsies of pediatric patients. Rejection of transplanted hearts is still the principal reason for death of transplanted pediatric patients. Organ rejection of transplants includes

hyperacute rejection, acute rejection and chronic rejection. Hyperacute rejection appears shortly after operation and is often easily recognized, as the patients are well monitored in this period. This is usually due to immune system changes that may occur after the transplantation. However, more problems are encountered concerning the recognition and the diagnosis of acute and chronic rejections, as well as cardiac allograft vasculopathy, or the graft coronary artery disease (GCAD). This type of rejection can occur at anytime after the heart transplantation, often several years after the operation [93, 96]. In these conditions, the coronary arteries develop progressive and diffuse (scattered and spread out) narrowing throughout their entire length, which result in nutrients and oxygen deprivation of the heart and lead to the failure of normal cardiomyocyte function. Acute rejection is defined as lymphatic inflammatory infiltration with associated damage and/or necrosis of cardiac cells or cardiac tissue [93]. Alteration of coronary vascular regulation during acute rejection may induce graft dysfunction and promote the occurrence of coronary atherosclerosis in transplant recipients [94]. Moreover, ischemia-reperfusion injury was also proposed to be an important alloantigen-independent factor [95] observed during cardiac rejection and leading to hypoxia in cardiomyocytes. Such modifications, which also include alterations in the cell oxidative metabolism, often develop rapidly. Some observations suggest that cardiac cells undergo changs in their oxidative state with the progression of cardiac rejection [84, 83], namely as a result of cell hypoxia, following oxidative modification of cardiac cells. Precise evaluation of the oxidative metabolism can therefore serve as an early indication of the rejection of transplanted hearts.

In human cardiomyocytes, a comprehensive study on the contribution of changes in NAD(P)H is largely missing. Our data show good reproducibility of results and comparison with commonly used models, such as the rat one. Our results indicate that the use of spectrally-resolved TCSPC method can improve the analysis of the metabolic state of isolated cardiac cells and suggest that human cells are more metabolically active than the rat ones in the same conditions. AF spectroscopy has been widely used in the early detection of different types of cancers [173 174] and was also attempted in examination of

transplanted tissues. In the heart, a strong correlation was found between changes in AF spectra and the rejection grade in rat heart allograft model [175], but more difficulties were encountered using human tissues [176], possibly due to use of frozen fractions, as well as lack of analysis of dynamic parameters of the recorded fluorescence. Our results of NAD(P)H fluorescence in paediatric heart transplanted patients with different rejection grades demonstrated higher steady-state NAD(P)H AF in R1 when compared to R0 rejection grade. Significant increase in the fluorescence intensity in R1 may indicate lesser metabolic activity and thus ATP production during rejection process. This result, observed in the absence of fluorescent lifetime modification is comparable to changes induced in ischemia-mimetic condition. These preliminary experimental data therefore gave us some promising direction, however, precise understanding of the processes that take place during rejection still needs recruitment of more cases with specific rejection grades and precise separation of individual components.

Based on data gathered in this contribution, we therefore propose to use the spectrally-resolved TCSPC approach as an interesting new multiparametric tool that can be applied to freshly-isolated cells from human biopsies, and eventually lead to new diagnostic approaches for early detection of allograft rejection. In addition to its higher sensitivity than conventional techniques, another advantage of this method is the possibility of its combination to multiphoton confocal microscopy, which, in the future, can result in the adaptation of this approach directly to tissue biopsy without the necessity of cell isolation.

5. Conclusions and Perspectives

In summary, in this contribution, we present the use of fluorescence spectral analysis coupled to fluorescence lifetime detection as a new sensitive tool to examine modifications of the oxidative mitochondrial metabolism in living cardiomyocytes. NAD(P)H fingerprinting is achieved by spectrally-resolved lifetime spectrometry approach.

We demonstrate that spectrally-resolved TCSPC recordings of cardiomyocyte AF lifetimes allow fast and reproducible measurements of NAD(P)H-based fluorophores and complex patterns of their spectra and lifetimes. Resolved fluorescence spectra and lifetimes of NAD(P)H are sensitive to regulation of mitochondrial respiration, as well as metabolic substrate availability in living cardiac cells. Changes in NAD(P)H fluorescence decay clearly correlated with modifications of mitochondrial oxidative metabolic states, indicator of mitochondrial functions. We also tested responses of NAD(P)H fluorescence when cardiomyocyte underwent ischemia-like condition. Accumulation of the NAD(P)H inside mitochondria corroborated biochemical changes in ischemia found previously.

Furthermore, we report spectrally-resolved lifetime characteristics of NAD(P)H fluorescence in living human cardiac cells, isolated from endomyocardial biopsies of pediatric heart transplanted patients. We have analyzed the kinetics of cellular NAD(P)H fluorescence in samples of patients with different rejection grades. We observed that human cells are more metabolically active than the rat ones in the same conditions, and that metabolic activity and thus ATP production decreased during rejection process. In perspective, we project to examine more subjects with different rejection grades of their transplanted hearts. In order to precisely identify specific fluorescence component and thus separate distinct populations of NADH molecules in living cells, we will also further examine application of advanced analytical methods.

Data gathered using this approach will bring an important insight into understanding of physiological regulation of NAD(P)H in cardiomyocytes, thus opening new horizons for the fluorescence lifetime analysis as a diagnostic tool of pathophysiological conditions, including ischemia, diabetes, or rejection of transplanted hearts.

6. BIBLIOGRAPHY

1. **Buckley NM, Penefsky ZJ, Litwak RS.** Comparative force-frequency relationships in human and other mammalian ventricular myocardium. *Pflugers Arch* 1972; 332(4): 259-70.

2. **Saks V, Dzeja P, Schlattner U, Vendelin M, Terzic A, Wallimann T.** Cardiac system bioenergetics: metabolic basis of the Frank-Starling law. *J Physiol* 2006 Mar 1; 571(Pt 2): 253-73.

3. **Brodde OE, Michel MC.** Adrenergic and muscarinic receptors in the human heart. *Pharmacol Rev* 1999 Dec; 51(4): 651-90.

4. **Scheffler IE.** A century of mitochondrial research: achievements and perspectives. *Mitochondrion* 2001 Jun; 1(1): 3-31.

5. **Maack C, O'Rourke B.** Excitation-contraction coupling and mitochondrial energetics. *Basic Res Cardiol* 2007 Sep; 102(5): 369-92.

6. **Bers DM.** Excitation-Contraction Coupling and Cardiac Contractile Force. 2 ed. Dordrecht, The Netherlands: Kluwer Academic Publisher, Dordrecht, The Netherlands.; 2001.

7. **Ernster L, Schatz G.** Mitochondria: a historical review. *J Cell Biol* 1981 Dec; 91(3 Pt 2): 227s-55s.

8. **Suga H.** Ventricular energetics. *Physiol Rev* 1990 Apr; 70(2): 247-77.

9. **Gibbs CL.** Cardiac energetics. *Physiol Rev* 1978 Jan; 58(1): 174-254.

10. **Bers DM.** Cardiac excitation-contraction coupling. *Nature* 2002 Jan 10; 415(6868): 198-205.

11. **Stanley WC, Recchia FA, Lopaschuk GD.** Myocardial substrate metabolism in the normal and failing heart. *Physiol Rev* 2005 Jul; 85(3): 1093-129.

12. **Keul J, Doll E, Keppler D, Reindell H.** [Variations of arterial substrate level under the influence of physical work]. *Int Z Angew Physiol* 1966 Aug 4; 22(4): 356-85.

13. **Stanley WC, Lopaschuk GD, Hall JL, McCormack JG.** Regulation of myocardial carbohydrate metabolism under normal and ischaemic conditions. Potential for pharmacological interventions. *Cardiovasc Res* 1997 Feb; 33(2): 243-57.

14. **Gertz EW, Wisneski JA, Stanley WC, Neese RA.** Myocardial substrate utilization during exercise in humans. Dual carbon-labeled carbohydrate isotope experiments. *J Clin Invest* 1988 Dec; 82(6): 2017-25.

15. **Berg JM.** Biochemistry. 5 ed. New York: Freeman and Co, U.S.A.; 2002.

16. **Denton RM, Randle PJ, Bridges BJ, Cooper RH, Kerbey AL, Pask HT, et al.** Regulation of mammalian pyruvate dehydrogenase. *Mol Cell Biochem* 1975 Oct 31; 9(1): 27-53.

17. **Williamson JR.** Mitochondrial function in the heart. *Annu Rev Physiol* 1979; 41: 485-506.

18. **Vary TC, Reibel DK, Neely JR.** Control of energy metabolism of heart muscle. *Annu Rev Physiol* 1981; 43: 419-30.

19. **Sharma N, Okere IC, Brunengraber DZ, McElfresh TA, King KL, Sterk JP, et al.** Regulation of pyruvate dehydrogenase activity and citric acid cycle intermediates during high cardiac power generation. *J Physiol* 2005 Jan 15; 562(Pt 2): 593-603.

20. **Wan B, LaNoue KF, Cheung JY, Scaduto RC, Jr.** Regulation of citric acid cycle by calcium. *J Biol Chem* 1989 Aug 15; 264(23): 13430-9.

21. **Zhou L, Cabrera ME, Okere IC, Sharma N, Stanley WC.** Regulation of myocardial substrate metabolism during increased energy expenditure: insights from computational studies. *Am J Physiol Heart Circ Physiol* 2006 Sep; 291(3): H1036-H1046.

22. **Poirier M, Vincent G, Reszko AE, Bouchard B, Kelleher JK, Brunengraber H, et al.** Probing the link between citrate and malonyl-CoA in perfused rat hearts. *Am J Physiol Heart Circ Physiol* 2002 Oct; 283(4): H1379-H1386.

23. **Depre C, Rider MH, Hue L.** Mechanisms of control of heart glycolysis. *Eur J Biochem* 1998 Dec 1; 258(2): 277-90.

24. **Ruderman NB, Saha AK, Vavvas D, Witters LA.** Malonyl-CoA, fuel sensing, and insulin resistance. *Am J Physiol* 1999 Jan; 276(1 Pt 1): E1-E18.

25. **Gavva SR, Wiethoff AJ, Zhao P, Malloy CR, Sherry AD.** A 13C isotopomer n.m.r. method for monitoring incomplete beta-oxidation of fatty acids in intact tissue. *Biochem J* 1994 Nov 1; 303 (Pt 3): 847-53.

26. **Forsey RG, Reid K, Brosnan JT.** Competition between fatty acids and carbohydrate or ketone bodies as metabolic fuels for the isolated perfused heart. *Can J Physiol Pharmacol* 1987 Mar; 65(3): 401-6.

27. **Hall CL.** Acyl-CoA dehydrogenases and electron-transferring flavoprotein. *Methods Enzymol* 1978; 53: 502-18.

28. **Wojtczak L, Schonfeld P.** Effect of fatty acids on energy coupling processes in mitochondria. *Biochim Biophys Acta* 1993 Nov 2; 1183(1): 41-57.

29. **Opie LH, Owen P.** Effects of increased mechanical work by isolated perfused rat heart during production or uptake of ketone bodies. Assessment of mitochondrial oxidized to reduced free nicotinamide-adenine dinucleotide ratios and oxaloacetate concentrations. *Biochem J* 1975 Jun; 148(3): 403-15.

30. **Kim DK, Heineman FW, Balaban RS.** Effects of beta-hydroxybutyrate on oxidative metabolism and phosphorylation potential in canine heart in vivo. *Am J Physiol* 1991 Jun; 260(6 Pt 2): H1767-H1773.

31. **Hasselbaink DM, Glatz JF, Luiken JJ, Roemen TH, Van d, V.** Ketone bodies disturb fatty acid handling in isolated cardiomyocytes derived from control and diabetic rats. *Biochem J* 2003 May 1; 371(Pt 3): 753-60.

32. **Schuchmann S, Kovacs R, Kann O, Heinemann U, Buchheim K.** Monitoring NAD(P)H autofluorescence to assess mitochondrial metabolic functions in rat hippocampal-entorhinal cortex slices. *Brain Res Brain Res Protoc* 2001 Jul; 7(3): 267-76.

33. **Aneba S., Cheng Y, Mateasik A, Comte B, Chorvat D, Chorvatova A.** Probing of Cardiomyocyte Metabolism by Spectrally Resolved Lifetime Detection of NAD(P)H Fluorescence. *Computers in Cardiology* 2007; in press.

34. **Belenky P, Bogan KL, Brenner C.** NAD^+ metabolism in health and disease. *Trends Biochem Sci* 2007 Jan; 32(1): 12-9.

35. **Pollak N, Dolle C, Ziegler M.** The power to reduce: pyridine nucleotides--small molecules with a multitude of functions. *Biochem J* 2007 Mar 1; 402(2): 205-18.

36. **Di LF, Ziegler M.** Pathophysiological relevance of mitochondria in NAD(+) metabolism. *FEBS Lett* 2001 Mar 9; 492(1-2): 4-8.

37. **Benderdour M, Charron G, Comte B, Ayoub R, Beaudry D, Foisy S, et al.** Decreased cardiac mitochondrial $NADP^+$-isocitrate dehydrogenase activity and

expression: a marker of oxidative stress in hypertrophy development. *Am J Physiol Heart Circ Physiol* 2004 Nov; 287(5): H2122-H2131.

38. **Eng J, Lynch RM, Balaban RS.** Nicotinamide adenine dinucleotide fluorescence spectroscopy and imaging of isolated cardiac myocytes. *Biophys J* 1989 Apr; 55(4): 621-30.

39. **Joubert F, Fales HM, Wen H, Combs CA, Balaban RS.** NADH enzyme-dependent fluorescence recovery after photobleaching (ED-FRAP): applications to enzyme and mitochondrial reaction kinetics, in vitro. *Biophys J* 2004 Jan; 86(1 Pt 1): 629-45.

40. **Vishwasrao HD, Heikal AA, Kasischke KA, Webb WW.** Conformational dependence of intracellular NADH on metabolic state revealed by associated fluorescence anisotropy. *J Biol Chem* 2005 Jul 1; 280(26): 25119-26.

41. **Nuutinen EM.** Subcellular origin of the surface fluorescence of reduced nicotinamide nucleotides in the isolated perfused rat heart. *Basic Res Cardiol* 1984 Jan; 79(1): 49-58.

42. **Veech RL, Eggleston LV, Krebs HA.** The redox state of free nicotinamide-adenine dinucleotide phosphate in the cytoplasm of rat liver. *Biochem J 1969* Dec; 115(4): 609-19.

43. **Lin SJ, Guarente L.** Nicotinamide adenine dinucleotide, a metabolic regulator of transcription, longevity and disease. *Curr Opin Cell Biol* 2003 Apr; 15(2): 241-6.

44. **Voet D, Voet JG.** Biochemistry. 3 ed. New York: John Wiley & Sons, Inc., .; 2004.

45. **Chance B, Thorell B.** Fluorescence measurements of mitochondrial pyridine nucleotide in aerobiosis and anaerobiosis. *Nature* 1959 Sep 26; 184: 931-4.

46. **Chance B.** Pyridine nucleotide as an indicator of the oxygen requirements for energy-linked functions of mitochondria. *Circ Res* 1976 May; 38(5 Suppl 1): I31-I38.

47. **Cortassa S, Aon MA, Marban E, Winslow RL, O'Rourke B.** An integrated model of cardiac mitochondrial energy metabolism and calcium dynamics. *Biophys J* 2003 Apr; 84(4): 2734-55.

48. **Joshi S, Huang YG.** ATP synthase complex from bovine heart mitochondria: the oligomycin sensitivity conferring protein is essential for dicyclohexyl

carbodiimide-sensitive ATPase. *Biochim Biophys Acta* 1991 Aug 26; 1067(2): 255-8.

49. **Tsubaki M.** Fourier-transform infrared study of cyanide binding to the Fea3-CuB binuclear site of bovine heart cytochrome c oxidase: implication of the redox-linked conformational change at the binuclear site. *Biochemistry* 1993 Jan 12; 32(1): 164-73.

50. **Heytler PG.** Uncouplers of oxidative phosphorylation. *Methods Enzymol* 1979; 55: 462-42.

51. **Lambert AJ, Brand MD.** Inhibitors of the quinone-binding site allow rapid superoxide production from mitochondrial NADH:ubiquinone oxidoreductase (complex I). *J Biol Chem* 2004 Sep 17; 279(38): 39414-20.

52. **Mitchell P.** Coupling of phosphorylation to electron and hydrogen transfer by a chemi-osmotic type of mechanism. *Nature* 1961 Jul 8; 191: 144-8.

53. **Mitchell P.** Possible molecular mechanisms of the protonmotive function of cytochrome systems. *J Theor Biol* 1976 Oct 21; 62(2): 327-67.

54. **Mitchell P.** Vectorial chemistry and the molecular mechanics of chemiosmotic coupling: power transmission by proticity. *Biochem Soc Trans* 1976; 4(3): 399-430.

55. **Ko YH, Hullihen J, Hong S, Pedersen PL.** Mitochondrial F(0)F(1) ATP synthase. Subunit regions on the F1 motor shielded by F(0), Functional significance, and evidence for an involvement of the unique F(0) subunit F(6). *J Biol Chem* 2000 Oct 20; 275(42): 32931-9.

56. **Dimroth P, Ballmoos C, Meier T.** Catalytic and mechanical cycles in F-ATP synthases. *European Molecular Biology Organization* 2006; 7(3): 276-82.

57. **Rich PR.** The molecular machinery of Keilin's respiratory chain. *Biochem Soc Trans* 2003 Dec; 31(Pt 6): 1095-105.

58. **Cortassa SC, Aon MA, O'Rourke B, Jacques R, Tseng HJ, Marban E, et al.** A computational model integrating electrophysiology, contraction and mitochondrial bioenergetics in the ventricular myocyte. *Biophys J* 2006 May 5.

59. **Balaban RS, Heineman FW.** Control of mitochondrial respiration in the heart in vivo. *Mol Cell Biochem* 1989 Sep 7; 89(2): 191-7.

60. **Brown GC.** Control of respiration and ATP synthesis in mammalian mitochondria and cells. *Biochem J* 1992 May 15; 284 (Pt 1): 1-13.

61. **Tager JM, Wanders RJ, Groen AK, Kunz W, Bohnensack R, Kuster U, et al.** Control of mitochondrial respiration. *FEBS Lett* 1983 Jan 10; 151(1): 1-9.

62. **Brand MD, Kesseler A.** Control analysis of energy metabolism in mitochondria. *Biochem Soc Trans* 1995 May; 23(2): 371-6.

63. **Bose S, French S, Evans FJ, Joubert F, Balaban RS.** Metabolic network control of oxidative phosphorylation: multiple roles of inorganic phosphate. *J Biol Chem* 2003 Oct 3; 278(40): 39155-65.

64. **Saks VA, Kuznetsov AV, Vendelin M, Guerrero K, Kay L, Seppet EK.** Functional coupling as a basic mechanism of feedback regulation of cardiac energy metabolism. *Mol Cell Biochem* 2004 Jan; 256-257(1-2): 185-99.

65. **Chance B, Williams GR.** A method for the localization of sites for oxidative phosphorylation. *Nature* 1955 Aug 6; 176(4475): 250-4.

66. **Katz LA, Koretsky AP, Balaban RS.** Respiratory control in the glucose perfused heart. A 31P NMR and NADH fluorescence study. *FEBS Lett* 1987 Sep 14; 221(2): 270-6.

67. **Katz LA, Swain JA, Portman MA, Balaban RS.** Relation between phosphate metabolites and oxygen consumption of heart in vivo. *Am J Physiol* 1989 Jan; 256(1 Pt 2): H265-H274.

68. **Korzeniewski B.** Oxygen consumption and metabolite concentrations during transitions between different work intensities in heart. *Am J Physiol Heart Circ Physiol* 2006 Sep; 291(3): H1466-H1474.

69. **Territo PR, French SA, Dunleavy MC, Evans FJ, Balaban RS.** Calcium activation of heart mitochondrial oxidative phosphorylation: rapid kinetics of mVO2, NADH, AND light scattering. *J Biol Chem* 2001 Jan 26; 276(4): 2586-99.

70. **Territo PR, Mootha VK, French SA, Balaban RS.** Ca(2+) activation of heart mitochondrial oxidative phosphorylation: role of the F(0)/F(1)-ATPase. *Am J Physiol Cell Physiol* 2000 Feb; 278(2): C423-C435.

71. **Territo PR, French SA, Balaban RS.** Simulation of cardiac work transitions, in vitro: effects of simultaneous Ca^{2+} and ATPase additions on isolated porcine heart mitochondria. *Cell Calcium* 2001 Jul; 30(1): 19-27.

72. **Solaini G, Harris DA.** Biochemical dysfunction in heart mitochondria exposed to ischaemia and reperfusion. *Biochem J* 2005 Sep 1; 390(Pt 2): 377-94.

73. **Smith DR, Stone D, Darley-Usmar VM.** Stimulation of mitochondrial oxygen consumption in isolated cardiomyocytes after hypoxia-reoxygenation. *Free Radic Res* 1996 Mar; 24(3): 159-66.

74. **Neely JR, Feuvray D.** Metabolic products and myocardial ischemia. *Am J Pathol* 1981 Feb; 102(2): 282-91.

75. **Hardy L, Clark JB, Darley-Usmar VM, Smith DR, Stone D.** Reoxygenation-dependent decrease in mitochondrial NADH:CoQ reductase (Complex I) activity in the hypoxic/reoxygenated rat heart. *Biochem J* 1991 Feb 15; 274 (Pt 1): 133-7.

76. **Cairns CB, Ferroggiaro AA, Walther JM, Harken AH, Banerjee A.** Postischemic administration of succinate reverses the impairment of oxidative phosphorylation after cardiac ischemia and reperfusion injury. *Circulation* 1997 Nov 4; 96(9 Suppl): II-5.

77. **Schluter KD, Jakob G, Ruiz-Meana M, Garcia-Dorado D, Piper HM.** Protection of reoxygenated cardiomyocytes against osmotic fragility by nitric oxide donors. *Am J Physiol* 1996 Aug; 271(2 Pt 2): H428-H434.

78. **Piper HM, Abdallah Y, Schafer C.** The first minutes of reperfusion: a window of opportunity for cardioprotection. *Cardiovasc Res* 2004 Feb 15; 61(3): 365-71.

79. **Piper HM, Siegmund B, Ladilov Y, Schluter KD.** Calcium and sodium control in hypoxic-reoxygenated cardiomyocytes. *Basic Res Cardiol* 1993 Sep; 88(5): 471-82.

80. **Piper HM, Noll T, Siegmund B.** Mitochondrial function in the oxygen depleted and reoxygenated myocardial cell. *Cardiovasc Res* 1994 Jan; 28(1): 1-15.

81. **Lesnefsky EJ, Moghaddas S, Tandler B, Kerner J, Hoppel CL.** Mitochondrial dysfunction in cardiac disease: ischemia--reperfusion, aging, and heart failure. *J Mol Cell Cardiol* 2001 Jun; 33(6): 1065-89.

82. **Bassien-Capsa V, Fouron JC, Comte B, Chorvatova A.** Structural, functional and metabolic remodeling of rat left ventricular myocytes in normal and in sodium-supplemented pregnancy. *Cardiovasc Res* 2006 Feb 1; 69(2): 423-31.

83. **Tanaka M, Mokhtari GK, Terry RD, Balsam LB, Lee KH, Kofidis T, et al.** Overexpression of human copper/zinc superoxide dismutase (SOD1) suppresses ischemia-reperfusion injury and subsequent development of graft coronary artery

disease in murine cardiac grafts. *Circulation* 2004 Sep 14; 110(11 Suppl 1): II200-II206.

84. **Tanaka M, Nakae S, Terry RD, Mokhtari GK, Gunawan F, Balsam LB, et al.** Cardiomyocyte-specific Bcl-2 overexpression attenuates ischemia-reperfusion injury, immune response during acute rejection, and graft coronary artery disease. *Blood* 2004 Dec 1; 104(12): 3789-96.

85. **Schaffer SW, Safer B, Ford C, Illingworth J, Williamson JR.** Respiratory acidosis and its reversibility in perfused rat heart: regulation of citric acid cycle activity. *Am J Physiol* 1978 Jan; 234(1): H40-H51.

86. **Aon MA, Cortassa S, Marban E, O'Rourke B.** Synchronized whole cell oscillations in mitochondrial metabolism triggered by a local release of reactive oxygen species in cardiac myocytes. *J Biol Chem* 2003 Nov 7; 278(45): 44735-44.

87. **Kussmaul L, Hirst J.** The mechanism of superoxide production by NADH:ubiquinone oxidoreductase (complex I) from bovine heart mitochondria. *Proc Natl Acad Sci U S A* 2006 May 16; 103(20): 7607-12.

88. **Raha S, Robinson BH.** Mitochondria, oxygen free radicals, disease and ageing. *Trends Biochem Sci* 2000 Oct; 25(10): 502-8.

89. **Balaban RS, Nemoto S, Finkel T.** Mitochondria, oxidants, and aging. *Cell* 2005 Feb 25; 120(4): 483-95.

90. **Lambert AJ, Brand MD.** Superoxide production by NADH:ubiquinone oxidoreductase (complex I) depends on the pH gradient across the mitochondrial inner membrane. *Biochem J* 2004 Sep 1; 382(Pt 2): 511-7.

91. **Brand MD, Affourtit C, Esteves TC, Green K, Lambert AJ, Miwa S, et al.** Mitochondrial superoxide: production, biological effects, and activation of uncoupling proteins. *Free Radic Biol Med* 2004 Sep 15; 37(6): 755-67.

92. **Turrens JF.** Mitochondrial formation of reactive oxygen species. *J Physiol* 2003 Oct 15; 552(Pt 2): 335-44.

93. **Stewart S, Winters GL, Fishbein MC, Tazelaar HD, Kobashigawa J, Abrams J, et al.** Revision of the 1990 working formulation for the standardization of nomenclature in the diagnosis of heart rejection. *J Heart Lung Transplant* 2005 Nov; 24(11): 1710-20.

94. **Bouchard D, Despatis MA, Buluran J, Cartier R.** Vascular effects of cyclosporin A and acute rejection in canine heart transplantation. *Ann Thorac Surg* 1997 Nov; 64(5): 1325-30.

95. **Gaudin PB, Rayburn BK, Hutchins GM, Kasper EK, Baughman KL, Goodman SN, et al.** Peritransplant injury to the myocardium associated with the development of accelerated arteriosclerosis in heart transplant recipients. *Am J Surg Pathol* 1994 Apr; 18(4): 338-46.

96. **Kuhn MA, Deming DD, Cephus CE, Mulla NF, Chinnock RE, Razzouk AJ, et al.** Moderate acute rejection detected during annual catheterization in pediatric heart transplant recipients. *J Heart Lung Transplant* 2003 Mar; 22(3): 276-80.

97. **Hilderson HJ.** Fluorescence Studies on Biological Membranes. In: Harris JR, editor. Subcellular Biochemistry.New York and London: Plenum Press. New York and London.; 1988.

98. **Romashko DN, Marban E, O'Rourke B.** Subcellular metabolic transients and mitochondrial redox waves in heart cells. *Proc Natl Acad Sci U S A* 1998 Feb 17; 95(4): 1618-23.

99. **Chorvat D, Jr., Bassien-Capsa V, Cagalinec M, Kirchnerova J, Mateasik A, Comte B, et al.** Mitochondrial autofluorescence induced by visible light in single cardiac myocytes studied by spectrally resolved confocal microscopy. *Laser Physics* 2004; 14(2): 220-30.

100. **Andersson H, Baechi T, Hoechl M, Richter C.** Autofluorescence of living cells. *J Microsc* 1998 Jul; 191 (Pt 1): 1-7.

101. **Aubin JE.** Autofluorescence of viable cultured mammalian cells. *J Histochem Cytochem* 1979 Jan; 27(1): 36-43.

102. **Benson RC, Meyer RA, Zaruba ME, McKhann GM.** Cellular autofluorescence--is it due to flavins? *J Histochem Cytochem* 1979 Jan; 27(1): 44-8.

103. **Chance B, Cohen P, Jobsis F, Schoener B.** Intracellular oxidation-reduction states in vivo. *Science* 1962 Aug 17; 137: 499-508.

104. **Monici M.** Cell and tissue autofluorescence research and diagnostic applications. *Biotechnol Annu Rev* 2005; 11: 227-56.

105. **Schweitzer D, Kolb A, Hammer M, Thamm E.** Basic investigations for 2-dimensional time-resolved fluorescence measurements at the fundus. *Int Ophthalmol* 2001; 23(4-6): 399-404.

106. **Becker W.** Advanced Time-Correlated Single Photon Counting techniques. 1 ed. New York: Springer; 2005.

107. **Becker W, Bergmann A, Haustein E, Petrasek Z, Schwille P, Biskup C, et al.** Fluorescence lifetime images and correlation spectra obtained by multidimensional time-correlated single photon counting. *Microsc Res Tech* 2006 Mar; 69(3): 186-95.

108. **Becker W, Bergmann A, Biskup C.** Multispectral fluorescence lifetime imaging by TCSPC. *Microsc Res Tech* 2007 May; 70(5): 403-9.

109. **Zhang J, Campbell RE, Ting AY, Tsien RY.** Creating new fluorescent probes for cell biology. *Nat Rev Mol Cell Biol* 2002 Dec; 3(12): 906-18.

110. **Sekar RB, Periasamy A.** Fluorescence resonance energy transfer (FRET) microscopy imaging of live cell protein localizations. *J Cell Biol* 2003 Mar 3; 160(5): 629-33.

111. **Lakowicz JR.** Principles of Fluorescence Spectroscopy. 2 ed. New York: Plenum Press.; 1999.

112. **Elangovan M, Day RN, Periasamy A.** Nanosecond fluorescence resonance energy transfer-fluorescence lifetime imaging microscopy to localize the protein interactions in a single living cell. *J Microsc* 2002 Jan; 205(Pt 1): 3-14.

113. **Chance B, Williams GR.** Respiratory enzymes in oxidative phosphorylation. III. The steady state. *J Biol Chem* 1955 Nov; 217(1): 409-27.

114. **Chance B.** Spectra and reaction kinetics of respiratory pigments of homogenized and intact cells. *Nature* 1952 Feb 9; 169(4293): 215-21.

115. **Mayevsky A, Rogatsky GG.** Mitochondrial function in vivo evaluated by NADH fluorescence: from animal models to human studies. *Am J Physiol Cell Physiol* 2007 Feb; 292(2): C615-C640.

116. **Chance B, Schoener B, Oshino R, Itshak F, Nakase Y.** Oxidation-reduction ratio studies of mitochondria in freeze-trapped samples. NADH and flavoprotein fluorescence signals. *J Biol Chem* 1979 Jun 10; 254(11): 4764-71.

117. **Cordeiro PG, Kirschner RE, Hu QY, Chiao JJ, Savage H, Alfano RR, et al.** Ultraviolet excitation fluorescence spectroscopy: a noninvasive method for the measurement of redox changes in ischemic myocutaneous flaps. *Plast Reconstr Surg* 1995 Sep; 96(3): 673-80.

118. **Schomacker KT, Frisoli JK, Compton CC, Flotte TJ, Richter JM, Nishioka NS, et al.** Ultraviolet laser-induced fluorescence of colonic tissue: basic biology and diagnostic potential. *Lasers Surg Med* 1992; 12(1): 63-78.

119. **Koretsky AP, Katz LA, Balaban RS.** Determination of pyridine nucleotide fluorescence from the perfused heart using an internal standard. *Am J Physiol* 1987 Oct; 253(4 Pt 2): H856-H862.

120. **Coremans JM, Ince C, Bruining HA, Puppels GJ.** (Semi-)quantitative analysis of reduced nicotinamide adenine dinucleotide fluorescence images of blood-perfused rat heart. *Biophys J* 1997 Apr; 72(4): 1849-60.

121. **Koretsky AP, Katz LA, Balaban RS.** The mechanism of respiratory control in the in vivo heart. *J Mol Cell Cardiol* 1989 Feb; 21 Suppl 1: 59-66.

122. **Kedem J, Mayevsky A, Sonn J, Acad BA.** An experimental approach for evaluation of the O_2 balance in local myocardial regions in vivo. *Q J Exp Physiol* 1981 Oct; 66(4): 501-14.

123. **Mills SA, Jobsis FF, Seaber AV.** A fluorometric study of oxidative metabolism in the in vivo canine heart during acute ischemia and hypoxia. *Ann Surg* 1977 Aug; 186(2): 193-200.

124. **Sundt TM, Jr., Anderson RE.** Reduced nicotinamide adenine dinucleotide fluorescence and cortical blood flow in ischemic and nonischemic squirrel monkey cortex. 2. effects of alterations in arterial carbon dioxide tension, blood pressure, and blood volume. *Stroke* 1975 May; 6(3): 279-83.

125. **Katz AM.** Discovery of phospholamban. A personal history. *Ann N Y Acad Sci* 1998 Sep 16; 853: 9-19.

126. **Wakita M, Nishimura G, Tamura M.** Some characteristics of the fluorescence lifetime of reduced pyridine nucleotides in isolated mitochondria, isolated hepatocytes, and perfused rat liver in situ. *J Biochem (Tokyo)* 1995 Dec; 118(6): 1151-60.

127. **Estabrook RW.** Fluorometric measurement of reduced pyridine nucleotide in cellular and subcellular particles. *Anal Biochem* 1962 Sep; 4: 231-45.

128. **Avi-Dor Y, Olson JM, Doherty MD, Kaplan NO.** Fluorescence of pyridine nucleotides in mitochovdria. *J Biol Chem* 1962; 237: 2377-83.

129. **Reiss PD, Zuurendonk PF, Veech RL.** Measurement of tissue purine, pyrimidine, and other nucleotides by radial compression high-performance liquid chromatography. *Anal Biochem* 1984 Jul; 140(1): 162-71.

130. **Yang H, Yang T, Baur JA, Perez E, Matsui T, Carmona JJ, et al.** Nutrient-sensitive mitochondrial NAD^+ levels dictate cell survival. *Cell* 2007 Sep 21; 130(6): 1095-107.

131. **Yamada K, Hara N, Shibata T, Osago H, Tsuchiya M.** The simultaneous measurement of nicotinamide adenine dinucleotide and related compounds by liquid chromatography/electrospray ionization tandem mass spectrometry. *Anal Biochem* 2006 May 15; 352(2): 282-5.

132. **Blinova K, Carroll S, Bose S, Smirnov AV, Harvey JJ, Knutson JR, et al.** Distribution of mitochondrial NADH fluorescence lifetimes: steady-state kinetics of matrix NADH interactions. *Biochemistry* 2005 Feb 22; 44(7): 2585-94.

133. **Todisco S, Agrimi G, Castegna A, Palmieri F.** Identification of the mitochondrial NAD^+ transporter in Saccharomyces cerevisiae. *J Biol Chem* 2006 Jan 20; 281(3): 1524-31.

134. **Schafer FQ, Buettner GR.** Redox environment of the cell as viewed through the redox state of the glutathione disulfide/glutathione couple. *Free Radic Biol Med* 2001 Jun 1; 30(11): 1191-212.

135. **Williamson DH, Lund P, Krebs HA.** The redox state of free nicotinamide-adenine dinucleotide in the cytoplasm and mitochondria of rat liver. *Biochem J* 1967 May; 103(2): 514-27.

136. **Tischler ME, Friedrichs D, Coll K, Williamson JR.** Pyridine nucleotide distributions and enzyme mass action ratios in hepatocytes from fed and starved rats. *Arch Biochem Biophys* 1977 Nov; 184(1): 222-36.

137. **Gafni A, Brand L.** Fluorescence decay studies of reduced nicotinamide adenine dinucleotide in solution and bound to liver alcohol dehydrogenase. *Biochemistry* 1976 Jul 27; 15(15): 3165-71.

138. **Gruber BA, Leonard NJ.** Dynamic and static quenching of 1,N6-ethenoadenine fluorescence in nicotinamide 1,N6-ethenoadenine dinucleotide and in 1,N6-

etheno-9-(3-(indol-3-yl) propyl) adenine. *Proc Natl Acad Sci U S A* 1975 Oct; 72(10): 3966-9.

139. **Lakowicz JR, Szmacinski H, Nowaczyk K, Johnson ML.** Fluorescence lifetime imaging of free and protein-bound NADH. *Proc Natl Acad Sci U S A* 1992 Feb 15; 89(4): 1271-5.

140. **Scholz TD, Laughlin MR, Balaban RS, Kupriyanov VV, Heineman FW.** Effect of substrate on mitochondrial NADH, cytosolic redox state, and phosphorylated compounds in isolated hearts. *Am J Physiol* 1995 Jan; 268(1 Pt 2): H82-H91.

141. **Thorell B, Chance B.** Microspectrography of respiratory enzymes within the single, mammalian cell under different metabolic conditions. *Exp Cell Res* 1960 Jun; 20: 43-55.

142. **Chance B, Thorell B.** Localization and kinetics of reduced pyridine nucleotide in living cells by microfluorometry. *J Biol Chem* 1959 Nov; 234: 3044-50.

143. **Chorvat D, Mateasik A, Kirchnerova J, Chorvatova A.** Application of spectral unmixing in multi-wavelength time-resolved spectroscopy. *Proceedings of SPIE: the International Society for Optical Engineering* 2007; 6771(Advanced Photon Counting Techniques II): 677105-1-677105-12.

144. **Chorvat D, Elzwiei F, Bassien-Capsa V, Mateasik A, Chorvatova A.** Assessment of Low-Intensity Fluorescence Signals in Living Cardiac Cells Using Time-Resolved Laser Spectroscopy. *Computers in Cardiology* 2007; in press.

145. **Kapusta P, Wahl M, Benda A, Hof M, Enderlein J.** Fluorescence lifetime correlation spectroscopy. *J Fluoresc* 2007 Jan; 17(1): 43-8.

146. **Becker W, Bergmann A, Hink MA, Konig K, Benndorf K, Biskup C.** Fluorescence lifetime imaging by time-correlated single-photon counting. *Microsc Res Tech* 2004 Jan 1; 63(1): 58-66.

147. **O'Connor DV, Phillips D.** Time-Correlated Single Photon Counting. 1 ed. London: Academic Press; 1984.

148. **Chorvat D, Jr., Chorvatova A.** Spectrally resolved time-correlated single photon counting: a novel approach for characterization of endogenous fluorescence in isolated cardiac myocytes. *Eur Biophys J* 2006 Oct 11.

149. **Miniati DN, Robbins RC.** Heart transplantation: a thirty-year perspective. *Annu Rev Med* 2002; 53: 189-205.

150. **Rodriguez ER.** The pathology of heart transplant biopsy specimens: revisiting the 1990 ISHLT working formulation. *J Heart Lung Transplant* 2003 Jan; 22(1): 3-15.

151. **Guinamard R, Chatelier A, Demion M, Potreau D, Patri S, Rahmati M, et al.** Functional characterization of a Ca(2+)-activated non-selective cation channel in human atrial cardiomyocytes. *J Physiol* 2004 Jul 1; 558(Pt 1): 75-83.

152. **Peeters GA, Sanguinetti MC, Eki Y, Konarzewska H, Renlund DG, Karwande SV, et al.** Method for isolation of human ventricular myocytes from single endocardial and epicardial biopsies. *Am J Physiol* 1995 Apr; 268(4 Pt 2): H1757-H1764.

153. **Pawley J.B.** Handbook of Biological Confocal Microscopy. 3 ed. Berlin: Springer; 2006.

154. **Vetrova EV, Kudryasheva NS, Visser AJ, van Hoek A.** Characteristics of endogenous flavin fluorescence of Photobacterium leiognathi luciferase and Vibrio fischeri NAD(P)H:FMN-oxidoreductase. *Luminescence* 2005 May; 20(3): 205-9.

155. **Park J.** AM1 semiempirical calculated potential energy surfaces for the isomerization of symmetrical carbocyanines. *Dyes and Pigments* 2000; 46: 155-61.

156. **Pouget J, Mugnier J, Valeur B.** Correction of systematic phase errors in frequency-domain fluorometry. *J Phys E: Sci Instrum* 1989; 89(22): 855-62.

157. **Perham RN.** Domains, motifs, and linkers in 2-oxo acid dehydrogenase multienzyme complexes: a paradigm in the design of a multifunctional protein. *Biochemistry* 1991 Sep 3; 30(35): 8501-12.

158. **Davies KJ, Doroshow JH.** Redox cycling of anthracyclines by cardiac mitochondria. I. Anthracycline radical formation by NADH dehydrogenase. *J Biol Chem* 1986 Mar 5; 261(7): 3060-7.

159. **Evans ND, Gnudi L, Rolinski OJ, Birch DJ, Pickup JC.** Glucose-dependent changes in NAD(P)H-related fluorescence lifetime of adipocytes and fibroblasts in vitro: potential for non-invasive glucose sensing in diabetes mellitus. *J Photochem Photobiol B* 2005 Aug 1; 80(2): 122-9.

160. **Hulsmann WC, Ashruf JF, Bruining HA, Ince C.** Imminent ischemia in normal and hypertrophic Langendorff rat hearts; effects of fatty acids and superoxide

dismutase monitored by NADH surface fluorescence. *Biochim Biophys Acta* 1993 Jun 19; 1181(3): 273-8.

161. **Lu J, Zang WJ, Yu XJ, Chen LN, Zhang CH, Jia B.** Effects of ischaemia-mimetic factors on isolated rat ventricular myocytes. *Exp Physiol* 2005 Jul; 90(4): 497-505.

162. **Chorvat D, Jr., Kirchnerova J, Cagalinec M, Smolka J, Mateasik A, Chorvatova A.** Spectral unmixing of flavin autofluorescence components in cardiac myocytes. *Biophys J* 2005 Dec; 89(6): L55-L57.

163. **Hull RV, Conger PS, III, Hoobler RJ.** Conformation of NADH studied by fluorescence excitation transfer spectroscopy. *Biophys Chem* 2001 Mar 15; 90(1): 9-16.

164. **Koretsky AP, Balaban RS.** Changes in pyridine nucleotide levels alter oxygen consumption and extra-mitochondrial phosphates in isolated mitochondria: a 31P-NMR and NAD(P)H fluorescence study. *Biochim Biophys Acta* 1987 Oct 7; 893(3): 398-408.

165. **Brandes R, Bers DM.** Simultaneous measurements of mitochondrial NADH and Ca(2+) during increased work in intact rat heart trabeculae. *Biophys J* 2002 Aug; 83(2): 587-604.

166. **Chance B, Baltscheffsky H.** Respiratory enzymes in oxidative phosphorylation. VII. Binding of intramitochondrial reduced pyridine nucleotide. *J Biol Chem* 1958 Sep; 233(3): 736-9.

167. **Ganote CE, McGarr J, Liu SY, Kaltenbach JP.** Oxygen-induced enzyme release. Assessment of mitochondrial function in anoxic myocardial injury and effects of the mitochondrial uncoupling agent 2,4-dinitrophenol (DNP). *J Mol Cell Cardiol* 1980 Apr; 12(4): 387-408.

168. **Brautigam CA, Chuang JL, Tomchick DR, Machius M, Chuang DT.** Crystal structure of human dihydrolipoamide dehydrogenase: NAD+/NADH binding and the structural basis of disease-causing mutations. *J Mol Biol* 2005 Jul 15; 350(3): 543-52.

169. **Van den Berg PA, Widengren J, Hink MA, Rigler R, Visser AJ.** Fluorescence correlation spectroscopy of flavins and flavoenzymes: photochemical and photophysical aspects. *Spectrochim Acta A Mol Biomol Spectrosc* 2001 Sep 14; 57(11): 2135-44.

170. **Porter DJ, Bright HJ, Voet D.** X-ray structures of two oxidation states of a flavin-nicotinamide biscoenzyme and models for flavin--nicotinamide interactions. *Nature* 1977 Sep 15; 269(5625): 213-7.

171. **Bastiaens PI, Squire A.** Fluorescence lifetime imaging microscopy: spatial resolution of biochemical processes in the cell. *Trends Cell Biol* 1999 Feb; 9(2): 48-52.

172. **Dennis SC, Gevers W, Opie LH.** Protons in ischemia: where do they come from; where do they go to? *J Mol Cell Cardiol* 1991 Sep; 23(9): 1077-86.

173. **Katz A, Savage HE, Schantz SP, McCormick SA, Alfano RR.** Noninvasive native fluorescence imaging of head and neck tumors. *Technol Cancer Res Treat* 2002 Feb; 1(1): 9-15.

174. **Yang Y, Katz A, Celmer EJ, Zurawska-Szczepaniak M, Alfano RR.** Fundamental differences of excitation spectrum between malignant and benign breast tissues. *Photochem Photobiol* 1997 Oct; 66(4): 518-22.

175. **Morgan DC, Wilson JE, MacAulay CE, MacKinnon NB, Kenyon JA, Gerla PS, et al.** New method for detection of heart allograft rejection: validation of sensitivity and reliability in a rat heterotopic allograft model. *Circulation* 1999 Sep 14; 100(11): 1236-41.

176. **Yamani MH, Van de Poll SW, Ratliff NB, Kuban BE, Starling RC, McCarthy PM, et al.** Fluorescence spectroscopy of endomyocardial tissue post-human heart transplantation: does it correlate with histopathology? *J Heart Lung Transplant* 2000 Nov; 19(11): 1077-80.

APPENDIX I:

ANEBA S., CHENG Y., MATEASIK A., COMTE B., CHORVAT D. JR, CHORVATOVA A., 2007: Probing of cardiomyocyte metabolism by spectrally-resolved lifetime detection of NAD(P)H fluorescence. ***The Computers in Cardiology.*** 39:349-352.

Probing of Cardiomyocyte Metabolism by Spectrally Resolved Lifetime Detection of NAD(P)H Fluorescence

S Aneba[1], Y Cheng[1], A Mateasik[2], B Comte[1,3], D Chorvat Jr[2], A Chorvatova[1,4]

[1]Research Centre, CHU Sainte-Justine, Montreal, Canada
[2]International Laser Centre, Bratislava, Slovakia
[3]Department of Nutrition, University of Montreal, Montreal, Canada
[4]Department of Pediatrics, University of Montreal, Montreal, Canada

Abstract

NAD(P)H, crucial in effective management of cellular oxidative metabolism and the principal electron donors for enzymatic reactions, is a major source of autofluorescence induced in cardiac cells following excitation by UV light. Spectrally-resolved time-correlated single photon counting was used to simultaneously measure the fluorescence spectra and fluorescence lifetimes of NAD(P)H, following excitation by a pulsed picosecond 375 nm laser diode. Spectra, as well as fluorescence lifetimes of NADH and NADPH molecules were investigated in solution at different concentrations Effects of their respective dehydrogenation by lipoamide dehydrogenase (LipDH) or glutathione reductase (GR) were also questioned. NAD(P)H autofluorescence recorded in vitro was compared to the one measured in freshly isolated cardiac cells. We observed a good comparability between NAD(P)H parameters recorded in solution and in cells.

1. Introduction

Endogenous fluorescence of NAD(P)H, induced following excitation with the UV light, is long used for non-invasive fluorescent probing of metabolic state. Blue autofluorescence of rat cardiac myocytes was demonstrated to correlate with metabolic changes and was mostly ascribed to mitochondrial NADH and NADPH [2]. Adenosine trisphosphate (ATP), produced in the process of mitochondrial oxidative phosphorylation, is the primary molecular energy source for the contraction of cardiac myocytes. This process is coupled to oxidation of reduced NADH, the principal electron donor for the electrochemical gradient indispensable for oxidative energy metabolism. The first step in this process, which accounts for 95% of ATP generation needed for cardiomyocyte contraction, is the dehydrogenation of NADH by Complex I of the mitochondrial respiratory chain. NADH consumption rate is long investigated using fluorescence techniques in tissues and isolated mitochondria. On the other hand, NADPH is an important cofactor for several enzymes involved in different metabolic pathways (i.e. pentose phosphate pathway, Krebs cycle) and is essential for antioxidant processes in the glutathione reductase (GR) reaction. This enzyme allows the recycling of glutathione by converting its oxidized form (GSSG) into reduced glutathione. Oxidative stress can modulate the cellular NADPH content through the release of peroxides and various by-products that has been shown to decrease the activity of several enzymes, such as the NADP-isocitrate dehydrogenase (NADP-ICDH) [1]. Here, we investigate NAD(P)H fingerprinting by spectrally-resolved lifetime spectroscopy. More precisely, we characterize fluorescence spectra and fluorescence lifetimes of NADH and NADPH in intracellular-like solutions and compare resolved data with spectral and temporal characteristics of endogenous NAD(P)H fluorescence, directly in living cardiomyocytes.

2. Methods

2.1. Cardiomyocyte isolation

Left ventricular myocytes were isolated from Sprague-Dawley rats (13-14 weeks old, Charles River, Canada) following retrograde perfusion of the heart with proteolytic enzymes [4]. All procedures were performed in accordance with Institutional Committee accredited by the Canadian Council for the Protection of Animals (CCPA). Myocytes were maintained in a storage solution at 4°C until used. Only cells that showed clearly defined striations were used in up to 10 hrs following isolation.

2.2. TCSPC

We have used time correlated single photon counting (TCSPC) setup based on inverted microscope (Axiovert 200M, Zeiss, Canada) [4]. In brief, a picosecond diode laser with emission line at 375 nm (BHL-375, Becker-Hickl, Boston Electronics, USA) was used as an excitation source (output power ~1 mW, repetition rate 20 MHz, pulse widths typically < 100 ps). The laser beams were combined by dichroic filters and reflected to the sample through epifluorescence path of Axiovert 200 inverted microscope to create slightly defocused elliptical spot (10-20 μm). The emitted fluorescence was spectrally decomposed by 16-channel photomultiplier array (PML-16, Becker-Hickl, Boston Electronics, USA), running in the photon-counting regime and feeding the time-correlated single photon counting interface card SPC 830 using SPCM software (both Becker-Hickl, Boston Electronics, USA), attached to the imaging spectrograph (Solar 100, Proscan, Germany). Fluorescence decays were measured for 30 s with 25 ns TAC time-base sampled by 1024 points. Cells were studied at room temperatures in 4-well chambers with UV-proof coverslip-based slides (LabTech).

2.3. Solutions, drugs and data analysis

The basic external solution contained (in mM): NaCl, 140; KCl, 5.4; $CaCl_2$, 2; $MgCl_2$, 1; glucose, 10; HEPES, 10; adjusted to pH 7.35 with NaOH. Basic intracellular solution contained (in mM): KCl, 140; NaCl, 10; glucose, 10; HEPES, 10; adjusted to pH 7.25 with NaOH. LipDH (porcine; 2 U/μL), NADH or NADPH in concentrations ranging from 1 to 20 μM were added to basic internal solution. NADPH was also produced from NADP-ICDH (3.9 U/mL) by reaction of Isocitrate (89 mM) and NADP (0.5 mM) with or without GSSG (50 nM) and GR (0.5 U/mL or 1 U/mL). Chemicals were from Sigma-Aldrich (Canada). Data were analyzed using SPCImage software (Becker-Hickl, Boston Electronics, USA), Origin 7.0 (OriginLab, USA) and custom-written procedures for data correction and analysis written in C++. Home-made database was used for appropriate data management. Data are shown as means ± standard errors (SEM).

3. Results

3.1. NADH and NADPH in vitro

Fluorescence spectra and fluorescence lifetimes of intrinsic NADH and NADPH fluorescence were recorded in vitro in intracellular media-mimicking solutions. Steady-state emission spectra measured simultaneously at 16 acquisition channels were determined as the total photon counts on each spectral channel. Concentrations ranging from 1 to 20 μM were used to question the dose dependence of spectral and lifetime properties of the NADH and NADPH fluorescence. Spectral intensity of NADH fluorescence followed linear concentration-dependence (Fig. 1A), as described previously [2].

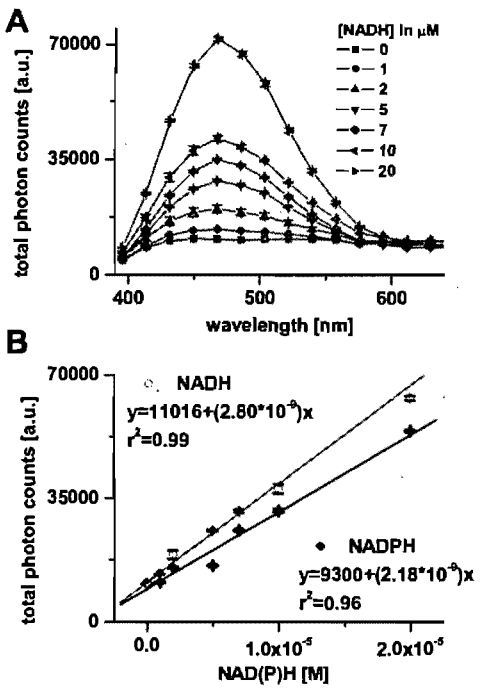

Figure 1. Emission spectra of NADH *in vitro* in intracellular solutions at concentrations ranging from 1 to 20 μM (n=5 samples each) (**A**). Concentration-dependence of the NADH and NADPH autofluorescence at spectral peak of 450 nm (**B**).

Normalized spectra superimposed perfectly for NADH concentrations between 1 to 20 μM (data not shown), confirming the same molecular origin. Free NADPH and NADH had autofluorescence with spectral maximum at 450 and 470 nm respectively in intracellular solution (Fig. 4). The spectral intensity of NADPH/NADH was linearly dependent on their concentration, as illustrated in Fig. 1B at 450 nm. Quantum yield of NADPH was smaller than that of NADH, as previously reported [2]. Normalized fluorescence intensity recorded in intra cellular medium showed slight shift of about 20 nm between NADPH and NADH (Fig. 4). At the fluorescence maximum wavelength of 450 nm we have resolved three fluorescence lifetimes for NADH (20 μM, n=10 samples): $\tau 1$ = 0.39±0.01 ns (with relative amplitude of 69.9±1.0%), $\tau 2$ = 1.46±0.05 ns (20.5±0.8%) and $\tau 3$ = 8.12±0.07 ns (9.8±0.2%), but only 2 significant ones for

NADPH (20 μM, n=5 samples): τ1 = 0.31±0.01 ns (74.6 ±2.4%) and τ2 = 0.75±0.02 ns (25.3±2.9%). Resolved lifetime parameters were independent on the studied emission wavelength, or concentrations (data not shown).

3.2. NADPH regulation by GR and NADH regulation by LipDH

NADPH produced *in vitro* from NADP-ICDH had same spectral and lifetime characteristics as NADPH in intracellular solution (data not shown). In the presence of GSSG, GR lowered (0.5 U/mL) or nearly completely abolished (1 U/mL) NADPH autofluorescence produced by NADP-ICDH (Fig. 2A), in agreement with dehydrogenation of NADPH by GR. Normalized and blank-corrected spectra showed no difference of NADPH spectral properties in the presence or absence of GR with GSSG and our data revealed no modifications of NADPH lifetime kinetic properties by GR (data not shown).

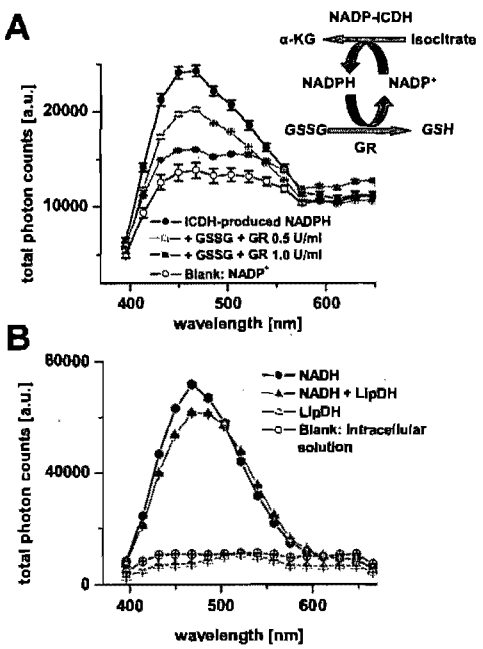

Figure 2. Normalized, background-corrected steady-state emission spectra of ICDH-produced NADPH in the absence and presence of GR (0.5 or 1 U/mL, n=5 samples each) (**A**) and of 20 μM NADH (n=10) in the absence and presence of 2 U/μL LipDH in intracellular solution (n=5) (**B**).

On the other hand, dehydrogenation of NADH (20 μM) to NAD^+ by LipDH (at 2 U/μL) - a disulfide oxidoreductase which is a part of the multienzyme Complex I - decreased fluorescence intensity (Fig. 2B). The effect was accompanied by a spectral broadening of about 10 nm towards red spectral region, as demonstrated by normalized emission spectra (Fig. 3A). NADH fluorescence decays were prolonged by LipDH (Fig. 3B) due to a significantly increased lifetime of the component 2 (at 504 nm, τ2 was prolonged from 1.84±0.12 ns to 2.74±0.18 ns, $p<0.05$).

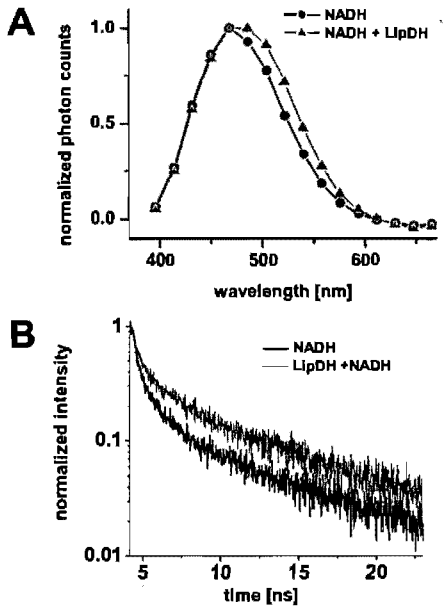

Figure 3. Comparison of normalized, background-corrected steady-state emission spectra of NADH (20 μM; n=10 samples) in the absence or presence LipDH (2 U/μL) in intracellular solution (n=5) (**A**). NADH normalized fluorescence lifetimes (20 μM) at 504 nm with or without LipDH (2 U/μL) (**B**).

3.3. Endogenous NAD(P)H in cardiac cells

To investigate the endogenous fluorescence of NAD(P)H in living cardiomyocytes, spectrally and time-resolved autofluorescence decays were recorded in cells bathed in basic external solutions. Normalized steady-state emission spectra of the cardiomyocyte auto fluorescence had spectral maximum at 450 nm (Fig. 4) and showed a slight blue-spectral shift when compared to NADH *in vitro*, while being closer to those of NADPH. Analysis of exponential decay of cardiomyocyte autofluorescence showed acceptable chi-square values ($\chi^2<1.2$; n=70/13 animals) and flat plot of weighted residuals when using at least a 3-exponential model, namely τ1 = 0.69±0.01 ns (69.3±1.0%), τ2 = 2.03±0.05 ns (27.6±0.9%) and τ3 = 12.68±0.08 ns (3.1±0.2%).

4. Discussion and conclusions

Although spectra of intrinsically fluorescing substances are now well characterized in cardiac tissue, the fluorescence lifetimes, considered to provide better quantitative measurement of different NAD(P)H conformations and/or molecular complexes contributing to the UV-excited autofluorescence of biological samples, are much less clearly identified in living cells. Here we demonstrate that NAD(P)H autofluorescence can be measured in living cardiomyocytes by time-resolved emission spectroscopy approach with good reproducibility. Recorded autofluorescence kinetics were comparable to already published data in cardiac mitochondria [2]. As expected, comparison with NADH and NADPH kinetics in vitro pointed to the NAD(P)H origins of the autofluorescence. While our data confirmed close spectral characteristics of NADH and NADPH molecules, curiously, we have identified differences in their lifetimes. This can be due to distinct kinetics of the two molecules, or the presence of impurities; kinetics of further purified molecules need to be done in the future.

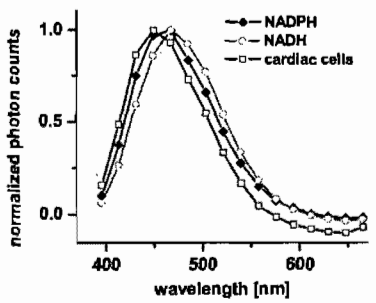

Figure 4. Normalized, background-corrected emission spectra, determined as total photon counts of NAD(P)H autofluorescence of single cardiac cells, compared to NADH and NADPH (both 20 μM) in basic extracellular solution.

The LipDH flavoprotein served as example to investigate NADH dehydrogenation. Observed increase in the lifetime kinetics can be related to conformational changes of NADH induced by the enzyme. Indeed, upon dehydrogenation, the oxidized form of the protein promotes the binding of the neutral dihydro-nicotinamide moiety of NADH [3], in addition to the formation of negatively charged charge-transfer complexes between transiently bound NAD^+ and covalently bound flavin adenine dinucleotide (FAD) cofactor. In this reduced form, nicotinamide moiety is in a different conformation from uniformly ordered structure of NADH juxtaposing nicotinamide and isoalloxazine flavin ring systems and is not proximal to FAD [3], which can be reflected in the change of fluorescence kinetics. On the other hand, appearance of the red-spectral shoulder points to possible presence of Förster resonant energy transfer (FRET). Being a flavoprotein, excitation of LipDH by visible light (420-460 nm) results in green FAD-autofluorescence with emission maximum around 500 nm [4]. As the LipDH-binding domain for NADH is in close proximity to FAD^+-binding one [3] and the 450 nm emission maximum of NADH corresponds exactly to an absorption peak of the FAD^+ moiety, this fulfils the prerequisites for the FRET between the two molecules. Nevertheless, since no decrease in NADH lifetime(s) was observed, further study is needed to fully understand significance of changes in NADH fluorescence following its binding to enzymes in living cells. Failure to observe lifetime kinetic changes following NADPH dehydrogenation by GR can be due to much faster kinetics of the NADPH molecule and/or much lower signal recorded in these experiments. Gathered data demonstrate the robustness of the TCSPC approach for NAD(P)H autofluorescence study directly in living cells. This approach brings an important insight into the understanding of metabolic state(s) of the heart in pathophysiological conditions.

Acknowledgements

Supported by CIHR (MOP 84450) grant to AC.

References

[1] Benderdour M, Charron G, Comte B, et al. Decreased cardiac mitochondrial $NADP^+$-isocitrate dehydrogenase activity and expression: a marker of oxidative stress in hypertrophy development. Am J Physiol Heart Circ Physiol 2004;287:H2122-H2131.

[2] Blinova K, Carroll S, Bose S et al. Distribution of mitochondrial NADH fluorescence lifetimes: steady-state kinetics of matrix NADH interactions. Biochemistry 2005;44:2585-2594.

[3] Brautigam CA, Chuang JL, Tomchick DR, Machius M, Chuang DT. Crystal structure of human dihydrolipoamide dehydrogenase: NAD^+/NADH binding and the structural basis of disease-causing mutations. J Mol Biol 2005;350:543-552.

[4] Chorvat D Jr, Chorvatova A. Spectrally resolved time-correlated single photon counting: a novel approach for characterization of endogenous fluorescence in isolated cardiac myocytes. Eur Biophys J 2006;36:73-83.

Address for correspondence

Dr. Chorvatova Alzbeta
Research Center of CHU Sainte Justine, University of Montreal
3175 Cote Sainte Catherine, H3T 1C5 Montreal, Canada
Email. [redacted]

APPENDIX II:

CHENG Y., DAHDAH N., POIRIER N., MIRO J., CHORVAT D. JR., CHORVATOVA A., 2007: Spectrally and time-resolved study of NADH autofluorescence in cardiomyocytes from human biopsies. ***Proceedings of SPIE, the International Society for Optical Engineering*** *Vol. 6771,* Advanced Photon Counting Techniques II: 677104-1 to 677104-13.

Invited Paper

Spectrally and Time-Resolved Study of NAD(P)H Autofluorescence in Cardiac Myocytes from Human Biopsies

Cheng Y.[1], Chorvat Jr. D.[2], Poirier N. [1,3], Miró J. [1,3], Dahdah N. [1,3] and Chorvatova A.[1,3*]

[1]Research Centre, CHU Sainte-Justine, Montreal, Canada, [2]Department of Biophotonics, International Laser Centre, Bratislava, Slovakia, [3]Department of Pediatrics, University of Montreal, Canada.

Correspondence should be addresses to: Alzbeta Chorvatova, Research Centre, CHU Sainte-Justine, 3175 Cote Sainte Catherine, H3T 1C5, Montreal, Qc, Canada, Tel. 514.345.4931/4366, Fax 514.345.4801, E-mail: [redacted]

Abstract

Rejection of transplanted hearts remains an important reason for death of transplanted children. Finding diagnostic tools for its detection can therefore improve the prognosis in this population of patients. Endomyocardial biopsy (EMB) by cardiac catheterization is currently accepted as the "gold standard" for the diagnosis of rejection. Here, we investigate new approach to monitor mitochondrial metabolic state of cardiac cells using spectrally-resolved autofluorescence lifetime detection of nicotinamide adenine dinucleotide (phosphate), or NAD(P)H, the principal electron donor in mitochondrial oxidative energy metabolism responsible for vital ATP supply of cardiomyocytes. NAD(P)H autofluorescence is long used for non-invasive fluorescent probing the metabolic state of the heart. In this contribution we report dynamic characteristics of NAD(P)H fluorescence decays in living human cardiomyocytes from EMB, following excitation by UV-pulsed laser diode and detection by spectrally-resolved time-correlated single photon counting. At least a 3-exponential decay model, with 0.5-0.7 ns, 1.9-2.4 ns and 9.0-15.0 ns lifetimes, is necessary to describe cardiomyocyte autofluorescence in human cells. When gathered data were compared to those recorded under same conditions in rats, autofluorescence in human hearts was found significantly lower in comparison to rat ones. Rotenone, the inhibitor of the Complex I of the respiratory chain, increased the fluorescence in human cardiac cells, making them more comparable to experimental rat model. These results suggest that human cardiac cells are more metabolically active than the rat ones in the same conditions. Presented work proposes a new tool for evaluation of oxidative metabolism changes in transplanted hearts.

Keywords: TCSPC, NAD(P)H Autofluorescence, Human Cardiac Biopsy.

1. INTRODUCTION

Rejection of transplanted hearts is the most important cause of death of transplanted children [11,13]. Search for new diagnostic tools is therefore crucial to insure its early detection and hence efficient prevention. The risk of rejection, highest in the first three postoperative months, decreases six month following transplantation mainly thanks to routine rejection surveillance. In this period, the main problem of the heart transplant recipients includes acute allograft rejection, cardiac allograft vasculopathy and infections which can occur at anytime after the transplantation, often several years after the operation [17,22]. In these conditions, the coronary arteries develop progressive and diffuse (scattered and spread out) narrowing throughout their entire length. Such type of narrowing is different from the fatty or calcified plaque that typically causes atherosclerotic coronary artery disease, but can, as well, result in nutrients and oxygen deprivation of the heart and lead to the failure of normal function of cardiac cells. Coronarography is used to monitor the presence of vascular rejection. Acute rejection is defined as lymphatic inflammatory infiltration with associated damage and/or necrosis of cardiac cells and this cardiac tissue [22]. Endomyocardial biopsy (EMB) with cardiac catheterization is currently accepted as the "gold standard" for the diagnosis of this type of rejection [18]. This method helps to estimate and grade the presence of rejection, but it does not always have the sufficient sensitivity to detect mild cases of the rejection at their early stages. At the same time, recently, new technologies were developed to monitor oxidative metabolic state of cardiac cells by measuring their endogenous fluorescence. We hypothesize that oxidative changes of

Advanced Photon Counting Techniques II, edited by Wolfgang Becker, Proc. of SPIE
Vol. 6771, 677104, (2007) · 0277-786X/07/$18 · doi: 10.1117/12.732876

cardiac cells occur at early stages of rejection of transplanted hearts and thus can serve as a diagnostic tool for its early detection.

Our goal is to investigate possible applications of the latest technologies at the level of living cardiomyocytes obtained from one additional endomyocardial biopsy, in the aim to better understand mechanisms underlying cardiac rejection and to propose new approaches for its diagnostics. We search for a new tool to improve the detection of rejection in its early stages and in this study, we investigate the possibility to study oxidative metabolic state of cardiac cells isolated from EMB of transplanted pediatric patients by analyzing their autofluorescence using spectrally-resolved fluorescence lifetime detection. We analyze mitochondrial oxidative metabolic changes of cardiomyocytes obtained from one additional biopsy during catheterization and EMB of pediatric patients with transplanted hearts. We characterize spectral and temporal characteristics of endogenous NAD(P)H fluorescence directly in living cardiomyocytes using simultaneous detection of their fluorescence spectra and fluorescence lifetimes. NAD(P)H fingerprinting by spectrally-resolved lifetime spectroscopy is investigated in cells isolated from human biopsies, together with changes of the autofluorescence intensity and its lifetimes following the modulation of NAD(P)H respiratory chain by rotenone. Gathered results are compared to data obtained in cells isolated using similar approach from hearts of rat experimental model.

2. MATERIAL AND METHODS

Cardiomyocyte Isolation from Human Biopsies

Cells were isolated from one additional biopsy during catheterization and EMB of pediatric patients with transplanted hearts (elective or triggered by a clinical or echocardiographic suspicion or rejection), performed routinely by the Cardiac Sciences Service at Sainte Justine Hospital during the regular check of patients. Cardiac tissue was obtained by the pediatric cardiologist (N.D., N.P. or J.M.) from the right ventricular EMB sample of children with cardiac transplantation using cardiac catheterization. Biopsies from transplanted children aging from several months to 18 years (mean age of 10 years) were used. The tissue of a weight of 1 to 5 mg, bulk of 1 to 2 mm^3 piece was promptly immersed in the isolation medium [14] (in mmol/L: NaCl, 35.0; KCl, 7.7; Na_2HPO_4, 16; $NaHCO_3$, 25; KH_2PO_4, 1.2; sucrose, 134.0; glucose, 10.0; and HEPES, 10.0; titrated to pH 7.30 with NaOH) under oxygenation with 5% CO_2 and 95% O_2 (using a portable device) and taken to the lab (in the same building), where the tissue were washed and cells isolated following enzymatic digestion with collagenase (Type V) and protease (type XXIV) for 20-50 min. All chemicals were from Sigma-Aldrich (Canada). The cell suspension was filtered with 250 μm pore size, centrifuged for 2 minutes at 100 x g and the pellet rinsed and resuspended in the isolation solution and used immediately after isolation (success rate of about 5%; see the right panel of the Fig. 1 for illustration of representing isolated cells from human biopsies). All procedures were performed in accordance with Institutional Ethical Committee and with the patient's (or their parent's) consent.

Cardiomyocyte Isolation from Rat Hearts

Sprague-Dawley rats (13-14 week old, Charles River, Canada) were sacrificed by decapitation. All procedures were performed in accordance with Institutional Committee accredited by the Canadian Council for the Protection of Animals (CCPA). Ventricular myocytes were isolated from chunks of tissue by same approach as described for human myocytes (success rate of about 10 %). Only cells that showed clearly defined striations were used.

Recording of Cardiomyocyte Autofluorescence by Spectrally-Resolved Time-Correlated Single Photon Counting (TCSPC)

To record kinetics of NAD(P)H autofluorescence in cardiac cells, we have used TCSPC setup on Axiovert 200 inverted microscope, as previously described [8]. In brief, picosecond laser diode with emission of 375 nm (BDL-375, Becker&Hickl, Boston Electronics, U.S.A.) was used at 20 MHz repetition rate as an excitation source with output power ~1 mW. The emitted fluorescence was spectrally separated from the laser excitation using standard dichroic filter cubes (395 nm dichroic and 397 nm long-pass filter for excitation at 375 nm) located in the microscope filter turret. Data were acquired by a 16-channel photomultiplier (PML-16, Becker&Hickl, Boston Electronics, U.S.A), after spectral decomposition via an imaging spectrograph (Solar 100, Proscan, Germany). The TCSPC card (SPC 830, Becker&Hickl, Boston Electronics, U.S.A), driven by SPCM_95 software (Becker&Hickl, Boston Electronics, U.S.A), was

synchronized by the laser diode driver. Fluorescence decays were measured simultaneously at 16 spectral channels with 25 ns Time-to-Amplitude Converter (TAC) time-base sampled by 1024 points, leading to the temporal resolution of 24.4 ps/channel. Decay kinetics were measured for 30 s, with the number of counts at each channel reaching maximum intensity of about 500-5000 counts and the typical background noise of 10-100 counts per channel, present mostly due to ambient light. Cells were mounted on an inverted microscope and studied at room temperature in 4-well chambers with UV-proof coverslip-based slides (LabTech, Canada). Rotenone (1 μmol/L) was added to cells for 5-25 min prior recording.

Data Analysis

Data were analyzed using SPCImage software (Becker&Hickl, Boston Electronics, U.S.A). All data were corrected for the systematic wobble of the temporal-shift in the detected photon histogram at different channels of the PMT array [3] using custom procedures for data correction and analysis written in C^{++} [8]. Home-made database was used for appropriate data management. Steady-state autofluorescence was evaluated as total photon counts for each spectral channel. Each lifetime component was assessed by examining its fluorescent lifetime (τ_i) and relative amplitude (a_i); see Chorvat et al., 2006 [8] for details on definition of terms and derived quantities. Data are shown as mean ± standard error (SEM). Comparison between means was made at spectral maximum of 450 nm, using one-way analysis of variance (ANOVA), followed by Tukey post-test.

3. RESULTS

NAD(P)H Autofluorescence in Human Cardiomyocytes

To investigate endogenous fluorescence of NAD(P)H, spectrally and time-resolved autofluorescence decays were recorded in living human cardiac myocytes (see an example of an original recording from one cell at the left panel of the Fig. 1 and Methods for details), following excitation of an elliptical spot (20 x 10 μm) by the 375 nm picosecond laser diode (see an example of the cell illumination at the Fig. 1, right panel). To study endogenous fluorescence in living cardiac cells we have used a newly-designed micro-spectrometer [8], based on the combination of inverted fluorescence microscope with TCSPC instrumentation. Steady-state emission spectra of the cardiomyocyte autofluorescence, determined from the total photon counts on each spectral channel (Fig. 2, left panel), had a spectral maximum at 450 nm, as illustrated by normalized spectra (Fig. 2, right panel). Exponential decay of cardiomyocyte autofluorescence (Fig. 3) showed acceptable chi-square values (χ^2<1.1) and flat plot of weighted residuals when analyzed using at least a 3-exponential model (see Table 1 for data at 450 nm emission wavelength). Fluorescence lifetimes were therefore estimated as a 3-exponental decay. We evaluated data only for spectral channels which intensity reached threshold of 500 counts in maximum, i.e. within the spectral range of 420 nm to 550 nm (Fig. 4). When illustrated in regard to emission wavelength between 420-550 nm, the lifetime of both the first and the second components exhibited a slight decrease, while that of the third component presented a slight increase at longer wavelengths within the assessed spectral range (Fig. 4, right panel). The relative amplitudes of all three lifetime components changed only slightly in the analyzed spectral region (within 10 % fraction of the total population, Fig. 4, left panel).

Comparison of NAD(P)H Autofluorescence in Human vs. in Rat Cardiomyocytes

The above data are, to our knowledge, first spectrally and time-resolved data recorded in human heart cells. We therefore wanted to make their comparison to models that are more commonly used for study of metabolic activity of cardiac cells, such as the rat one. When compared to cells isolated by the same experimental approach from rat hearts, we have found significantly smaller total photon counts in human cells. This result was accompanied by significantly smaller relative amplitude of the component 1, against significantly higher relative amplitude of the component 2. We also observed a tendency of the lifetime of the component 1 and 3 to increase in human cells, but this change was not significant. We hypothesized that this result can be related to a lower amount of NAD(P)H present in human cells due to higher metabolic activity of the respiratory chain and thus more substantial ATP production. NADH is well known main electron donor necessary for creation of the electrochemical gradient in cardiac cells, used in the process of oxidative metabolism for ATP generation. This process is initiated following dehydrogenation of NADH by the Complex I of the respiratory chain. To account for the hypothesis of higher metabolic activity, we have therefore analyzed AF in human cells in the presence of rotenone, an inhibitor of the Complex I of the respiratory chain [1,10]. As expected, rotenone

increased the total photon counts of the human cells (Fig. 2), while modifying fluorescent decays (Fig. 3) by rising the relative amplitude of the first component and decreasing the second one (Fig. 4). In the presence of rotenone, human cells were therefore more comparable to rat ones. These data point to possible higher metabolic activity in control conditions in human cells, when compared to the commonly used rat model. However, a more profound study of autofluorescence using confocal microscopy is needed in the future to avoid differences due to signal dependence on the cell size.

4. DISCUSSION

In the present contribution, we evaluated for the first time spectrally-resolved lifetime characteristics of NAD(P)H autofluorescence in living cardiac cells isolated from human endomyocardial biopsies of pediatric patients. We have analyzed the kinetics of cell NAD(P)H autofluorescence and its responsiveness to rotenone, the inhibitor of the Complex I. Our data indicate that the use of spectrally-resolved TCSPC method greatly improves the analysis of the metabolic state of isolated cardiac cells and suggest that human cells are more metabolically active than the rat ones in the same conditions.

Rejection of transplanted hearts is still the principal reason for death of transplanted pediatric patients. Organ rejection of transplants includes hyperacute rejection, acute rejection and chronic rejection. Hyperacute rejection appears shortly after operation and is often easily recognized, as the patients are well monitored in this period. This is usually due to immune system changes that may occur after the transplantation. However, more problems are encountered concerning the recognition and the diagnosis of acute and chronic rejections, or the Graft Coronary Artery Disease (GCAD). This type of rejection can occur at anytime after the transplantation, often several years after the operation. In these conditions, the coronary arteries develop progressive and diffuse (scattered and spread out) narrowing throughout their entire length. Such type of narrowing is different from the fatty or calcified plaque that typically causes atherosclerotic coronary artery disease, but can, as well, result in nutrients and oxygen deprivation of the heart and lead to the failure of normal cardiomyocyte function. Such modifications, which also include alterations in the cell oxidative metabolism, often develop rapidly. Some observations suggest that cardiac cells undergo modifications in their oxidative state with the progression of cardiac rejection [23,24], namely as a result of cell hypoxia, following oxidative changes of cardiac cells. Precise evaluation of the oxidative metabolism can therefore serve as an early indication of the rejection of transplanted hearts.

The heart is a pump converting chemical energy into mechanical work and the power for this work is gathered almost entirely from oxidation of carbon fuels and to a great extent these fuels are provided by coronary (myocardial) blood flow. Such oxidative metabolism is primarily the function of mitochondria in the process of oxidative phosphorylation. Because of the high oxidative metabolism, heart cells have elevated oxidative capacity, demonstrated by their ultrastructure: 25–35% of total cardiomyocyte volume is occupied by mitochondria [2]. During hypoxia or ischemia, the supply of O_2 to the respiratory chain fails, leading to blocking of the tricarboxylic acid cycle and no energy being available from oxidative phosphorylation. This results in an accumulation of cytoplasmic NADH which is accompanied, in ischemia, by an accumulation of lactate and a decrease in cytoplasmic pH (5.5–6) [21,25]. Many researchers have identified Complex I as a major site of damage to the respiratory chain in ischemia [4,15] and observed a reduction in oxidation rate for NADH-linked substrates by up to 60%.

In recent years, new technological approaches were developed to investigate oxidative metabolic changes in tissues and cells. Our previously obtained data in rat cardiomyocytes [7-9] clearly demonstrated that metabolic state can be determined directly in living cardiac cells by monitoring their naturally occurring autofluorescence. Bulk of AF, generated after excitation with UV or visible light is localized in mitochondria and is mainly resulting from mitochondrial oxidized flavins (FAD^*) and reduced NAD(P)H [20], principal endogenous indicators of cellular oxidative metabolism. These molecules exist in their free forms, or as cofactors in enzymes of inner mitochondrial membrane and are involved in the mitochondrial respiratory chain and in the fatty acid oxidation. ATP, produced in the process of mitochondrial oxidative phosphorylation, is the primary molecular source of energy for the contraction of cardiac cells. This process is coupled to oxidation of reduced NADH, the principal electron donor for electrochemical gradient necessary for oxidative energy metabolism which accounts for 95% of ATP generation in cardiomyocyte mitochondria. Endogenous fluorescence of NADH, induced following excitation with the UV light, is long used for non-invasive fluorescent probing of metabolic state [5] and has been an extremely useful tool for monitoring of energy metabolism

[6]. Blue autofluorescence of rat cardiac myocytes was demonstrated to correlate with metabolic changes and was ascribed to mitochondrial NADH [12].

In human cardiomyocytes, a comprehensive study on the contribution of changes in NADH is largely missing. Our data show good reproducibility of results and comparison with commonly used models, such as the rat one. Autofluoresence spectroscopy has been widely used in the early detection of different types of cancers [16,27] and was also attempted in examination of transplanted tissues. In the heart, a strong correlation was found between changes in autofluorescence spectra and the rejection grade in rat heart allograft model [19], but more difficulties were encountered using human tissues [26], possibly due to use of frozen fractions, as well as lack of analysis of dynamic parameters of the recorded fluorescence. Fluorescence lifetimes reflect the characteristic time that the molecule spends in the excited state and are specific for different molecular conformations. They are also sensitive to interactions of the fluorescing molecule with its surroundings. Thus, in multi-compartment complex systems such as in cells, the observed fluorescence is often described by multi-exponential decays, even if in *in vitro* conditions the studied molecule has single-exponential characteristics. Based on data gathered in this contribution, we therefore propose to use the spectrally-resolved TCSPC approach as an interesting new multiparametric tool that can be applied to freshly-isolated cells from human biopsies. In addition to its higher sensitivity than conventional techniques, another advantage of this method is the possibility of its combination to multiphoton confocal microscopy, which, in the future, can result in the adaptation of this approach directly to tissue biopsy without the necessity of cell isolation.

5. SUMMARY

Spectrally-resolved fluorescence lifetime detection was tested as a promising new tool for quantitative analysis of intrinsic cellular autofluorescence signals in living cardiomyocytes and hence for assessment of changes in oxidative metabolism in the heart of transplanted patients. This work is the first study evaluating the lifetime characteristics of NAD(P)H fluorescence and thus the cardiac metabolic state in cells from human biopsy. In the future, this approach will be tested to compare oxidative metabolic state of human cardiac myocytes at different stages of rejection, to improve the detection of early or mild cases of rejection, particularly in the case of doubtful histological results and hence in the decision-making for rapid initiation of the necessary treatment. Using the described method will not only enhance our understanding of mechanisms underlying the rejection of transplanted hearts in pediatric patients, but it may eventually also improve the diagnostics of cardiac transplant rejection by supplementing the currently used histological analysis.

Acknowledgements

This work was supported by Canadian Foundation for Innovation (N° 9684) and Groupe de Recherche Universitaire sur Médicament grant to AC. AC is recipient of fellowship from Fonds de la Recherche en Santé du Québec (N° 2948). We would like to thank Mme Sylvie Michaud for the patient recruitment, Anton Mateasik for custom-written procedures for data correction and analysis and Qian Wu for creation of database for data management.

6. REFERENCES

[1] Balaban, R. S.; Heineman, F. W. Control of mitochondrial respiration in the heart in vivo. *Mol. Cell Biochem.* **89**:191-197; 1989.

[2] Bassien-Capsa, V.; Fouron, J. C.; Comte, B.; Chorvatova, A. Structural, functional and metabolic remodeling of rat left ventricular myocytes in normal and in sodium-supplemented pregnancy. *Cardiovasc. Res.* **69**:423-431; 2006.

[3] Becker, W. Advanced Time-Correlated Single Photon Counting techniques: New York Springer; 2005.

[4] Cairns, C. B.; Ferroggiaro, A. A.; Walther, J. M.; Harken, A. H.; Banerjee, A. Postischemic administration of succinate reverses the impairment of oxidative phosphorylation after cardiac ischemia and reperfusion injury. *Circulation* **96**:II-5; 1997.

[5] Chance, B. Pyridine nucleotide as an indicator of the oxygen requirements for energy-linked functions of mitochondria. *Circ. Res.* **38**:I31-I38; 1976.

[6] Chance, B.; Schoener, B.; Oshino, R.; Itshak, F.; Nakase, Y. Oxidation-reduction ratio studies of mitochondria in freeze-trapped samples. NADH and flavoprotein fluorescence signals. *J. Biol. Chem.* **254**:4764-4771; 1979.

[7] Chorvat, D., Jr.; Bassien-Capsa, V.; Cagalinec, M.; Kirchnerova, J.; Mateasik, A.; Comte, B.; Chorvatova, A. Mitochondrial autofluorescence induced by visible light in single cardiac myocytes studied by spectrally resolved confocal microscopy. *Laser Physics* **14**:220-230; 2004.

[8] Chorvat, D., Jr.; Chorvatova, A. Spectrally resolved time-correlated single photon counting: a novel approach for characterization of endogenous fluorescence in isolated cardiac myocytes. *Eur. Biophys. J.* 2006.

[9] Chorvat, D., Jr.; Kirchnerova, J.; Cagalinec, M.; Smolka, J.; Mateasik, A.; Chorvatova, A. Spectral unmixing of flavin autofluorescence components in cardiac myocytes. *Biophys. J.* **89**:L55-L57; 2005.

[10] Davies, K. J.; Doroshow, J. H. Redox cycling of anthracyclines by cardiac mitochondria. I. Anthracycline radical formation by NADH dehydrogenase. *J. Biol. Chem.* **261**:3060-3067; 1986.

[11] Dipchand, A. I. Heart transplantation: Literature review 2004-2005. *Pediatr. Transplant.* **10**:279-287; 2006.

[12] Eng, J.; Lynch, R. M.; Balaban, R. S. Nicotinamide adenine dinucleotide fluorescence spectroscopy and imaging of isolated cardiac myocytes. *Biophys. J.* **55**:621-630; 1989.

[13] Feingold, B.; Webber, S. A. Heart transplantation: Literature review 2003-2004. *Pediatr. Transplant.* **9**:430-439; 2005.

[14] Guinamard, R.; Chatelier, A.; Demion, M.; Potreau, D.; Patri, S.; Rahmati, M.; Bois, P. Functional characterization of a Ca(2+)-activated non-selective cation channel in human atrial cardiomyocytes. *J. Physiol* **558**:75-83; 2004.

[15] Hardy, L.; Clark, J. B.; Darley-Usmar, V. M.; Smith, D. R.; Stone, D. Reoxygenation-dependent decrease in mitochondrial NADH:CoQ reductase (Complex I) activity in the hypoxic/reoxygenated rat heart. *Biochem. J.* **274 (Pt 1)**:133-137; 1991.

[16] Katz, A.; Savage, H. E.; Schantz, S. P.; McCormick, S. A.; Alfano, R. R. Noninvasive native fluorescence imaging of head and neck tumors. *Technol. Cancer Res. Treat.* **1**:9-15; 2002.

[17] Kuhn, M. A.; Deming, D. D.; Cephus, C. E.; Mulla, N. F.; Chinnock, R. E.; Razzouk, A. J.; Larsen, R. L. Moderate acute rejection detected during annual catheterization in pediatric heart transplant recipients. *J Heart Lung Transplant.* **22**:276-280; 2003.

[18] Miniati, D. N.; Robbins, R. C. Heart transplantation: a thirty-year perspective. *Annu. Rev. Med.* **53**:189-205; 2002.

[19] Morgan, D. C.; Wilson, J. E.; MacAulay, C. E.; MacKinnon, N. B.; Kenyon, J. A.; Gerla, P. S.; Dong, C.; Zeng, H.; Whitehead, P. D.; Thompson, C. R.; McManus, B. M. New method for detection of heart allograft rejection: validation of sensitivity and reliability in a rat heterotopic allograft model. *Circulation* **100**:1236-1241; 1999.

[20] Romashko, D. N.; Marban, E.; O'Rourke, B. Subcellular metabolic transients and mitochondrial redox waves in heart cells. *Proc. Natl. Acad. Sci. U. S. A* **95**:1618-1623; 1998.

[21] Smith, D. R.; Stone, D.; Darley-Usmar, V. M. Stimulation of mitochondrial oxygen consumption in isolated cardiomyocytes after hypoxia-reoxygenation. *Free Radic. Res.* **24**:159-166; 1996.

[22] Stewart, S.; Winters, G. L.; Fishbein, M. C.; Tazelaar, H. D.; Kobashigawa, J.; Abrams, J.; Andersen, C. B.; Angelini, A.; Berry, G. J.; Burke, M. M.; Demetris, A. J.; Hammond, E.; Itescu, S.; Marboe, C. C.; McManus, B.; Reed, E. F.; Reinsmoen, N. L.; Rodriguez, E. R.; Rose, A. G.; Rose, M.; Suciu-Focia, N.; Zeevi, A.; Billingham, M. E. Revision of the 1990 working formulation for the standardization of nomenclature in the diagnosis of heart rejection. *J Heart Lung Transplant.* **24**:1710-1720; 2005.

[23] Tanaka, M.; Mokhtari, G. K.; Terry, R. D.; Balsam, L. B.; Lee, K. H.; Kofidis, T.; Tsao, P. S.; Robbins, R. C. Overexpression of human copper/zinc superoxide dismutase (SOD1) suppresses ischemia-reperfusion injury and subsequent development of graft coronary artery disease in murine cardiac grafts. *Circulation* **110**:II200-II206; 2004.

[24] Tanaka, M.; Nakae, S.; Terry, R. D.; Mokhtari, G. K.; Gunawan, F.; Balsam, L. B.; Kaneda, H.; Kofidis, T.; Tsao, P. S.; Robbins, R. C. Cardiomyocyte-specific Bcl-2 overexpression attenuates ischemia-reperfusion injury, immune response during acute rejection, and graft coronary artery disease. *Blood* **104**:3789-3796; 2004.

[25] Vuorinen, K.; Ylitalo, K.; Peuhkurinen, K.; Raatikainen, P.; Ala-Rami, A.; Hassinen, I. E. Mechanisms of ischemic preconditioning in rat myocardium. Roles of adenosine, cellular energy state, and mitochondrial F1F0-ATPase. *Circulation* **91**:2810-2818; 1995.

[26] Yamani, M. H.; van de Poll, S. W.; Ratliff, N. B.; Kuban, B. E.; Starling, R. C.; McCarthy, P. M.; Young, J. B. Fluorescence spectroscopy of endomyocardial tissue post-human heart transplantation: does it correlate with histopathology? *J. Heart Lung Transplant.* **19**:1077-1080; 2000.

[27] Yang, Y.; Katz, A.; Celmer, E. J.; Zurawska-Szczepaniak, M.; Alfano, R. R. Fundamental differences of excitation spectrum between malignant and benign breast tissues. *Photochem. Photobiol.* **66**:518-522; 1997.

LEGENDS

Fig. 1. Representative original recordings of time- and spectrally-resolved autofluorescence of single human cardiomyocyte in control conditions measured simultaneously at 16 acquisition channels (recorded for 30 s with 25 ns TAC time-base and sampled by 1024 points), following excitation with 375 nm pulsed laser (left). Example of the recorded cells (right).

Fig. 2. Steady-state (left) and normalized (right), background-corrected autofluorescence emission spectra of human cardiomyocyte autofluorescence determined as total photon counts, recorded in the control conditions and in the presence of 1 μM rotenone.

Fig. 3. Normalized fluorescence decays at 450 nm of autofluorescence in human cardiomyocyte in control conditions and in the presence of 1 μM rotenone, compared to fluorescence decays gathered in rats.

Fig. 4. Relative amplitudes a1, a2 and a3 (left panel) and mean spectrally-resolved fluorescence lifetimes τ1, τ2 and τ3 (right panel).

Table 1. Fluorescence parameters of cardiomyocyte autofluorescence ($\lambda_{excitation/emission}$ = 375 nm/450 nm). Data are shown as mean ± SEM (number of cells); *p<0.05 vs. control human cells.

Figure 1.

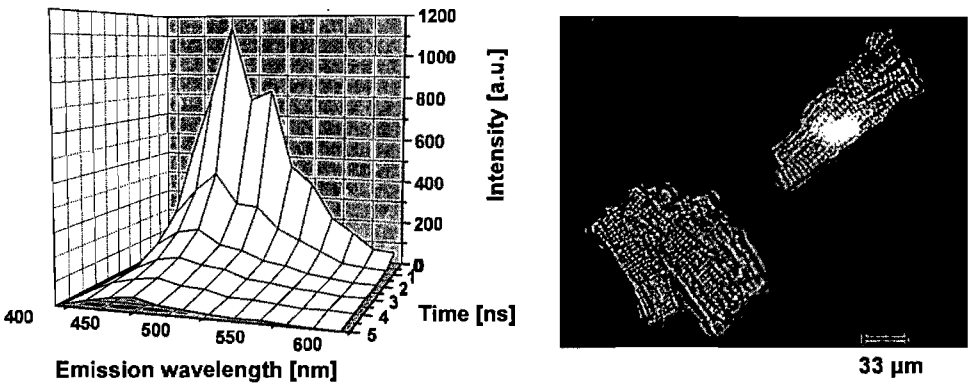

Fig. 1. Representative original recordings of time- and spectrally-resolved autofluorescence of single human cardiomyocyte in control conditions measured simultaneously at 16 acquisition channels (recorded for 30 s with 25 ns TAC time-base and sampled by 1024 points), following excitation with 375 nm pulsed laser (left). Example of the recorded cells (right).

Figure 2.

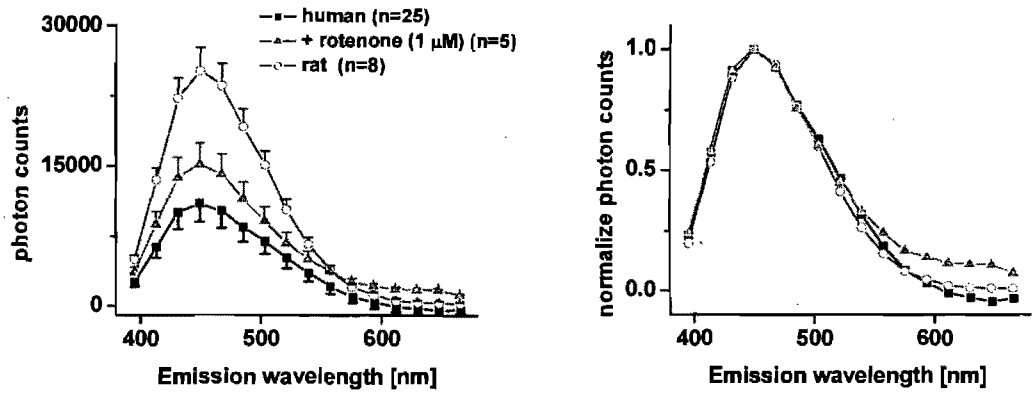

Fig. 2. Steady-state (left) and normalized (right), background-corrected autofluorescence emission spectra of human cardiomyocyte autofluorescence determined as total photon counts, recorded in the control conditions and in the presence of 1 μM rotenone.

Figure 3.

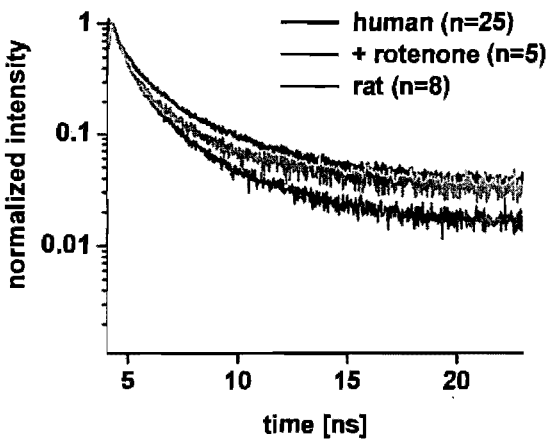

Fig. 3. Normalized fluorescence decays at 450 nm of autofluorescence in human cardiomyocyte in control conditions and in the presence of 1 μM rotenone, compared to fluorescence decays gathered in rats.

Figure 4.

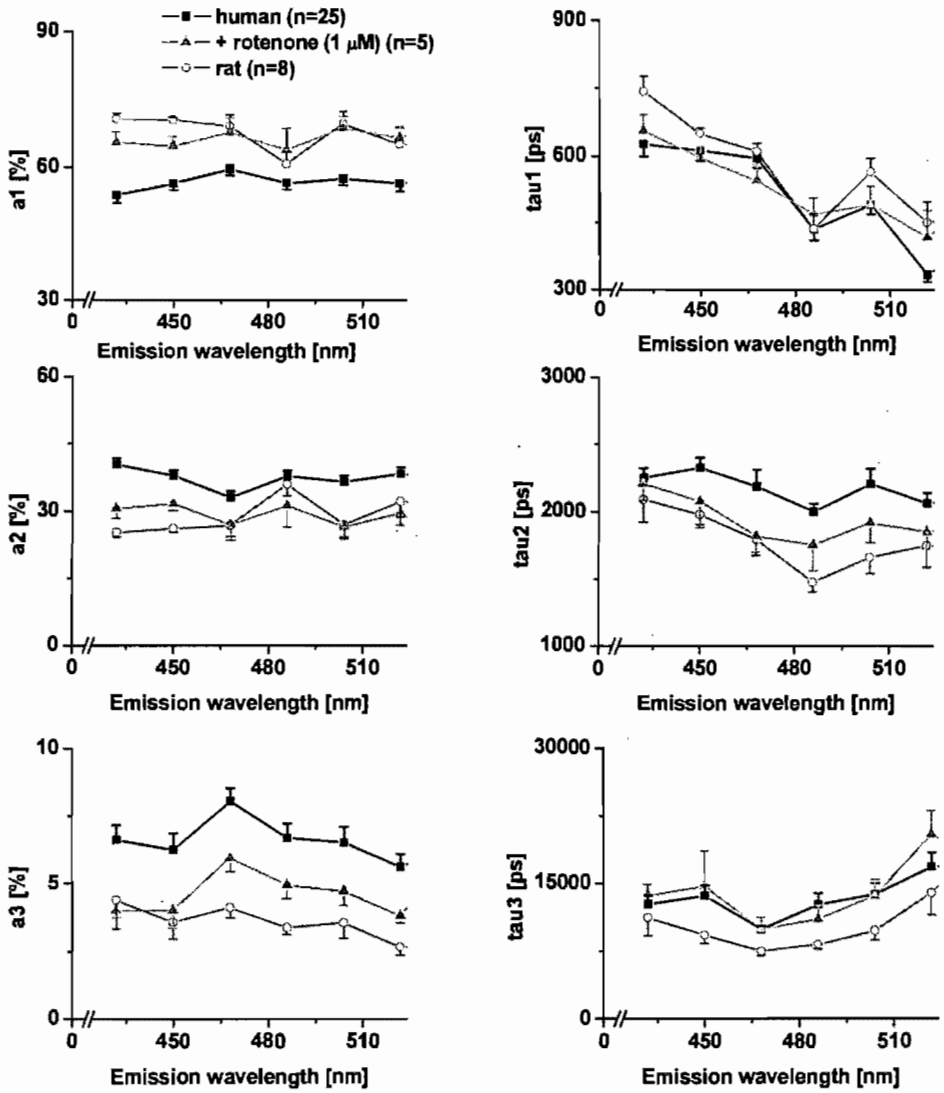

Fig. 4. Relative amplitudes a1, a2 and a3 (left panel) and mean spectrally-resolved fluorescence lifetimes τ1, τ2 and τ3 (right panel).

Table 1.

	Total photon counts [a.u.]	a_1	τ_1 [ps]	a_2	τ_2 [ps]	a_3	τ_3 [ps]
Human (25)	11022±1961	56.04±1.56	612.54±22.49	37.84±1.16	2324.75±73.83	6.23±0.63	13634.98±1139.30
Human + Rotenone (5)	15194±2324	64.60±2.09*	596.44±25.56	31.60±1.44*	2076.53±195.19	4.02±0.66	14658.67±3987.45
Rat (8)	25175±2489*	70.38±0.56*	649.30±13.03	26.25±0.80*	1979.27±74.67	3.59±0.61	9337.82±928.39

Table 1. Fluorescence parameters of cardiomyocyte autofluorescence ($\lambda_{excitation/emission}$ = 375 nm/450 nm). Data are shown as mean ± SEM (number of cells); *$p<0.05$ vs. control human cells.